MONITORING AND DIAGNOSIS OF ROTATING MACHINERY BY USING VIBRATION ANALYSIS TECHNOLOGY

Engr. Md. Lutfar Rahman
General Manager (MTS)

ABSTRACT: This paper presents machine health monitoring and malfunction diagnostics methods using vibration data in correlation with operational process data. The advantage of vibration analysis systems is emphasized as a part of preventive/predictive maintenance programs. Training Institute for Chemical Industries (TICI), BCIC is rendering this type of specialized technical services to various industrial & technical organizations of Bangladesh since long. This paper includes case study of Vibration analysis & diagnosis of 35 MW Gas Turbine Generator (GTG), Bhola Rental Power Plant, Bhola & Vibration analysis & Dynamic mass balancing of Centrifuge, Joypurhat Sugar mills Ltd., Joypurhat.

Keywords: Monitoring, Diagnosis, Data formats, Vibration severity

1. INTRODUCTION

One of the widely used methods for detection and diagnosis of the rotating machinery malfunctions is one by vibration analysis technology. In this technology, machinery malfunctions detection and diagnostics procedure can be roughly divided into four steps, namely; vibration measurement, signal processing, feature extraction and feature recognition.

2. CASE STUDY

Case History# 1- *35 MW Gas Turbine Generator (GTG), Bhola Rental Power Plant, Bhola*
Case History# 2- *Centrifuge, Joypurhat Sugar mills Ltd., Joypurhat.*

3. Case History# 1-- 35 MW Gas Turbine Generator (GTG), Bhola Rental Power Plant

Venture Energy Resources Ltd. authority requested TICI to analyze vibration data and diagnosis of their 35 MW Gas Turbine Generator (GTG), Bhola Rental Power Plant, Bhola. Maintenance of Generator (stator rewinding) of the said machine train was carried out by in-house maintenance personnel of Bhola Rental Power Plant with foreign experts' assistance. After maintenance when the machine train was restarted, it was suffering from high vibration problem. TICI was requested to attend the job. TICI vibration analysis team attended the job on 06.05.2012. Vibration data was recorded at start-up, steady state & coasted down condition.

Operators' Information
Overall level of vibration level is high. Vibration increases with the increase of load. Vibration decreases with the increase of frequencies (at 49.2 Hz vibration is maximum and at 51.1 Hz it is minimum)

Table 1. Steady state data at 30 MW load

Probe Location	Probe Position	Composite Vibration in mm/sec	1X Vibration in mm/sec	2X Vibration in mm/sec	3X Vibration in mm/sec
Bearing-1 Compressor end	Vertical	8.27	3.00	0.23	0.02
	Horizontal	10.10	5.70	0.35	0.09
	Axial	35.6	3.39	0.23	0.26
Bearing Generator NDE	Vertical	5.45	2.35	0.24	0.19
	Horizontal	10.4	5.94	0.91	0.07
	Axial	23.2	9.24	8.06	0.49

4. 1 ANALYSIS (at Compressor)

In half spectrum plots 1X is the dominating frequency. So mass unbalance, increased bearing clearance are the suspected causes.

In full spectrum plot existence of 1X forward & reverse component indicates mass unbalance. Forward component is key for balancing. Reverse component can be reduced by the forward component reduction.

Highly elliptical shape orbit indicates pre-loaded compressor bearing.

From start-up data, in Bode Plots vibration amplitude increase exponentially with the increase of speed which is the indication of mass unbalance. In Polar Plots outward nature of 1X amplitude indicates mass unbalance.

Vibration frequencies 1020 cpm and 1980 cpm indicate fluid induced instability (oil whirl) due to improper wedge effect in bearings (improper bearing alignment). The tilting pads/bearings assure unstable position during loaded condition.

In axial direction, existence of synchronous and super harmonic frequencies indicates mechanical looseness.

4.2 ANALYSIS *(*at Generator)

In axial direction, the existence of 1X & 2X vibration frequency where 2X is the dominating frequency indicates misalignment.

Axial vibration is higher than radial vibrations indicate misalignment..

5. REMARKS

1. Misalignment in the machine train.
2. Mass unbalance in the turbine rotor.
3. Fluid induced instability (oil whirl)
4. Increased bearing clearance

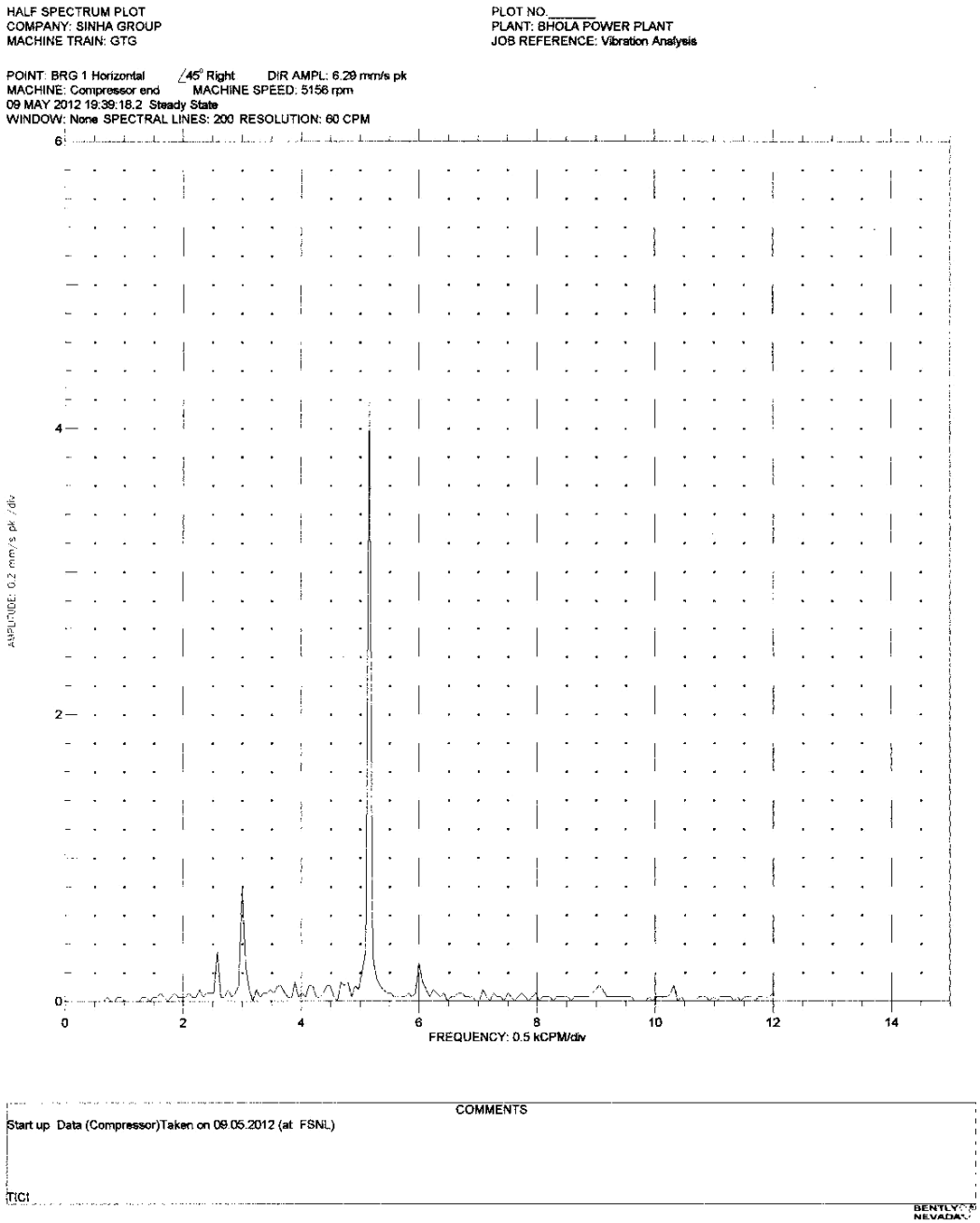

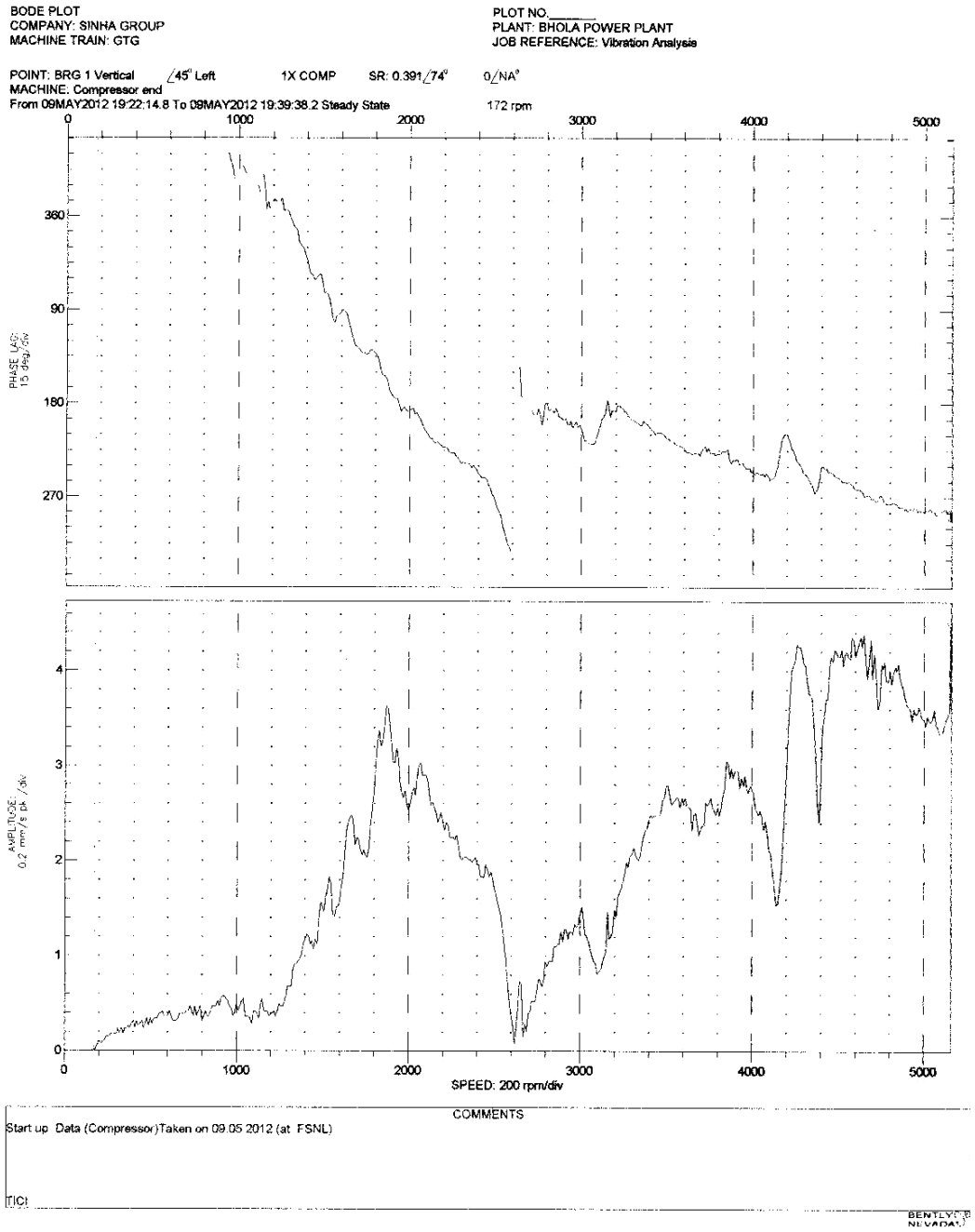

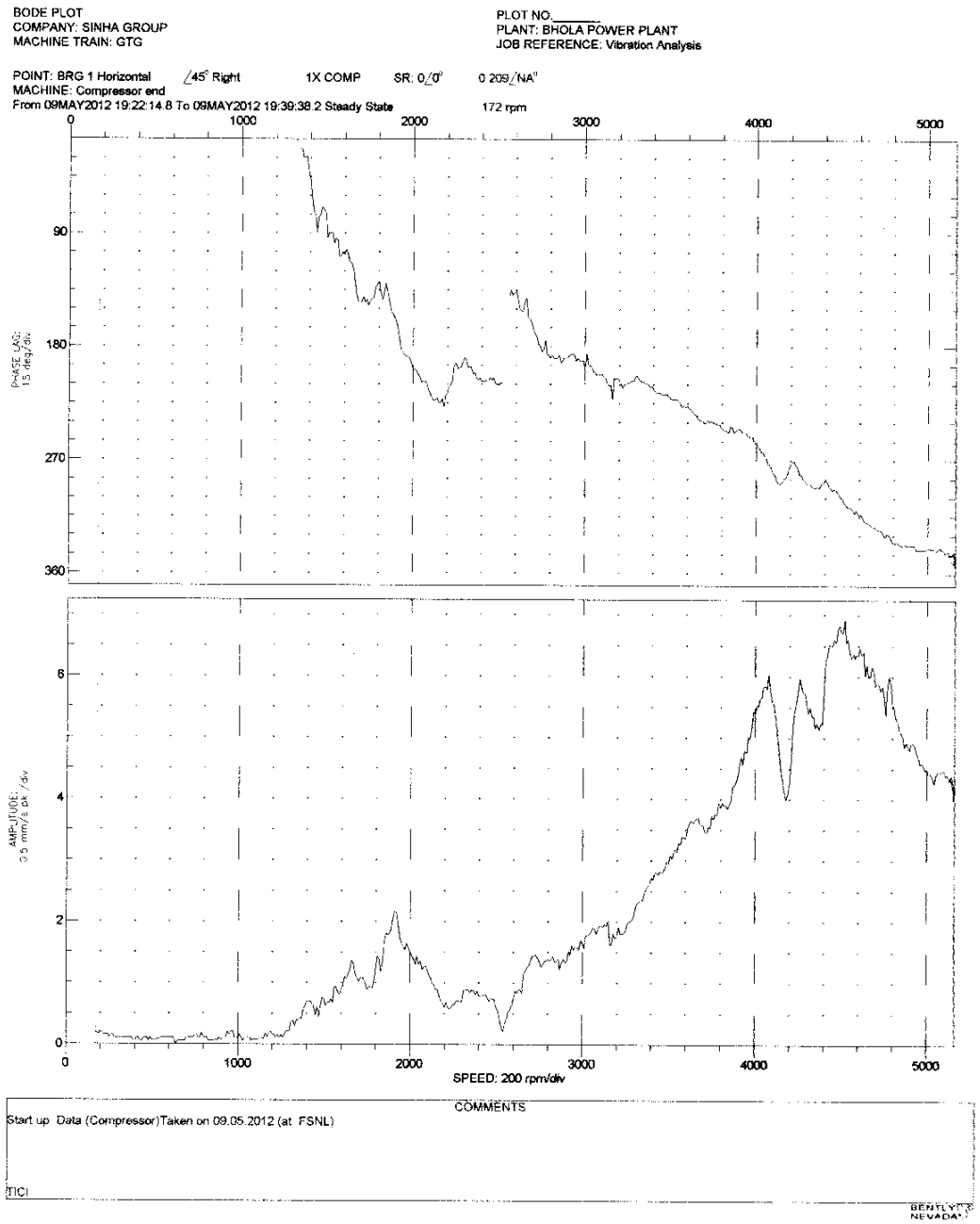

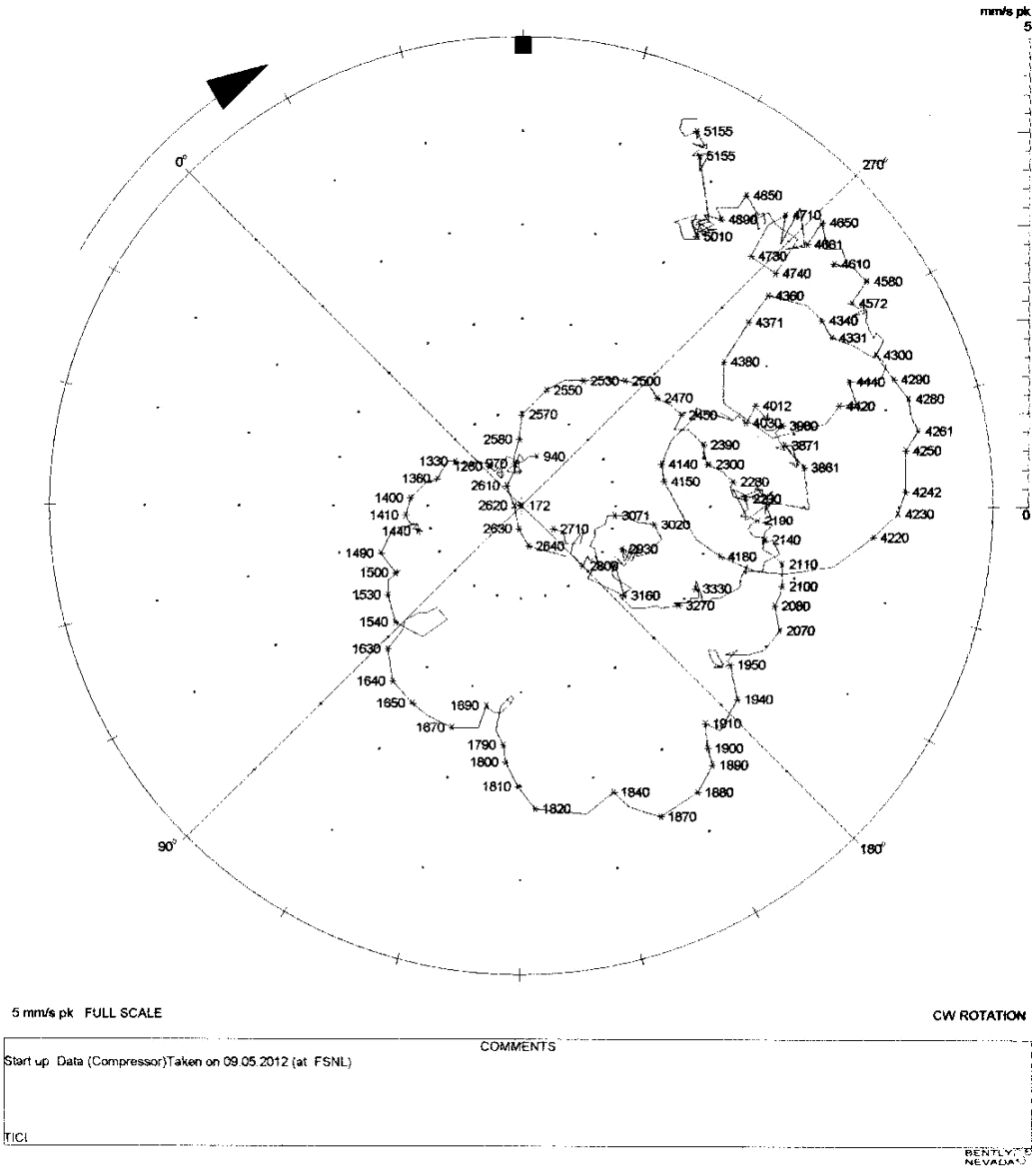

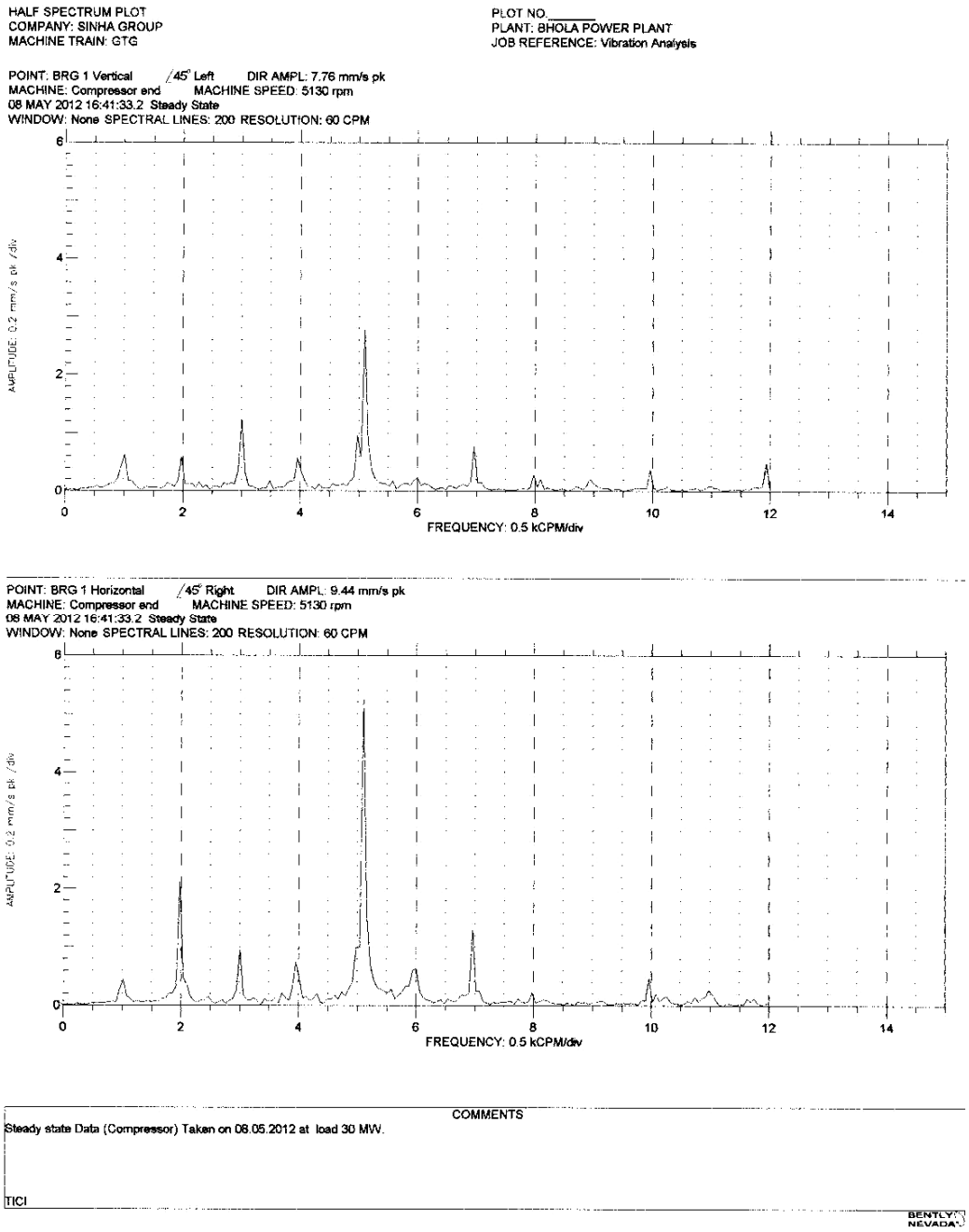

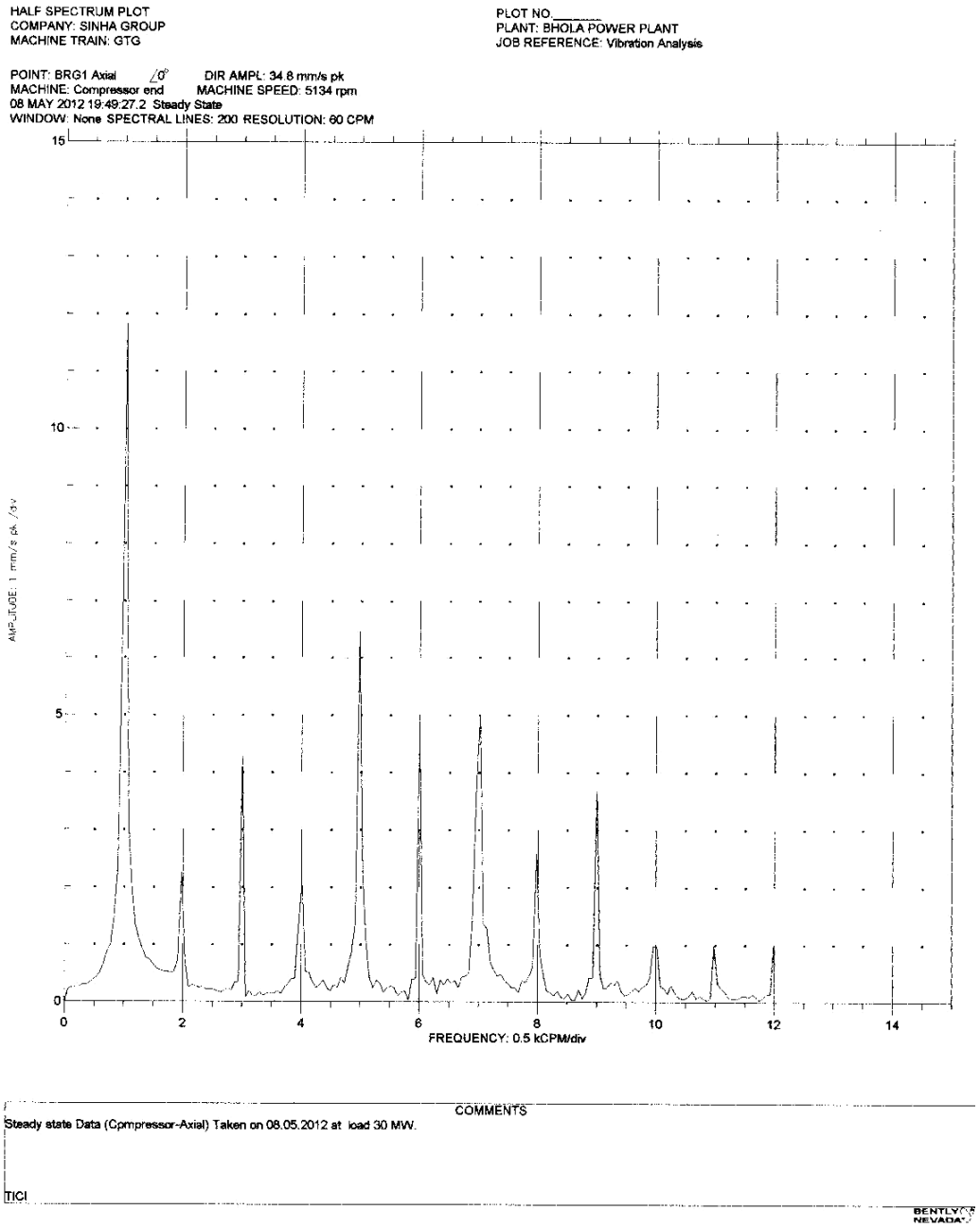

6. Case History# 2—Dynamic mass balancing of Centrifuge, Joypurhat Sugar mills Ltd., Joypurhat.

After yearly scheduled repair & maintenance work of the centrifugal machines (centriguge), it was necessary to find out the cause of high vibration and subsequent in-situ dynamic mass balancing of the said machines. TICI was requested by Joypurhat Sugar Mills Ltd., Joypurhat authority to perform dynamic mass balancing of the centrifugal machine (BMA). TICI vibration analysis team attended the problem on 22.12.2011 and undertook necessary action.

To evaluate the machine condition, Transient and Steady state data of the centrifugal machine (centrifuge) were recorded. Transient data (start-up data) was plotted in Bode & Polar formats while

steady state data was plotted in Spectrum formats. Vibration data were also recorded in Tabular list before & after balancing.

Level of vibration before balancing

Composite vibration : 41.5 mm/sec pk
1X vibration : 40.9 mm/sec pk
2X vibration : 1.20 mm/sec pk

According to Vibration Severity Chart ISO Std. 2372, the machine is operating in "Unsatisfactory" zone

Nature of change of 1X vibration amplitude with rpm in Bode & Polar plots show that there is *mass unbalance in the rotor.*

According to the above findings, dynamic balancing of the machine "BMA" was carried-out. To find out the correct mass & angle, trial mass was added several times in the single plane dynamic balancing steps. Finally 167 gm was added at 342 deg. & 171 gm at 352 deg.

Steady state data of the machine was plotted in Spectrum format after mass balancing. Transient data (start-up data) was plotted in Bode & Polar formats

Level of vibration after balancing
Composite vibration : 5.28 inch/sec pk
1X vibration : 5.26 inch/sec pk
2X vibration : 0.369 inch/sec pk

According to **Vibration Severity Chart ISO Std. 2372**, the machine is operating in **"Satisfactory"** zone

Now the machine is dynamically balanced and it is capable to run at rated load for normal operation.

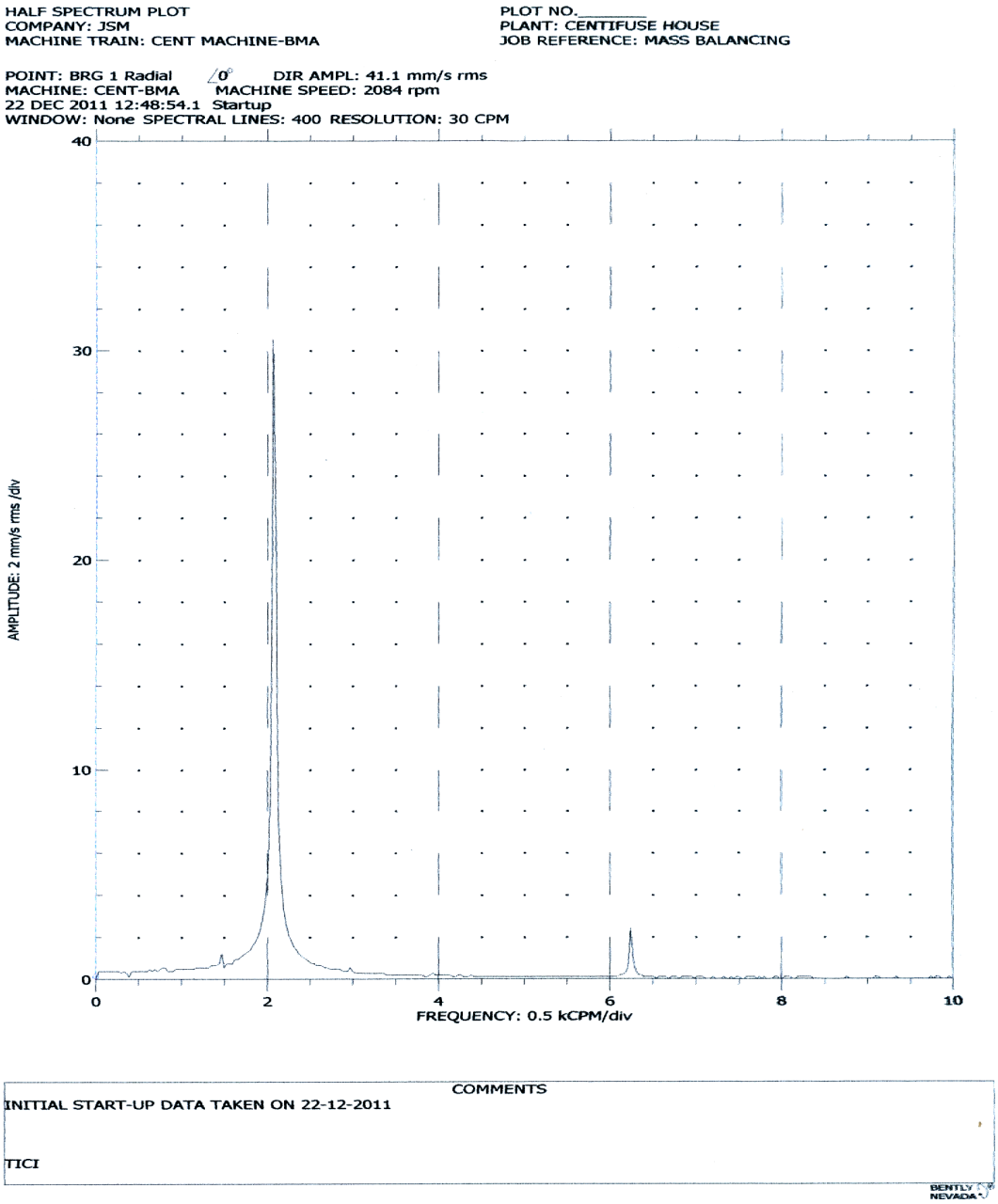

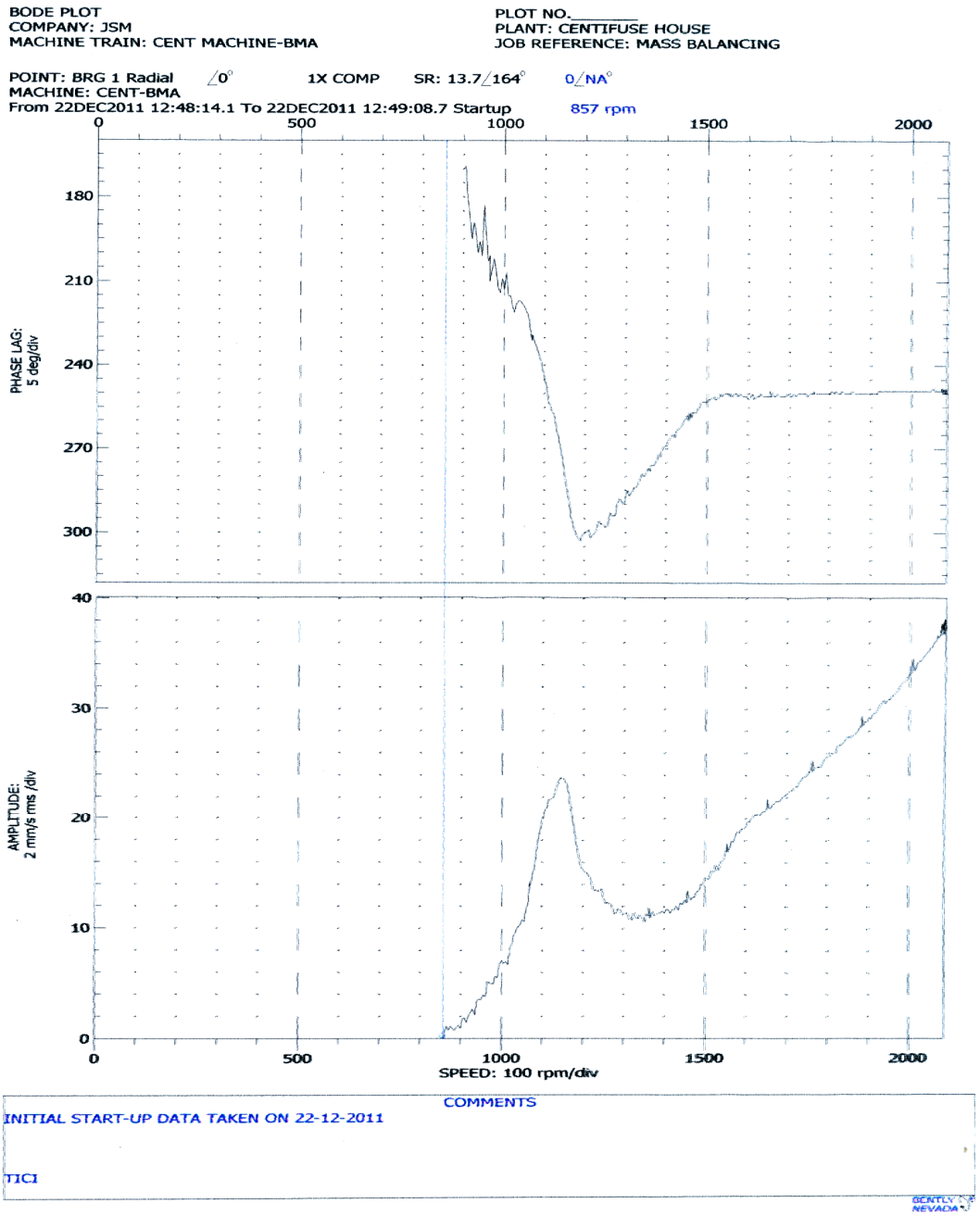

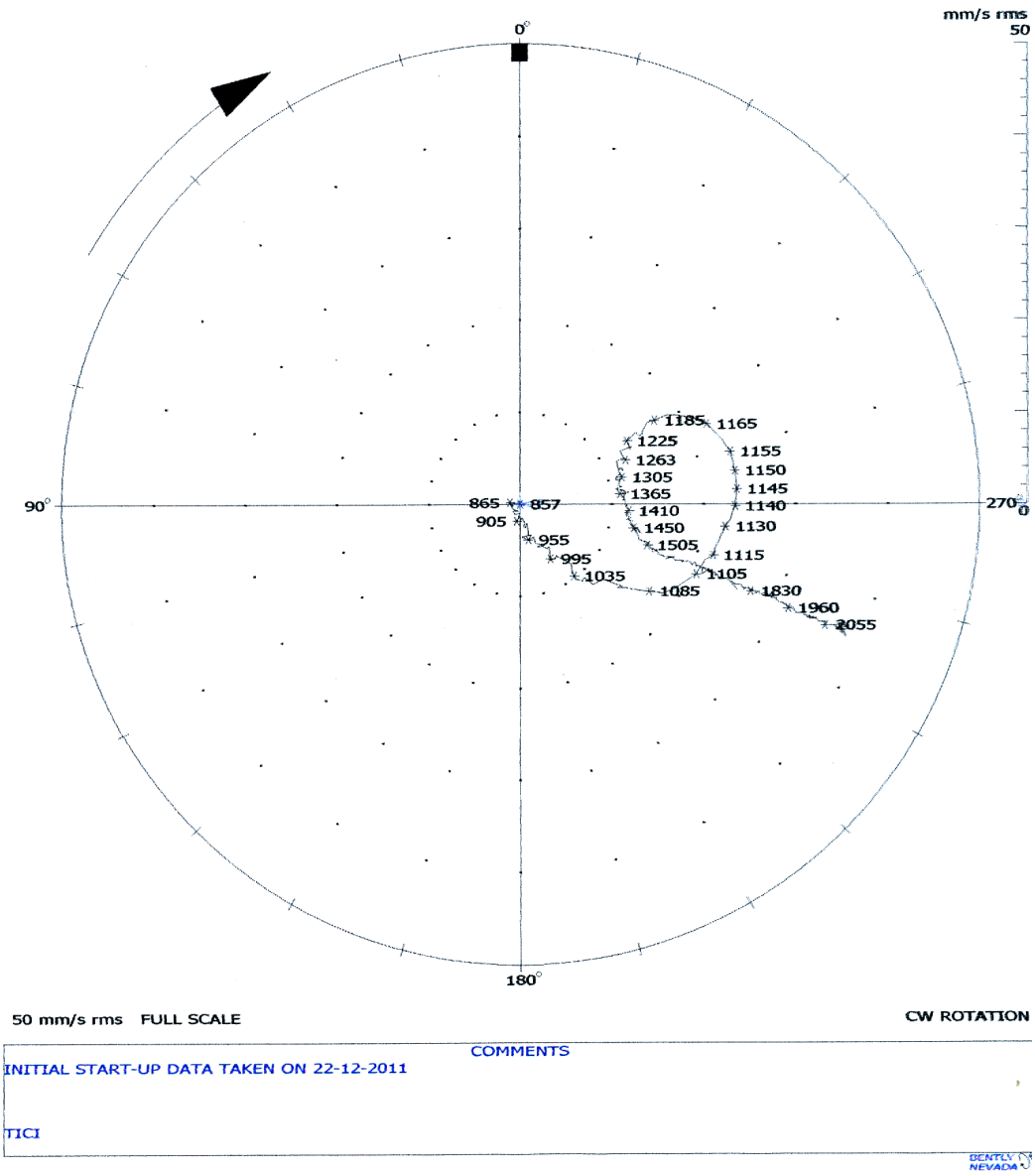

HALF SPECTRUM PLOT
COMPANY: JSM
MACHINE TRAIN: CENT MACHINE-BMA

PLOT NO._____
PLANT: CENTIFUSE HOUSE
JOB REFERENCE: MASS BALANCING

POINT: BRG 1 Radial ∠0° DIR AMPL: 5.35 mm/s rms
MACHINE: CENT-BMA MACHINE SPEED: 2084 rpm
22 DEC 2011 17:08:40.2 Startup
WINDOW: None SPECTRAL LINES: 400 RESOLUTION: 30 CPM

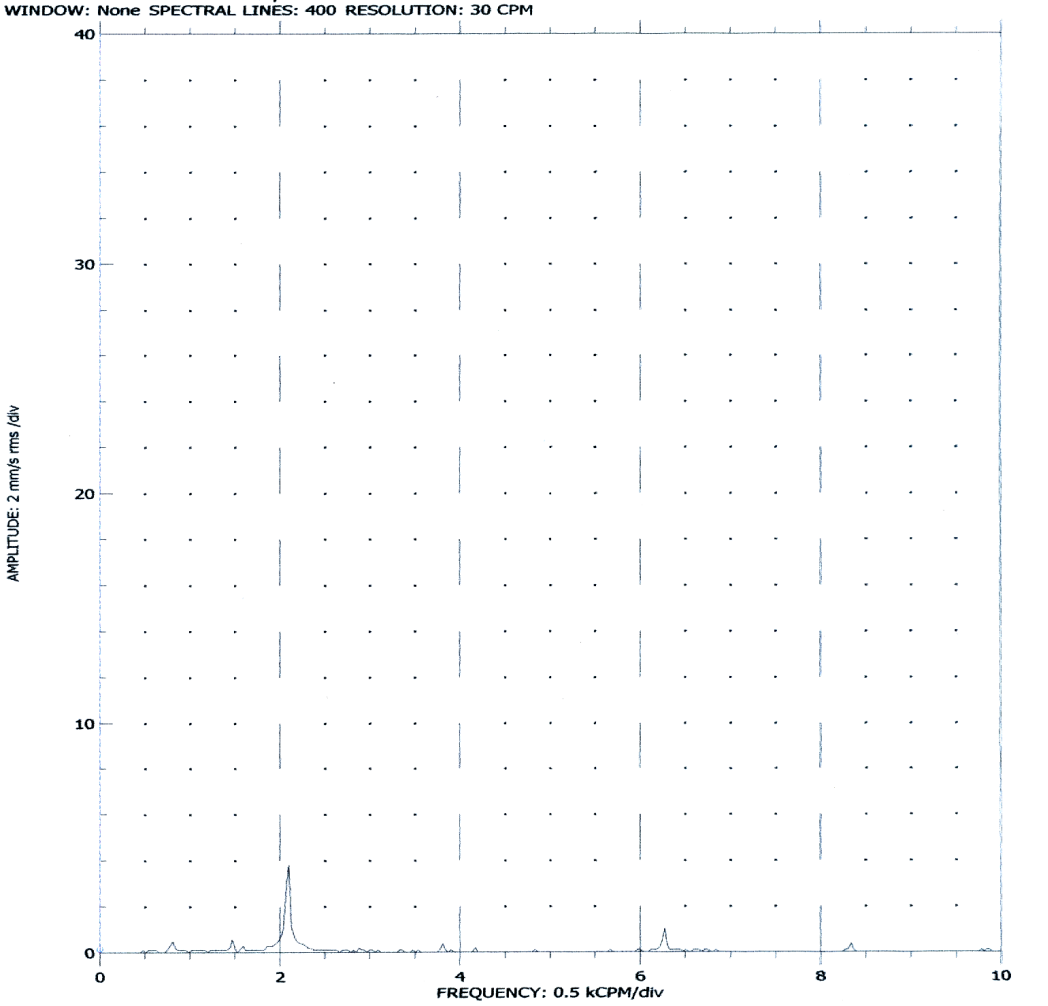

COMMENTS
FINAL DATA AFTER ADDING MASS 167 GM AT 342 DEG. & 171 GM AT 352 DEG. TAKEN ON 22-12-2011

TICI

BENTLY NEVADA

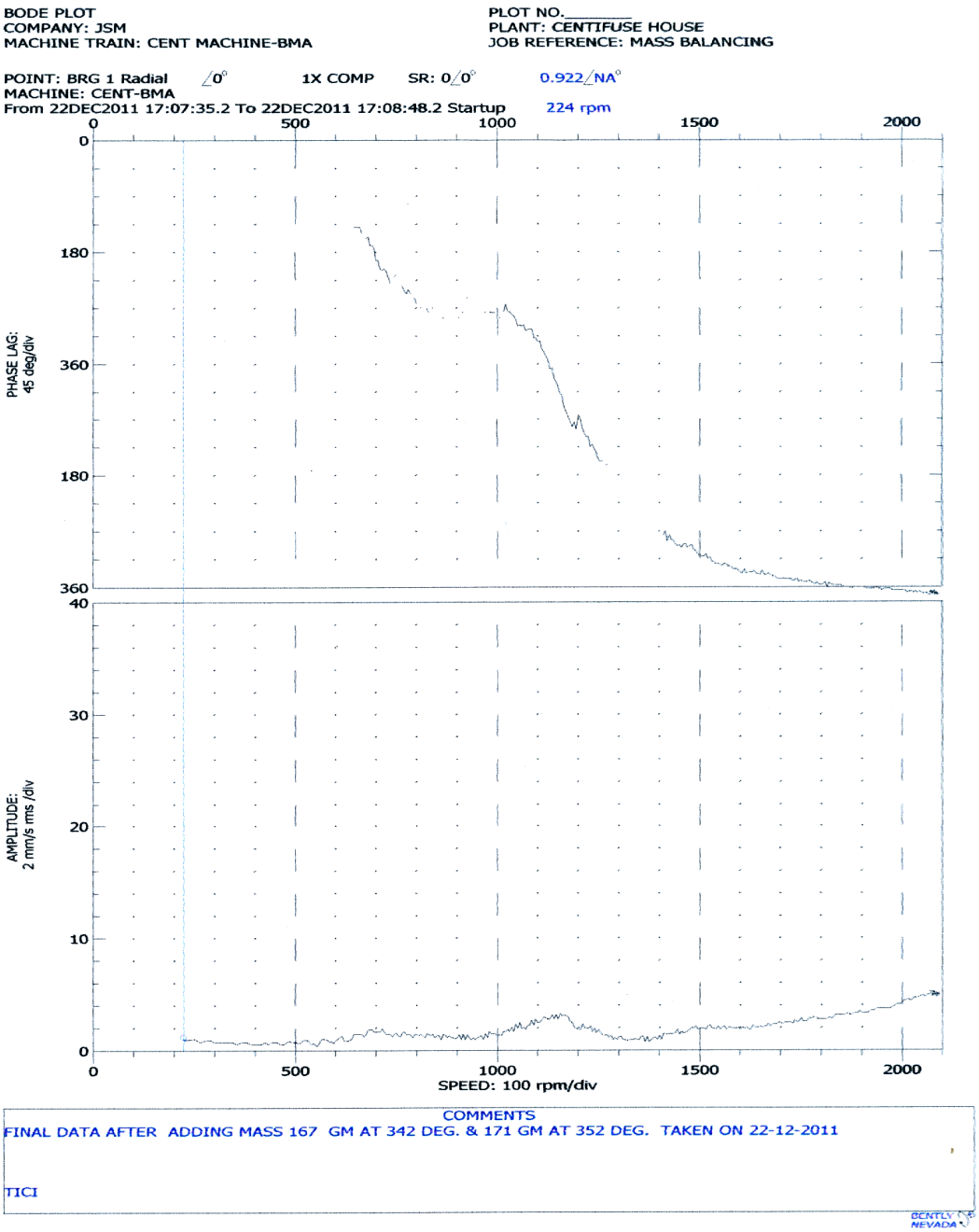

VIBRATION ANALYSIS OF A CRACKED BEAM

A.R.Biswal
Department of Mechanical Engineering
National Institute of Technology, Rourkela-769008, INDIA.
alokbiswal82@gmail.com,

R.K.Behera
Department of Mechanical Engineering
National Institute of Technology, Rourkela-769008, INDIA.
rkbehera@nitrkl.ac.in

T.Roy
Department of Mechanical Engineering
National Institute of Technology, Rourkela-769008, INDIA
tarapada@nitrkl.ac.in

ABSTRACT: The present day structures and machineries are designed based on optimizing of multi-objectives such as maximum strength, maximum life, minimum weight and minimum cost. Due to this they are flexible and allow having a very high level of stresses. This leads to development of cracks in their elements. Many engineering structures may have structural defects such as cracks due to long-term service. So it is very much essential to know the property of structures and response of such structures in various cases. An important problem in most of the structural element is active vibration control. The simplest way to tackle such problem is to make the element smart, adaptive and self-controlling. In this article the natural frequencies and mode shapes of an uncracked and cracked Timoshenko beam is studied by using finite element method (FEM) and MATLAB programme. The effect of piezoelectric patches on natural frequencies of the uncracked and cracked Timoshenko beam along with piezoelectric bimorph is studied for electro-mechanical validation.

Keywords: Cracked beam, Timoshenko beam, finite element method, piezoelectricity, bimorph beam.

1. INTRODUCTION

Presence of crack in a structural member is a serious threat to the performance of the structure. The effects of crack on the dynamic behaviour of the structural elements have been the subject of several investigations for the last few decades. Due to the existence of such cracks the frequencies of natural vibration, amplitudes of forced vibration, and areas of dynamic stability change. In order to identify the magnitude and location of the crack, analysis of these changes is essential. The information from the analysis enables one to determine the degree of sustainability of the structural element and the whole structure.

Beams are one of the most commonly used elements in structures and machines, and fatigue cracks are the main cause of beams failure. Papadopoulos and Dimarogonas [1] revealed the introduction of local flexibility due to presence of transverse crack in a structural member whose dimension depends on the number of degrees of freedom considered. It has been observed that the local flexibility matrix is mainly appropriate for the analysis of a cracked beam if one employs an analytical method by solving the differential equations piece wisely [2]. One way to detect cracks on structures is to employ modal testing in which changes in modal parameters such as variations in frequencies and mode shapes are used to detect damage. The detection of structural damage through changes in frequencies was discussed by Salawu [3]. Moreover, Dilena and Morassi [4] proposed damage identification based on changes in the nodes of mode shapes. They demonstrated that appropriate use of resonances and anti-resonances can be used to avoid the non-uniqueness of damage location for symmetrical beams.

Identification of cracks in beam structures using Timoshenko and Euler beam formulation has been studied by Swamidas *et al*. [5]. In their paper Timoshenko and Euler beam formulations have been used to estimate the influence of crack size and location on natural frequencies of cracked beam. Frequency contour method has been used to identify the crack size and location properly. Ali *et al*.[6] have studied the free vibration analysis of a cantilever beam. It has been observed that the presence of crack in the beam, will affect the natural frequency. The magnitude for the change of natural frequency depends on the change of (number, depth and location) for the crack.Also the change of dynamic property will effect on stiffness and dynamic behaviour.

Shin *et al*. [7] have developed a method to find the lowest four natural frequencies of the cracked structure by finite element method. They have obtained the approximate crack location by using Armon's Rank-ordering method that uses the above four natural frequencies. A method for shaft crack detection have proposed by Xiang *et al*. [8] which is based on combination of wave-let based elements and genetic algorithm. The experimental investigations of the effects of cracks and damages on the structures have been reported by Owolabi et al. [9]. Al-Qaisia *et al*. [10] have utilized the reduction of Eigen frequencies and sensitivity analysis to localize a crack in a non-rotating shaft coupled to an elastic foundation. The shaft was modelled by the finite element method and coupled to an experimentally identified foundation model. Sahin *et al*. [11] have introduced different damage scenarios by reducing the local thickness of the selected elements at different locations along with finite element model (FEM) for quantification and localization of damage in beam-like structures in their research. Nahvi *et al*. [12] have developed an analytical, as well as experimental approach to the crack detection in cantilever beams by vibration analysis.

E.Viola *et al*. [13] have used a finite element method for static and dynamic analysis of a cracked prismatic beam on the basis of Hamilton's principle. The crack section was modelled as an elastic hinge by considering fracture mechanics theory. Kisa *et al*. [14] have developed the component mode synthesis technique along with finite element method for free vibration analysis of uniform and stepped cracked beam with circular cross section. The finite element analysis of a cracked cantilever beam and the relation between the modal natural frequencies with crack depth, modal natural frequency with crack location has been studied by Sutar [15]. Only single crack at different depth and at different location are evaluated. The analysis reveals a relationship between crack depth and modal natural frequency. Zheng [16] has described an overall flexibility matrix instead of local flexibility matrix in order to find out the total flexibility matrix and the stiffness matrix of the cracked beam. It has been observed that the consideration of 'overall additional flexibility matrix', due to the presence of the crack, can indeed give more accurate results than those obtained from using the local flexibility matrix. The overall additional flexibility matrix parameters are computed by 128-point (1D) and 128 ×128(2D) Gauss quadrature and then further best fitted using the least-squares method. The best-fitted formulas agree very well with the numerical integration results [17]. After getting the stiffness matrix of a cracked beam element standard FEM procedure can be followed, which will lead to a generalized eigenvalue problem and thus the natural frequencies can be obtained.

Active vibration control through piezoelectric transducer patches is used to dampen out the critical modes which have high influence on the spindle location [18], [19]. Piezoelectric materials generate an electric potential from an applied mechanical stress and also exhibit the inverse effect of expanding when subjected to an applied voltage. The development of ceramics that possess very strong mechanical electrical coupling properties is one of the driving factors behind the advent of active vibration control as a more viable solution to vibration than passive control techniques. Extensive researches have been made in modeling of piezoelectric materials in building actuators and sensors for structure. Crawley and Luis [20] emphasized on the derivation of sensor / actuator modeling of piezo-electric materials. The control analysis of cantilever beams using these sensors / actuators have been studied by Bailey and Hubbard [21]. The concept of smart structure, its benefits and applications has been given by Culshaw [18] .A Finite Element Model (FEM) has been developed by Hanagud, *et al.*, [22] for an active beam with many distributed piezoceramic sensors / actuators coupled by signal conditioning systems and applied optimal output feedback control. Experiments have been performed by Fanson *et al.*, [23] on a beam with piezoelectric using positive position feedback.

2. FINITE ELEMENT MODELING OF A CRACKED TIMOSHENKO BEAM ELEMENT

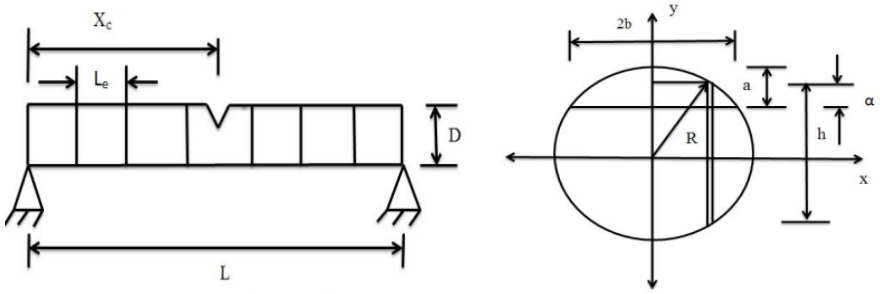

Fig. 1: Simply supported beam with crack subjected to shear force and bending moment.

Figure 1 shows a simply supported beam of circular cross-section having diameter '*D*' with a single transverse crack with constant depth '*a*'. The crack is at a distance of 'X_c' from the left end of the beam. The beam is divided into number of equal elements having length 'L_e'.
Where

$$b = \sqrt{Da - a^2}$$
$$h = \sqrt{D^2 - 4x^2}$$
$$\alpha = \frac{1}{2}\left[\sqrt{D^2 - 4x^2} - (D - 2a)\right].$$

The additional strain energy due to the existence of the crack can be expressed as [24], [25].

$$\Pi_c = \int_{Ac} G dA \qquad (1)$$

Where '*G*' is the strain energy release rate function. The strain energy release rate function can be expressed as

$$G = \frac{1}{E'}\left[(K_{I2} + K_{I3})^2 + K_{II2}{}^2\right] \qquad (2)$$

Where $E'=E$ for plane stress problem, $E'=E/1-\mu^2$ for plane strain problem. K_{I2},K_{I3},K_{II2} are the stress intensity factors. The values of stress intensity factor can be can be expressed as

$$K_{ni} = \sigma_i \sqrt{\pi\alpha} F_n\left(\frac{\alpha}{h}\right). \qquad (3)$$

Using Paris equation

$$\delta_i = \frac{\partial \Pi_c}{\partial P_i} \qquad (i = 2,3). \qquad (4)$$

The overall additional flexibility matrix C_{ij} can be obtained as [25]

$$C_{ij} = \frac{\partial \delta_i}{\partial P_j} = \frac{\partial^2 \Pi_c}{\partial P_i \partial P_j} \qquad (i,\ j = 2,3). \qquad (5)$$

Substituting the equation (3) in (2) & (1) and then in (5) we get

$$C_{ij} = \frac{1}{E'}\frac{\partial^2}{\partial P_i P_j}\int_{-\sqrt{(Da-a^2)}}^{\sqrt{(Da-a^2)}}\int_{0}^{\frac{1}{2}\left[\sqrt{(Da-4x^2)}-(D-2a)\right]}\left[\left\{\frac{32\,P_2 L_c h}{\pi D^4}\sqrt{\pi\alpha}\,F_2\left(\frac{\alpha}{h}\right)\right.\right. \text{(i, j=2, 3)} \qquad (6)$$
$$\left.\left. + \frac{32\,P_3 h}{\pi D^4}\sqrt{\pi\alpha}\,F_2\left(\frac{\alpha}{h}\right)\right\}^2 + \frac{16\,P_2{}^2}{\pi^2 D^4}\pi\alpha\,F_{II}{}^2\left(\frac{\alpha}{h}\right)\right] d\alpha\, dx$$

2.1 Overall additional flexibility matrix under conventional FEM co-ordinate system

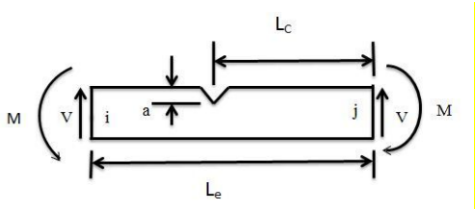

Fig. 2: Cracked Timoshenko beam element.

Figure 2 shows a cracked beam element with generated loading. The beam is subjected to shearing force '*V*' and bending moment '*M*' at each node. The corresponding displacements are denoted as '*y*' and 'θ'. 'L_c' denotes the distance between the right hand side end node and the crack location. '*a*' denotes the crack depth. The beam element has length 'L_e', cross-sectional area '*A*' and flexural rigidity '*EI*'.Under the FEM co-ordinate and notation system, the relationship between the displacement and the forces can be expressed as

$$\begin{Bmatrix} y_j - y_i - \theta_i \\ \theta_j - \theta_i \end{Bmatrix} = C_{ovl} \begin{Bmatrix} V_j \\ M_j \end{Bmatrix}.$$

2.2 Flexibility matrix for intact Timoshenko beam element

The flexibility matrix C_{intact} of the intact Timoshenko beam element can be written as

$$\begin{Bmatrix} y_j - y_i - \theta_i \\ \theta_j - \theta_i \end{Bmatrix} = C_{\text{int}\ act} \begin{Bmatrix} V_j \\ M_j \end{Bmatrix}.$$

2.3 Total flexibility matrix of the cracked Timoshenko beam element

The Total flexibility matrix of the cracked Timoshenko beam element is obtained by the combination of over-all additional flexibility matrix and flexibility matrix of an intact beam

$$C_{total} = C_{ovl} + C_{\text{int}act}$$

2.4 Stiffness matrix of a cracked Timoshenko beam element

Through the equilibrium conditions, the stiffness matrix 'K_c' of a cracked beam element can be obtained as follows [26] [27]

$$K_c = LC_{total}^{-1} L^T.$$

Where

$$L = \begin{bmatrix} -1 & 0 \\ -L_e & -1 \\ 1 & 0 \\ 0 & 1 \end{bmatrix}$$

2.5 Finite element modelling of piezoelectric beam element

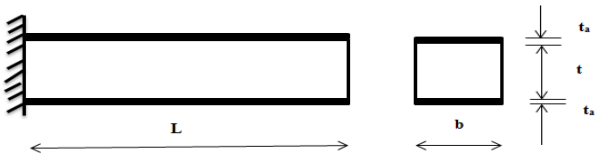

Fig. 3: Piezo-electric beam element.

The regular beam elements with the piezoelectric patches are shown in Figure 3. The piezoelectric element is obtained by bonding the regular beam element with a layer of two piezoelectric patches, one above and the other below at two finite element positions as a collocated pair. The bottom layer acts as the sensor and the top layer acts as an actuator. The element is assumed to have three degrees

of freedom at each nodal point, which are, transverse deflection *w*, an angle of rotation or slope θ and an electrical degree of freedom, i.e., the sensor voltage. The effect of shear is negligible in the piezoelectric patches, since they are very thin and light as compared to the thickness of the beam. In modeling of the smart beam, the following assumptions are made. The mass and stiffness of the adhesive used to bond the sensor / actuator pair to the master structure is being neglected. The smart cantilever beam model is developed using 2 piezoelectric beam elements, which includes sensor and actuator dynamics and remaining beam elements as regular beam elements based on Timoshenko beam theory assumptions. The mass and stiffness matrix of the piezoelectric beam element (regular beam element with piezoelectric patches at the top and bottom surfaces) as a collocated pair is given by

$$[M] = [M_b] + [M_p]$$
$$\text{and} \quad [K] = [K_b] + [K_p]$$

A piezoelectric bimorph beam is composed of two piezoelectric layers joined together with opposite polarities. Piezoelectric bimorphs are widely used for actuation and sensing. In the actuation mode, on the application of an electric field across the beam thickness, one layer contracts while the other expands. This results in the bending of the entire structure and tip deflection. In the sensing mode, the bimorph is used to measure an external load by monitoring the piezoelectrically induced electrode voltages. Figure 4 shows a piezoelectric bimorph beam with thickness of 't_p' of each piezo layer and width of '$2w_p$'.The piezoelectric constitutive equations are given by [30]

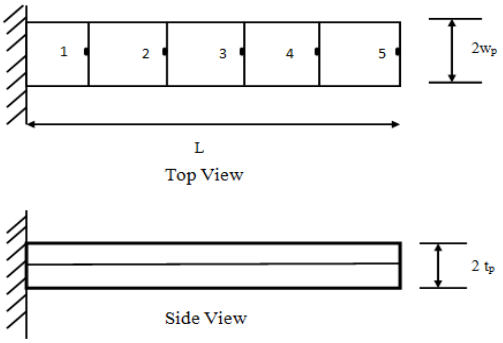

Fig. 4: Piezoelectric bimorph beam.

$$\{T\} = [c]\{S\} - [e]^T\{E\}$$
$$\{D\} = [e]\{S\} + [\varepsilon]\{E\}.$$

Where*{T},{S}* are longitudinal stress and strain, *[c]* is the compliance matrix, *{E}* is the effective electric field, *{D}* is the electric displacement, *[e]*is the piezoelectric coupling coefficient and *[ε]* is the permittivity. A finite element coupled –field formulation is developed to model the dynamics of the piezoelectric bimorph. For mechanical domain, the bimorph is modeled as an equivalent single layer using 1D Timoshenko beam element having 2 degrees of freedom per node denoting the transverse and angular displacements. The equations of motion of a piezoelectric structure can be derived from the Lagrangian and the virtual work which must include both the mechanical and the electrical contributions. The element equations of motion are then obtained by using Lagrange's equation .Upon assembly the equation of motion for the coupled electro-mechanical system are given by [28]

$$\begin{bmatrix} [M] & 0 \\ 0 & 0 \end{bmatrix} \begin{bmatrix} \ddot{x} \\ \ddot{\theta} \end{bmatrix} + \begin{bmatrix} [K_{uu}] & [K_{ud}] \\ [K_{du}] & [K_{dd}] \end{bmatrix} \begin{bmatrix} x \\ \theta \end{bmatrix} = \begin{bmatrix} 0 \\ 0 \end{bmatrix}.$$

Where $M = \rho \int_v N^T N dV$, $K_{uu} = \int_v B^T cB dV$, $K_{ud} = -\int_v B^T e\Phi dV$, $K_{dd} = -\int_v \Phi^T S\Phi dV$

3. RESULT AND DISCUSSION

For numerical analysis a simply supported beam with a transverse crack is taken into consideration. The various geometric and physical properties of the beam are *L*=1m, *D*=2cm, *E*=206Gpa,

ρ=7800Kg/m^3& μ=0.3.The present result for natural frequencies of uncracked Timoshenko beam is compared with the theoretical result as well as the result obtained by [29].The natural frequencies of cracked beam with various positions and various relative crack depth ratio are also found.

Table 1. Natural frequencies of uncracked Timoshenko beam.

ω (rad/sec)	Present Result	Theoretical [29]
ω_1	253.425	253.426
ω_2	1013.703	1013.703
ω_3	2280.835	2280.835

Table 2. Natural frequencies of Cracked Timoshenko beam, Xc/L=0.20.

ω (rad/sec)	Xc/L	α/D=0.2	α/D =0.3	α/D =0.4	α/D =0.5
ω_1	0.2	252.053	250.716	249.371	248.275
ω_2	0.2	1013.396	1012.553	1010.952	1008.875
ω_3	0.2	2183.378	1944.381	1700.315	1552.258

Table 3. Natural frequencies of Cracked Timoshenko beam, Xc/L=0.50.

ω (rad/sec)	Xc/L	α/D=0.2	α/D =0.3	α/D =0.4	α/D =0.5
ω_1	0.5	252.772	252.100	251.389	250.784
ω_2	0.5	982.0696	953.609	927.4137	907.8555
ω_3	0.5	2284.857	2281.51	2268.067	2248.615

Table 4. Natural frequencies of Cracked Timoshenko beam, Xc/L=0.60.

ω (rad/sec)	Xc/L	α/D=0.2	α/D =0.3	α/D =0.4	α/D =0.5
ω_1	0.6	251.221	249.088	246.960	245.240
ω_2	0.6	1018.711	1024.418	1031.028	1037.089
ω_3	0.6	2162.823	2058.453	1966.404	1900.875

Table 5. Natural frequencies of Cracked Timoshenko beam, Xc/L=0.80.

ω (rad/sec)	Xc/L	α/D=0.2	α/D =0.3	α/D =0.4	α/D =0.5
ω_1	0.8	250.544	247.810	245.130	242.997
ω_2	0.8	1001.11	989.0831	977.321	968.032
ω_3	0.8	2321.405	2350.619	2369.132	2377.006

Table [1] represents the comparison of first three natural frequencies of uncracked Timoshenko beam with theoretical values. Table [2-5] represents the natural frequencies of a cracked Timoshenko beam at various crack positions and relative crack depths. It is observed that natural frequency decreases as crack depth increase. Figures 5-7 show the mode shapes for uncracked and cracked Timoshenko beam with relative crack position of 0.5 and relative crack depth of 0.2. It is observed that for cracked beam there is a jump at the respective position of crack.

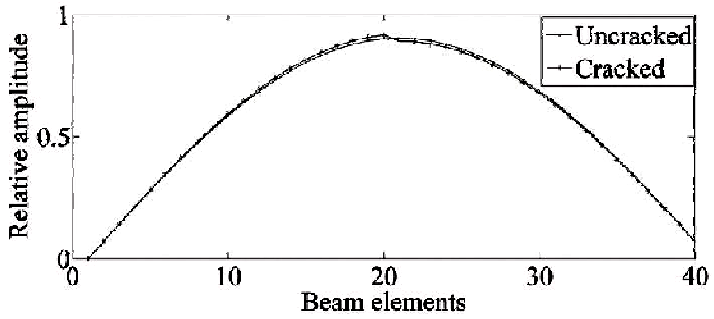

Fig. 5: First mode shape for uncracked and cracked beam, $X_C/L=0.5,\alpha/D=0.2$

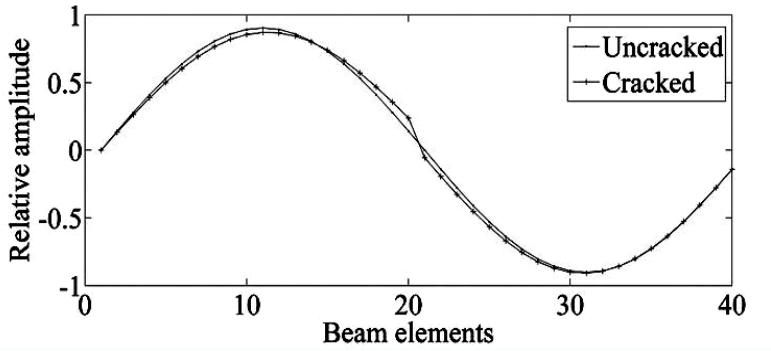

Fig. 6: Second mode shape for uncracked and Cracked beam, $X_C/L=0.5,\alpha/D=0.2$.

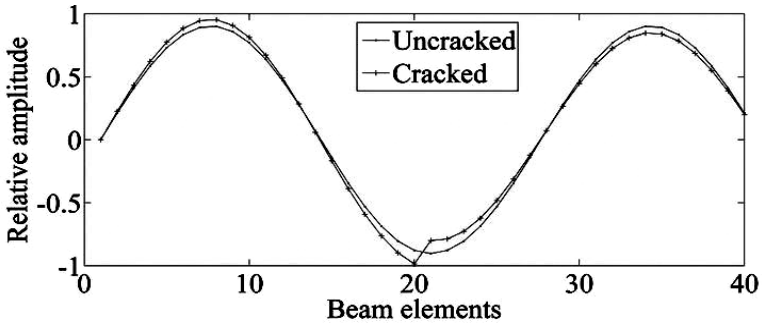

Fig. 7: Third mode shape for uncracked and cracked beam ,$X_C/L=0.5,\alpha/D=0.2$.

A piezoelectric bimorph beam with two PVDF layers bonded together and polarized in opposite directions is considered for Electro-Mechanical validation .The dimensions of the bimorph beam is (100×5×1)mm. The following mechanical and piezoelectric properties used for the PVDF beam are $E_{11}=E_{22}=E_{33}$=2Gpa, ρ=1800kg/m^3, e_{31}=0.0460 C/m^2, ε_{11}=1.062 nF/m. The e_{33} coefficient is assumed to be zero. The bimorph beam has been discretized into five equal elements. A unit voltage has been applied across the thickness and the calculated transverse deflections at the five nodes obtained from the present code have also been compared with other results.

Table 6. Deflections of a piezoelectric bimorph beam.

Location (mm)	20.0	40.0	60.0	80.0	100.0
present (deflection(10^{-4}mm))	0.154	0.587	1.239	2.05	2.956
Mixed model (Chee et al.(1999))	0.138	0.552	1.242	2.208	3.45
Plate FE(FDST)(Suleman and Venkaya(1995))	0.14	0.55	1.24	2.21	3.45
Shell FE(FDST)(Tzou and Ye(1996))	0.132	0.528	1.19	2.11	3.30

Experimental (Tzou and Tseng.(1990))	0.138	0.552	1.24	2.21	3.45

Table 7. Deflections of Cracked Bimorph beam (10^{-4}mm), Xc/L=0.50.

Location (mm)	α/h=0.2	α/h=0.3	α/h=0.4
20.0	0.154	0.154	0.154
40.0	0.587	0.587	0.587
60.0	1.787	2.126	2.435
80.0	2.786	3.125	3.434
100.0	3.882	4.22	4.529

Table 8. Deflections of Cracked Bimorph beam (10^{-4}mm), Xc/L=0.70.

Location (mm)	α/h=0.2	α/h=0.3	α/h=0.4
20.0	0.154	0.154	0.154
40.0	0.587	0.587	0.587
60.0	1.239	1.239	1.239
80.0	2.419	2.647	2.856
100.0	3.453	3.681	3.89

Table 9. Deflections of Cracked Bimorph beam (10^{-4}mm), Xc/L=0.90.

Location (mm)	α/h=0.2	α/h=0.3	α/h=0.4
20.0	0.154	0.154	0.154
40.0	0.587	0.587	0.587
60.0	1.239	1.239	1.239
80.0	2.05	2.05	2.05
100.0	3.143	3.258	3.364

Table -6 represents the deflections of bimorph beam at various node positions and is compared with existing results. Table 7-9 represents the deflections of a cracked bimorph beam with various relative positions of crack and relative crack depths.

4. CONCLUSION

In this paper an overall additional flexibility matrix is used for evaluating the natural frequencies of a cracked Timoshenko beam. From the results obtained it has been observed that the presence of crack in the beam decreases the natural frequencies. The magnitude for the change of natural frequencies depends upon the change of relative crack depth and location for the crack. The Electro-Mechanical validation is carried out by considering a bimorph beam. It is seen that the present result agree well with the existing results.The cracked bimorph beam is studied with various relative positions of crack along with different crack dephs.It is observed that due to presence of crack in different positions of the beam the deflection increases.

5. REFERENCES

[1] C. A. Papadopoulos and A. D. Dimarogonas, Coupled longitudinal and bending vibrations of a rotating shaft with an open crack. Journal of Sound and Vibration. **(1987)**, Vol. 117, No. 1, pp 81–93.
[2] E. I. Shifrin and R. Ruotolo, Natural frequencies of a beam with an arbitrary number of cracks. Journal of Sound and Vibration. **(1999)**, Vol. 222, pp. 409–423.
[3] O. S. Salawu, Detection of structural damage through changes in frequency: a review. Engineering Structures. **(1997)**, Vol. 19, pp. 718-723.
[4] M. Dilena and A. Morassi, Identification of crack location in vibrating beams from changes in node positions. Journal of Sound and Vibration. **(2002)**, Vol. 255, pp. 915-930.
[5] A. S. J. Swamidas, X.Yang and R.Seshadri, Identification of cracking in beam structures using Timoshenko and Euler beam formulations **(2004)**.

[6] A. T. Z. Ali, A. J. N. Aswan, M. Faizal and A. Nisreen, Free vibration Analysis and Dynamic Behaviour for Beams with cracks. International Journal of Science Engineering and Technology **(2009)**.
[7] L. Y. Shin, C. M. Jee, A study on crack detection using Eigen frequency Test data. Computers and Structures. **(2000)**, Vol. 77, pp. 327-342.
[8] J. Xiang, Y. Zhong, X. Chen and Z. He, Crack detection in a shaft by combination of wavelet based elements and genetic algorithm. International journal of solids and structures. **(2008)**, Vol. 45, pp. 4782-4795.
[9] G. M. Owolabi and A. S. J. Swamidas, Crack detection in beams using changes in frequencies and amplitudes of frequency response functions. Journal of Sound and Vibration. **(2003)**, Vol. 265, pp. 1-22.
[10] A. Al-Qaisia and G. Catania, Crack localization in non-rotating shafts coupled to elastic foundation using sensitivity analysis techniques. Journal of Quality in Maintenance Engineering. **(2003)**, Vol. 9, pp. 176 – 201.
[11] M. Sahin and R. A. Shenoi, Quantification and localization of damage in beam-like structures by using artificial neural networks with experimental validation. Engineering Structures. **(2003)**, Vol. 25, No. 14, pp. 1785-1802.
[12] H. Nahvi and M.Jabbari, Crack detection in beams using experimental modal data and finite element model. International Journal of Mechanical Sciences. **(2005)**, Vol. 47, pp. 482-490.
[13] E. Viola, L. Nobile and L. Federici, Formulation of cracked beam element for structural analysis. **(2002)**.
[14] M. Kisa and M. A.Gruel, Free vibration analysis of uniform and stepped cracked beams with circular cross section. International Journal of Engineering Science. **(2007)**.
[15] M. K. Sutar, Finite element analysis of a cracked cantilever beam. International Journal of Advanced Engineering Research and Studies. E-ISSN2249–8974.
[16] D. Y. Zheng and N. J. Kessissoglou, Free vibration analysis of a cracked beam by finite element method. Journal of Sound and Vibration. **(2004)**, Vol. 273, pp. 457–475.
[17] P. J. Davis and P. Rabinowitz, Methods of Numerical Integration. **(1975)**.
[18] B. Culshaw, Smart Structures: A concept or a reality. Journal of Systems and Control Engg. **(2006)**, Vol. 26, pp. 1-8.
[19] S. Rao and M. Sunar, Piezoelectricity and its uses in disturbance sensing and control of flexible structures: A survey. Applied Mechanics. **(1994)**, Vo. 47, No. 2, pp. 113–119.
[20] E. F. Crawley and J. D. Luis, Use of piezoelectric actuators as elements of intelligent structures. AIAA. **(1987)**, Vol. 25, pp. 1373–1385.
[21] T. Baily and J. E. Hubbard Jr., Distributed piezoelectric polymer active vibration control of a cantilever beam. Journal of Guidance, Control and Dynamicsl. **(1985)**, Vol. 8, No. 5, pp. 605–611.
[22] S. Hanagud, M. W. Obal and A. J. Callise, Optimal vibration control by the use of piezoceramic sensors and actuators. Journal of Guidance, Control and Dynamics. **(1992)**, Vol. 15, No. 5, pp. 1199–1206.
[23] J. L. Fanson and T. K. Caughey, Positive position feedback control for structures. AIAA. **(1990)**, Vol. 18, No. 4, pp. 717–723.
[24] A. D. Dimarogonas and C. A. Papadopoulos, Vibration of cracked shafts in bending. Journal of Sound and Vibration. **(1983)**, Vol. 91, No. 4, pp. 583–593.
[25] H. Tada, P. C. Paris and G. R. Irwin, The Stress Analysis of Cracks Handbook. ASME Press. New York **(2000)**.
[26] Z. Xiaoqing, H. Qiang and L. Fen, Analytical Approach for Detection of Multiple Cracks in a Beam. Journal of Engineering Mechanics. **(2010)**, Vol. 136, No. 3, pp. 345-357.
[27] D. R. K. Parhi and A. K. Dash, Faults detection by finite element analysis of a multi cracked beam using vibration signatures. International Journal of Vehicle Noise and Vibration. **(2010)**, Vol. 6, No. 1, pp. 40-54.
[28] T. Roy, P. Manikandan and D. Chakraborty, Improved shell finite element for piezothermoelestic analysis of smart fibre reinforced composite structures. Finite Elements in Analysis and Design. **(2010)**, Vol. 46, pp. 710-720.
[29] S. S. Rao, Mechanical vibrations, fourth edition.
[30] M. Arafa, O. Aldraihem and A. Baz, Modeling and characterisation of linear piezometer. journal of intelligent material systems and structures. **(2009)**.
[31] C. Y. K. Chee, L. Tong and P. G. Steven, A mixed model for composite beams with piezoelectric actuators and sensors. Smart materials and structures. **(1999)**, Vol. 8, pp. 417-432.

[32] A. Sulemean and V. B. Venkay, A simple finite element formulation for a laminated composite plate with piezoelectric layers. journal of intelligent material system and structures. **(1995)**, Vol. 6, pp. 776-782.
[33] H. S. Tzou and R. Ye, Analysis of Piezoelectric Structures with Laminated Piezoelectric Triangular Shell Elements. American Institute of Aeronautics and Astronautics. **(1996)**, Vol. 34, pp. 110-115.
[34] T. S. Tzou and C. I. Tseng, Distributed piezoelectric sensors/actuator design for dynamic measurement /control of distributed parameter system: A piezoelectric finite element approach. Journal of sound and vibration. **(1990)**, Vol. 138, pp. 17-34.

DESIGN AND FABRICATION OF AN AUTOMATIC PICK UP AND PLACING SYSTEM WITH THREE PHASE MOTION ON THE BASIS OF SMALL GRADE PRODUCTION ARRANGING

MD. Nahian Bin Hossain and Tawsif Ahmed
Department of Mechanical Engineering
Bangladesh University of Engineering and Technology (BUET), Dhaka-1000, Bangladesh.

ABSTRACT: The main objective of this paper is to make a model of an automatic pick up and placing system with three phase motion that can be easily applicable on bottle or packet arranging on small industries. As the large scale automation in small industries is practically hindered due to the shortage of capital, so it is necessary to develop an automatic system which is cost viable and operationally effective for small grade of production. Modeling with CAD and fabrication of the system is done through phase by phase analysis. System reliability, practical application and cost effectiveness is considered during design process. With the freedom of three phase motion the system presents itself as a good choice for small scale packet or bottle arranging automation. Overall fabrication is fully dependent on locally available accessories. So any further improvement or repairing of the system is very simple.

Keywords: Automatic, pick up, placing, motion, cost.

1. INTRODUCTION

1.1. OVERVIEW

Recent rise in the production cost has become a major concern for the industries. Demands for products also increasing. The only solve to these problems is to decrease production time and production unit. An automatic pick up and placing system with 3P motion can contribute a lot to this.

1.2. OBJECTIVES

The paper provides an overview on a machine which can automatically arrange bottles in row and column through 3P motion. The goal was to improve it such a stage that it can be used to industry or small packing system. This report is the guide to different facts, ideas, machine and electrical components used and different stages of works done to accomplish the goal of the project.

1.3. ORGANIZATION OF PAPER

This paper is organized in four sections. The first section describes about 3P motion. The second section gives a brief description on models mechanical structure. The third section describes about the electrical part. The fourth section is about the automation. The fifth section shows the economic aspects of our model. Finally, the paper provides a summary of the findings and recommendations for future work.

2. 3P MOTION AND ITS FEATURES

3P motion denotes three phase motion. In a simple sense it indicates to the freely three axis movement of a mechanical component. Proper control over the system can provide a well automation. In this model the bottle arranging mechanism can move smoothly on X, Y & Z axis. For a well-controlled and overall compact arranging system, three phase motion is must. Introducing the three phase mechanism perfectly also broads the way of future development reliability of the system.

3. DEVELOPMENT OF MECHANICAL STRUCTURE

3.1. DESIGN OVREVIEW

The design is focused on some general criteria such as system flexibility, local availability of components, system reliability &cost. For a wide range of bottle handling and long term use of the system, flexibility and cost have great importance. System modeling is done through SOLIDWORKS. CAD drawing of our model is shown is Figure 1.

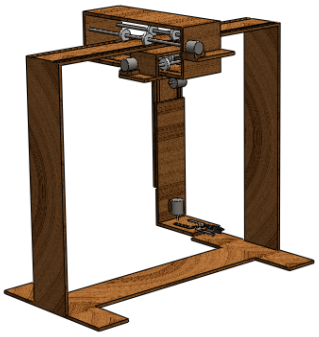

Fig. 1: CAD Model of 3P Automatic Pick up and Placing Arrangement

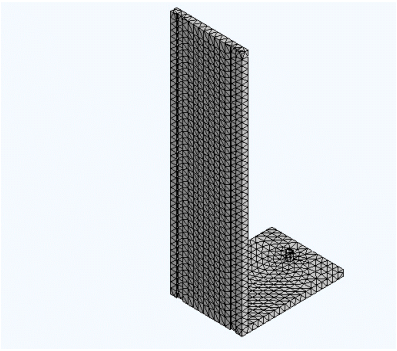

Fig. 2: Surface Mesh Setup for the Arm of 3P Automatic Pick up and Placing Arrangement

3.2. STRUCTURAL UTENSILS

Easy available and most regular equipment is used for making the model. Main structure has been made using wood. For attaining 3P motion three different ball bearing channels are there. For the bottle gripper a simple mechanism, the cross connection of X-type plate of metal, is used which is controlled by a DC motor. 3P motion of the arm has been powered by three DC gear motors.

3.3. FINDINGS OF STRUCTURAL ANALYSIS

Results of the simulation of the mechanical structure is presented here in Table 1, Figure 2, Figure 3 and Figure 4.

Table 1. Simulations Results for Stress Analysis of the 3P Automatic Pick up and Placing Arrangement Arm

Name	Type	Min	Max
Equivalent Stress	VON: von Mises Stress	1.43635N/m^2	3.03816e+005 N/m^2
Maximum shear stress	*Maximum Shear Stress*	8.97e-001 N/m^2	1.78715e+005 N/m^2
Displacement	Resultant Displacement	0 m	1.92745e-003 m
Factor of Safety	Fatigue Tool	1.1853	15
Factor of Safety	Max von Mises Stress	2.9828	15

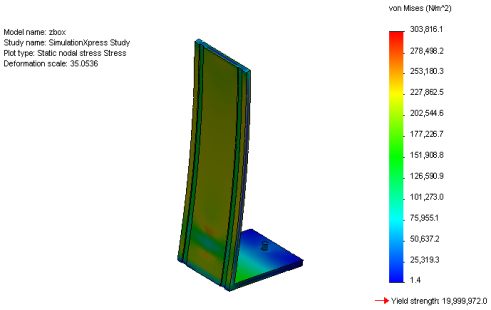

Fig. 3: Simulation Xpress Study for Static Nodal Stress

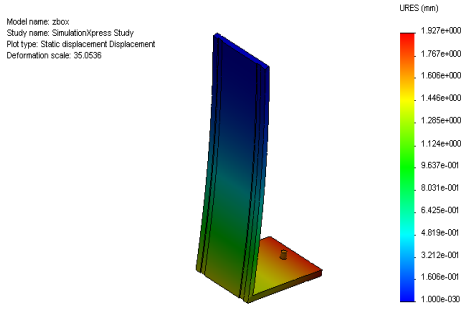

Fig. 4: Simulation Xpress Study for Static Displacement

4. DEVELOPMENT OF ELECTRICAL STRUCTURE

4.1. CIRCUIT OVERVIEW

The circuit is designed and simulated through PROTEUS. An overview of the whole circuit is shown at Figure 5 and PROTIUS simulation has given in Figure 6.

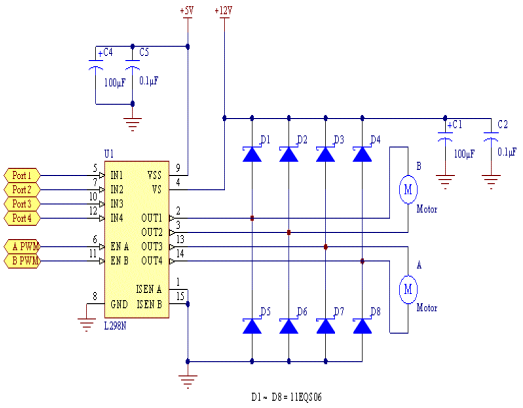

Figure 5. Layout of Electric Circuit

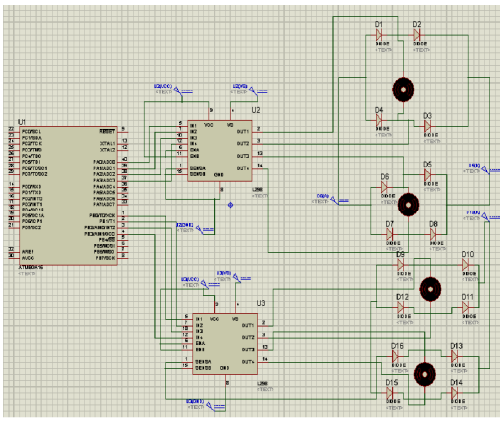

Figure 6. PROTEUS Simulation of Electric Circuit

4.2. ELECTRICAL UTENSILS

Microcontrollers are designed for embedded applications, in contrast to the microprocessors used in personal computers or other general purpose applications which is must for designing an automated system. For our simple model 'Atmega16' is the perfect one that's why it was used. Pin mapping for the 'Atmega16' has been shown in Figure 8. For controlling the motors by the microcontroller motor driver L298N was used. This motor driver IC is popular for stepper motor or dual DC brushed motor control projects. The interface is the same as that of the L293 and the TI SN754410, so this IC can also be used with our dual serial motor controller PIC to make a higher-power dual serial motor controller. We have this chip in the L298N version, which is staggered-lead, through-hole package that can be used with breadboards and other prototyping boards. Figure 7 shows the pin mapping of L298N.

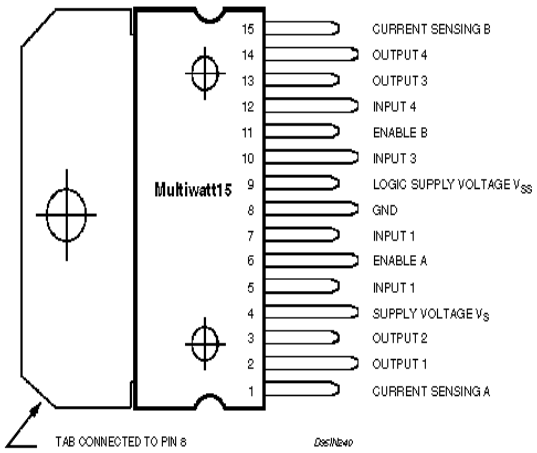

Figure 7. L298N

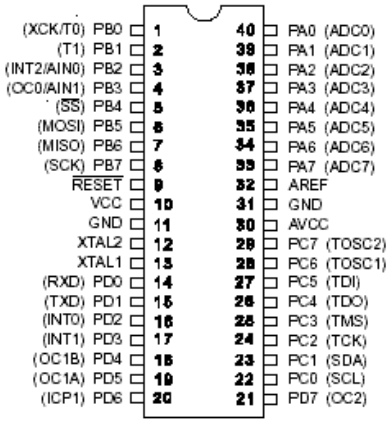

Figure 8. The pin mapping for the Atmega16

5. AUTOMATION OF THE MODEL

The automation which is the most complicated part. For making the system automated AVR programming has been done in C interface. AVR timer programming and AVR interrupt both are performed for avoiding time delay and controlling four different motor by one microcontroller. Program has been made optimized to get better response and better performance.

5.1. CODE

C code for AVR programming is following

```
#include<avr/io.h>
#include<util/delay.h>

void main()
{
        DDRA=0xFF;     //initialization
        DDRB=0xFF;
        PORTB=0b00000010;  //adv     01
                _delay_ms(2500);
        PORTB=0;
                _delay_ms(2000);
        PORTA=0b00000010;      //catch
                _delay_ms(2500);
        PORTA=0;
                _delay_ms(2000);
        PORTA=0b00001000;      //pull
                _delay_ms(11000);
        PORTA=0;
                _delay_ms(2000);
        PORTB=0b00001000;      //right
                _delay_ms(21400);
        PORTB=0;
                _delay_ms(2000);
        PORTA=0b00000100;      //down
                _delay_ms(11000);
        PORTA=0;
                _delay_ms(2000);
        PORTA=0b00000001;      //release  //01//02
                _delay_ms(2500);
        PORTA=0;
                _delay_ms(2000);
        PORTA=0b00001000;      //up
                _delay_ms(11000);
        PORTA=0;
                _delay_ms(2000);
        PORTB=0b00000100;      //left
                _delay_ms(21400);
        PORTB=0;
                _delay_ms(2000);
        PORTA=0b00000100;      //down
                _delay_ms(11000);
        PORTA=0;
                _delay_ms(2000);
        PORTA=0b00000010;      //hold
                _delay_ms(2500);
        PORTA=0;
                _delay_ms(2000);
        PORTA=0b00001000;      //up
                _delay_ms(11000);
        PORTA=0;
                _delay_ms(2000);
```

```
PORTB=0b00001000;      //right
        _delay_ms(15000);
PORTB=0;
        _delay_ms(2000);
PORTA=0b00000100;      //down
        _delay_ms(11000);
PORTA=0;
        _delay_ms(2000);
PORTA=0b00000001;      //release //002//03
        _delay_ms(2500);
PORTA=0;
        _delay_ms(2000);
PORTA=0b00001000;      //up
        _delay_ms(11000);
PORTA=0;
        _delay_ms(2000);
PORTB=0b00000100;      //left
        _delay_ms(15000);
PORTB=0;
        _delay_ms(2000);
PORTA=0b00000100;      //down
        _delay_ms(11000);
PORTA=0;
        _delay_ms(2000);
PORTA=0b00000010;      //hold
        _delay_ms(2500);
PORTA=0;
        _delay_ms(2000);
PORTA=0b00001000;      //up
        _delay_ms(11000);
PORTA=0;
        _delay_ms(2000);
PORTB=0b00000001;      //back
        _delay_ms(2500);
PORTB=0;
        _delay_ms(2000);
PORTB=0b00001000;      //right
        _delay_ms(21400);
PORTB=0;
        _delay_ms(2000);
PORTA=0b00000100;      //down
        _delay_ms(11000);
PORTA=0;
        _delay_ms(2000);
PORTA=0b00000001;      //release //0003
        _delay_ms(2500); //
PORTA=0;
        _delay_ms(2000);
PORTA=0b00001000;      //up
        _delay_ms(11000);
PORTA=0;
        _delay_ms(2000);
PORTB=0b00000100;      //left
        _delay_ms(21400);
PORTB=0;
        _delay_ms(2000);
PORTA=0b00000100;      //down
        _delay_ms(11000);
PORTA=0;
```

```
            _delay_ms(2000);
        PORTB=0b00000010;      //adv
            _delay_ms(2500);
        PORTB=0;
            _delay_ms(2000);
        PORTA=0b00000010;      //hold
            _delay_ms(2500);
        PORTA=0;
            _delay_ms(2000);
        PORTA=0b00001000;      //up
            _delay_ms(11000);
        PORTA=0;
            _delay_ms(2000);
        PORTB=0b00000001;      //back
            _delay_ms(2500);
        PORTB=0;
            _delay_ms(2000);
        PORTB=0b00001000;      //right
            _delay_ms(15000);
        PORTB=0;
            _delay_ms(2000);
        PORTA=0b00000100;      //down
            _delay_ms(11000);
        PORTA=0;
            _delay_ms(2000);
        PORTA=0b00000001;      //release
            _delay_ms(2500);
        PORTA=0;
            _delay_ms(2000);
        PORTA=0b00001000;      //up
            _delay_ms(11000);
        PORTA=0;
            _delay_ms(2000);
        PORTB=0b00000100;      //left
            _delay_ms(15000);
        PORTB=0;
            _delay_ms(2000);
        PORTA=0b00000100;      //down
            _delay_ms(11000);
        PORTA=0;
            _delay_ms(2000);

while(1)
        {
        }
}
```

6. ECONOMIC ASPECTS

A simple cost analysis is shown in the Table 2. Which provides an overview of the expense of the model. It shows us, this system is highly economical for small grade industries. Although it's a long journey to find a perfect model for industrial practical application, but this model reveals a way for low cost automatic arranging system.

Table 2. Cost Analysis of the Model

Serial No	Name of the component	Price(Tk)
1	Wooden frame	550
2	Iron shaft	45

3	Nylon bar	80
4	Ball bearing channel	60
5	Gear motor	1600
6	Bread board	300
7	Diode	16
8	IC (L298N)	280
9	Wires	50
10	Adaptor	240
11	Miscellaneous	200
	Total	3421

7. CONCLUTION

Although the system represents a simple way of bottle arranging for small grade industries some salient features may improve the usefulness of the system. More critical application of dynamic balancing and reduction of over friction impact needs more analysis. Using of T-beam at slots can make the movement quicker. Multi stage arranging will be achievable with simple change of coding. Optimization of cost with high quality components can also be applied.

8. REFERENCES

[1] R. C. Dorf and A. Kusiak, Handbook of Automation and Manufacturing. Jhon Wiley & Sons. New York. **(1994)**.
[2] A. G. Ulsoy, Control of Machining Processes," Journal of Dynamic Systems. ASME. **(1993)**, pp. 301-307.
[3] R. C. Dorf, The Encyclopedia of Robotics. Jhon Wiley & Sons. New York. **(1988)**.
[4] N. Kyura and H. Oho, Mechatronics-An Industrial Perspective. IEEE/ASME Transactions on Mechatronics. **(1996)**, Vol. 1, No. 1, pp. 10-15.
[5] C. M. Close and D. K. Frederick, Modeling and Analysis of Dynamic System. 2nd ed. Houghton Miffilin, Boston. **(1995)**.
[6] Richard C. Dorf and Robert H. Bishop, Modern Control System. 11th ed. Pearson Education. **(2008)**.
[7] N. S. Nise, Control Systems Engineering. 4th ed. Jhon Wiley & Sons, New York. **(2003)**.

NONLINEAR BENDING ANALYSIS OF SHEAR DEFORMABLE LAMINATED COMPOSITE FLAT PANEL

T. R. Mahapatra[1], S. K. Panda[2]
[1]School of Mechanical Engineering, KIIT University, Bhubaneswar, 751024, Odisha, India
[2]Department of Mechanical Engineering, National Institute of Technology Rourkela, Rourkela, 769008, Odisha, India

ABSTRACT: In this article, geometrical nonlinear bending behavior of laminated flat panel is investigated under mechanical loading. As a first step, a general nonlinear mathematical model of laminated composite plate has been developed in the framework of higher order shear deformation theory. The nonlinearity in geometry is considered in Green-Lagrange sense and all the nonlinear higher order terms are taken in the mathematical model to achieve a realistic flexural condition of composite. A suitable finite element model is proposed to discretise the domain using a nine noded isoparametric Lagrangian element with nine degrees of freedom per node to obtain the elemental equations. The nonlinear equations are solved using a direct iterative method. The nonlinear bending responses are compared with those available published literature and some new results are plotted to examine the efficacy of the present proposed model.

Keywords Laminated Composites, Green-Lagrange nonlinearity, HSDT, Bending.

1. INTRODUCTION AND PROBLEM DEFINITION

Laminated composites are widely used in many weight sensitive industries as a compromise between stiffness/strength and weight. Today's most of the structural engineering components are firstly replaced by laminated material and are exposed to combined action of loading during their service condition. These structures are comparatively flexible in comparison to their metallic counterpart and bending behavior is one of the important considerations in design engineering. Large deformation results in change in the geometry of the structure and subsequently induces nonlinearity in the geometry. It is also well known that the laminated structures are prone to fail due to shear stress in comparison to the normal stress. This necessitates the development of pragmatic model for the accurate prediction of the structural responses.

Many studies have already been reported in open literature addressing the issue of static and dynamic behaviour of laminated structures in past. In this regard few past investigations are discussed here for sake of continuity and conciseness of the present objective. The linear and geometrically nonlinear bending of isotropic and multilayered composite plates was studied by Argyris and Tenek [1] using the natural mode method. Zhang and Kim [2] developed three noded 18-degrees of freedom (d.o.f.) flat triangular plate element for linear and geometrically nonlinear analysis of thin to moderately thick laminated composite plates. The plate model is developed based on the first order shear deflection theory (FSDT) by taking von-Karman type nonlinear kinematics. Flat quadrilateral plate/shell element of 4-noded, 24 d.o.f to analyze linear and geometrically nonlinear behavior of thin to moderately thick laminated composite plates developed by Zhang and Yang [3]. The model is developed based on the FSDT and von-Karman's large deflection theory. Lee *et. al.* [4] presented a nonlinear finite element model using third-order shear deformation theory for the analysis of laminated composite shell structures with smart material laminae. Singh *et. al.* [5] investigated stochastic nonlinear bending response of a laminated composite plate with uncertain system properties subjected to transverse distributed static load. The nonlinear finite element formulation was based on higher order shear deformation theory (HSDT) in the von Karman sense. Study of the nonlinear static behavior of the composite plates embedded with magnetostrictive materials is carried out by Kishore *et. al.* [6]. Their model is based on the third order shear deformation theory taking into account the geometric nonlinearity in von-Karman sense. Baltacioglu *et. al.* [7] investigated the nonlinear static deflections of rectangular laminated thick plates on elastic foundation using the discrete singular convolution method in the frame work of the FSDT and by using the von Karman equation. Reddy *et. al.* [8] studied the bending analysis of a simply supported composite laminated plate under uniformly distributed load for various aspect ratios, modulus ratios and side-to-thickness ratios using finite element method. Based on the FSDT and using nonlinear von-Karman theory

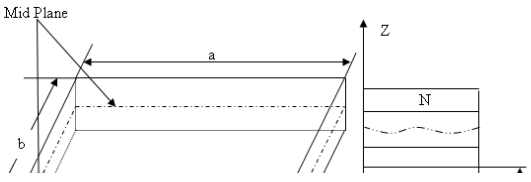

Fig. 1: Laminated Composite flat panel

Golmakani and Alamatian [9 and 10] studied large deflection behavior of the moderately thick RFG solid/annular sector plates with different boundary conditions subjected to uniform and non-uniform transverse loads by taking Winkler or two-parameter Pasternak elastic foundations. Civalek [11] investigated nonlinear dynamic response of rectangular laminated composite plate resting on nonlinear Pasternak type elastic foundations. He used the FSDT and the von Karman nonlinear equation for plate formulation.

Though numerous theoretical development, analytical/numerical solutions are been proposed for the nonlinear bending analysis of laminated structures but, nonlinear mathematical modeling considering the nonlinearity in Green-Lagrange sense in the framework of the HSDT are very limited. Hence, to evaluate the bending behavior of laminated structures, a general nonlinear mathematical model is developed based on the HSDT to evaluate the in-plane and out of plane stress and strains correctly. A suitable finite element is proposed to discretise the domain by using a nine noded isoparametric Lagrangian element. The nonlinear governing equations are solved using direct iterative method.

2. THEORETICAL FORMULATION

A laminated composite plate with *N* number of anisotropic layers of uniform thickness having *a*, *b*, and *h* as length width and thickness respectively is considered (Figure 1). Z_k and Z_{k-1} be the top and bottom *Z*-coordinates of the k^{th} lamina.

The displacement field for the laminated flat plate considered to derive the mathematical model is based on the HSDT [12].

$$\begin{aligned}
\bar{u}(x,y,z,t) &= u(x,y,t) + z\phi_1(x,y,t) + z^2\psi_1(x,y,t) + z^3\theta_1(x,y,t) \\
\bar{v}(x,y,z,t) &= v(x,y,t) + z\phi_2(x,y,t) + z^2\psi_2(x,y,t) + z^3\theta_2(x,y,t) \\
\bar{w}(x,y,z,t) &= w(x,y,z)
\end{aligned} \tag{1}$$

This displacement field represents the transverse shear strains as quadratic function of thickness coordinate and requires zero transverse normal strain. Here, $(\bar{u}, \bar{v}, \bar{w})$ represents the displacements at any point of the plate along the (X, Y, Z) coordinates, (*u*, *v*, *w*) are the corresponding displacements of the points on the mid-plane, rotations at normal to the mid-plane with respect to the y and x-axes are represented by $\phi_1$and ϕ_2 respectively and Ψ_1, Ψ_2, θ_1, θ_2 are higher order terms of Taylor series expansion defined at the mid-plane.
The strain–displacement relations of the laminated plate incorporating Green-Lagrange type geometric nonlinearity can be expressed as follows:

$$\varepsilon_{xx} = \left(\frac{\partial \bar{u}}{\partial x}\right) + \frac{1}{2}\left\{\left(\frac{\partial \bar{u}}{\partial x}\right)^2 + \left(\frac{\partial \bar{v}}{\partial x}\right)^2 + \left(\frac{\partial \bar{w}}{\partial x}\right)^2\right\}$$

$$\varepsilon_{yy} = \left(\frac{\partial \bar{v}}{\partial y}\right) + \frac{1}{2}\left\{\left(\frac{\partial \bar{u}}{\partial y}\right)^2 + \left(\frac{\partial \bar{v}}{\partial y}\right)^2 + \left(\frac{\partial \bar{w}}{\partial y}\right)^2\right\}$$

$$\gamma_{xy} = \left(\frac{\partial \bar{u}}{\partial y} + \frac{\partial \bar{v}}{\partial x}\right) + \left[\left(\frac{\partial \bar{u}}{\partial x}\right)\left(\frac{\partial \bar{u}}{\partial y}\right) + \left(\frac{\partial \bar{v}}{\partial x}\right)\left(\frac{\partial \bar{v}}{\partial y}\right) + \left(\frac{\partial \bar{w}}{\partial x}\right)\left(\frac{\partial \bar{w}}{\partial y}\right)\right]$$

(2)

This can further be re arranged as

$$\{\varepsilon\} = \{\bar{\varepsilon}_L\} + \{\bar{\varepsilon}_{NL}\} \tag{3}$$

Using equation (1) in (2), the total strain can be expressed as

$$\{\varepsilon\} = [\mathrm{H}]_L \{\bar{\varepsilon}_L\} + \frac{1}{2}[\mathrm{H}]_{NL} \{\bar{\varepsilon}_{NL}\} \tag{4}$$

where,

$$\{\bar{\varepsilon}_L\} = \begin{Bmatrix} \varepsilon_1^0 & \varepsilon_2^0 & \varepsilon_6^0 & \varepsilon_5^0 & \varepsilon_4^0 & k_1^1 & k_2^1 & k_6^1 & k_5^1 & k_4^1 \\ k_1^2 & k_2^2 & k_6^2 & k_5^2 & k_4^2 & k_1^3 & k_2^3 & k_6^3 & k_5^3 & k_4^3 \end{Bmatrix}^T$$

is the mid plane linear strain and

$$\{\bar{\varepsilon}_{NL}\} = \frac{1}{2}\begin{Bmatrix} \varepsilon_1^4 & \varepsilon_2^4 & \varepsilon_6^4 & \varepsilon_5^4 & \varepsilon_4^4 & k_1^5 & k_2^5 & k_6^5 & k_5^5 & k_4^5 & k_1^6 & k_2^6 & k_6^6 & k_5^6 & k_4^6 & k_1^7 & k_2^7 \\ k_6^7 & k_5^7 & k_4^7 & k_1^8 & k_2^8 & k_6^8 & k_5^8 & k_4^8 & k_1^9 & k_2^9 & k_6^9 & k_5^9 & k_4^9 & k_1^{10} & k_2^{10} & k_6^{10} & \end{Bmatrix}^T$$

is the mid plane nonlinear strain. The superscripts 0-3 and 4-10 accounts for the bending, curvature and higher order strain terms in linear and nonlinear strain vectors respectively. The stress-strain relation for a general k^{th} lamina of the laminated composite plate for any arbitrary fiber orientation angle is given by

$$\{\sigma\}^k = \left[\bar{Q}\right]^k \{\varepsilon\}^k \tag{5}$$

where, $\{\sigma\}^k = \{\sigma_1 \quad \sigma_2 \quad \sigma_6 \quad \sigma_5 \quad \sigma_4\}^T$ is the total stress vector measured at the stress free state, $\{\varepsilon\}^k = \{\varepsilon_1 \quad \varepsilon_2 \quad \varepsilon_6 \quad \varepsilon_5 \quad \varepsilon_4\}^T$ is the strain vector, and $\left[\bar{Q}\right]^k$ is the transferred reduced stiffness matrix.

2.1 STRAIN ENERGY EXPRESSION

The total strain energy of the laminated plate is given by

$$U = \frac{1}{2}\int_V \{\varepsilon\}_i^{\mathrm{T}} \{\sigma\}_i dV \tag{6}$$

Using the expressions for stress and total strain this can be modified as

$$U = \frac{1}{2}\iiint \{\varepsilon\}^T [D]\{\varepsilon\}\, dx\, dy\, dz \tag{7}$$

where, $[\mathrm{D}] = \sum_{k=1}^{NL} \int_{z_{k-1}}^{z_k} [\mathrm{H}]\left[\bar{Q}\right]^k [\mathrm{H}] dz$ and '*NL*' is number of layer.

2.2 WORK DONE EXPRESSION

The work done (*W*) in Green-Lagrange sense for the laminated plate can be obtained as

$$W = \int_A \{\delta\}^T q dA \tag{8}$$

3. FINITE ELEMENT SOLUTION SCHEME

A nine noded quadrilateral Lagrangian isoparametric element is employed for finite element modeling. In the finite element method, the domain is discretized into a set of finite elements. For NN number of nodes per element, the displacement vector $\{\delta^*\}$ is represented as

$$\{\delta^*\} = \sum_{i=1}^{NN} [N_i]\{\delta_i\} \tag{9}$$

where, $[N_i] and \{\delta_i\}$ are the interpolation (shape function) function and displacement vector for the i^{th} node respectively. The governing equation for the nonlinear bending analysis of laminated composite flat panel is obtained by using Hamilton's principle.

This result in $\delta\Pi = 0$ (10)

where, $\Pi = (U\text{-}W)$

Using Eqs. (6)- (9), Eq. (10) can be expressed following $[K_L + K_{NL}]\{\delta\} = \{F\}$ (11)

Where, [M] is the global mass matrix, $[K_L]$ and $[K_{NL}]$ are the global linear and nonlinear stiffness matrices, which depend on the displacement vector linearly and quadratically respectively. The above equation is solved by using a direct iterative method.

4. RESULT AND DISCUSSION

A general nonlinear mathematical model of laminated panel is developed and discretised using suitable finite element model. A computer code has been developed in MATLAB 7.10.0 environment based on the developed nonlinear model. The nonlinear responses are obtained using direct iterative method and compared with available published literature. For all the analysis each layer of the laminated plate are considered to be of equal thickness.

4.1 CONVERGENCE AND VALIDATION

A $[0^0/90^0]_S$ cross ply square plate, subjected to uniformly distributed load (UDL), with material properties and boundary conditions identical with [2]. The convergence study for six different load values (Q = 0.4, 0.6, 0.8, 1.2, 1.6, 2.0) and the results for different mesh sizes are presented in Fig. 2. Based on the convergence study it can be concluded that a (6×6) mesh is adequate to predict the bending behavior of the flat panel. In order to validate the proposed model, results are also obtained and compared with those available in reference [1] and [2] and presented in Fig. 3. The present results are showing higher values of linear and nonlinear bending responses in comparison to both the references. This is due to the fact that, all the higher order nonlinear terms are included in the present formulation which makes the model more flexible or realistic. This demonstrates a need of an improved mathematical model in terms of mid-plane kinematics and geometric nonlinearity in Green-Lagrange sense.

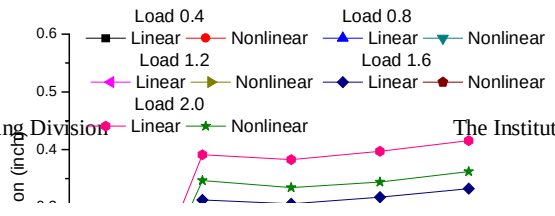

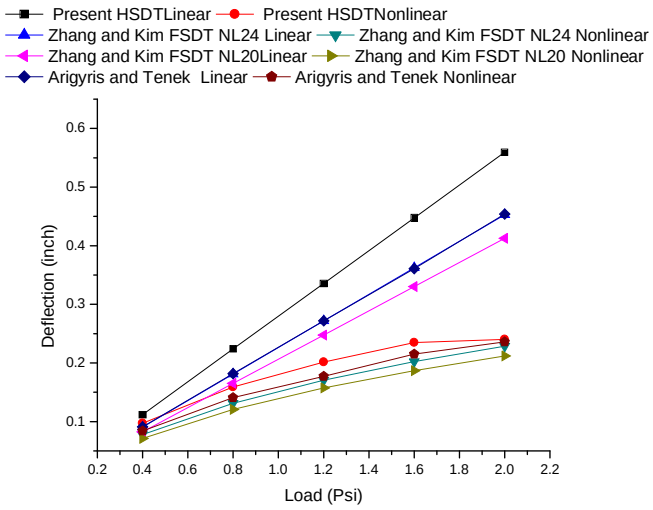

Fig.3: Comparison study of linear and nonlinear bending of laminated composite flat panel

4.2 NUMERICAL ILLUSTRATIONS

Some numerical examples are presented in this section in order to reveal absolute understanding of the nonlinear bending analysis of symmetric and un-symmetric cross/angle-ply laminated plates. The material properties and boundary conditions used for the analysis are as follows.

Material: $E_1/E_2 = 25$, $G_{12}/E_2 = 0.5$, $G_{23}/E_2 = 0.2$, $\nu_{12} = 0.3$, $G_{13} = G_{12}$.

Support conditions:
(a) Simply support (SSSS):
$v = w = \Phi_2 = \Psi_2 = \theta_2 = 0$ at X = 0, a and
$u = w = \Phi_1 = \Psi_1 = \theta_1 = 0$ at Y = 0, b and
(b) Clamped condition (CCCC):
$u = v = w = \Phi_1 = \Phi_2 = \Psi_1 = \Psi_2 = \theta_1 = \theta_2 = 0$ for both X = 0, a and Y = 0, b.

4.2.1 ILLUSTRATION 1:

Simply supported, moderately thick (a/h = 10), symmetric/un-symmetric, cross-ply $(0^0/90^0)_s$ and angle-ply laminated plates with material properties as stated above are analyzed to observe the influence of aspect ratio (a/b) on the center deflection and results are plotted in Fig. 4. It is noted that, both the nondimensional linear and nonlinear deflections decrease with increase in aspect ratio. Higher center deflections are observed in the case of the symmetric angle-ply laminates, as compared to cross-ply laminates under a given value of load and aspect ratio. The differences between linear and nonlinear values decrease with increase in aspect ratio for the same value of load; but become equal for both for cross ply and angle ply laminates at higher values of aspect ratio.

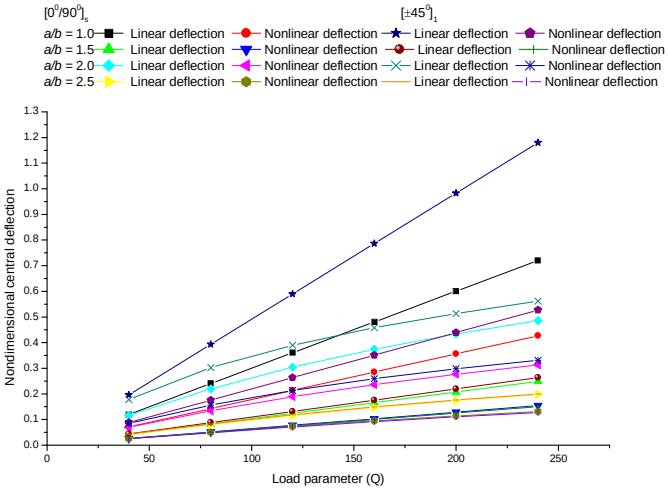

Fig.4. Effect of aspect ratio (a/b) on linear and nonlinear deflection of laminated composite flat panel bending of laminated composite panel

4.2.2 ILLUSTRATION 2:

Square, anti-symmetric, cross-ply $(0^0/90^0)_2$ and angle-ply [0/30 /-30 /90] laminated plates with all sides clamped support condition and having above declared material properties are analyzed to examine the influence of thickness of the laminated plate on the center deflection. The results plotted in Fig.5 shows that both the non dimensional linear and nonlinear deflections decrease with increase in thickness ratio. Lower values of center deflections are observed in case of cross ply laminates as compared to angle ply laminates. The differences between linear and nonlinear values for thinner plates are smaller than that for thicker plates.

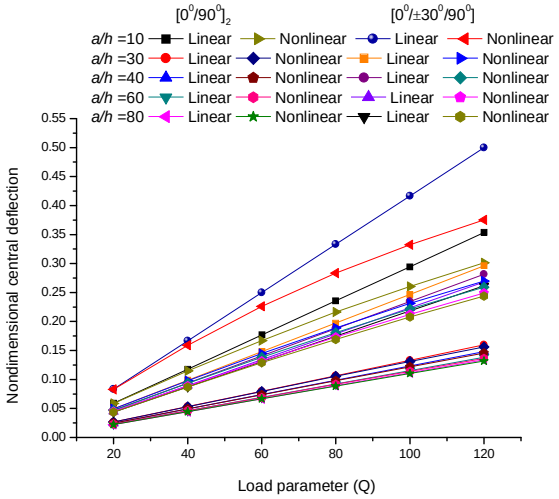

Fig.5. Effect of thickness ratio (a/h) on linear and nonlinear deflection of laminated composite flat panel

5. CONCLUSION

The nonlinear bending analysis of shear deformable laminated composite flat plates has been studied by taking the geometrical nonlinearity in Green-Lagrange sense in the framework of the HSDT. All the nonlinear higher order terms are considered in the mathematical model to attain a more realistic case. The sets of governing equations are obtained using Hamilton's principle and discretised using a nonlinear finite element approach. The validation study shows the necessity of present nonlinear model for the more accurate analysis of nonlinear bending in shear deformable laminated plates. In order to judge the effectiveness of the present model, some new results are also obtained for different parameters. Both the linear and nonlinear non-dimensional central deflections for laminated flat panel decrease with increase in aspect ratio and thickness ratio. Higher center deflections are observed in the case of the asymmetric angle-ply laminates and the differences between non-dimensional linear and nonlinear values for thinner plates are smaller than that for thicker plates.

6. REFERENCES

[1] J. Argyris and L. Tenek, Linear and geometrically nonlinear bending of isotropic and multilayered composite plates by the natural mode method. Computer Methods Applied Mechanics and Engineering. **(1994)**, Vol. 113, pp. 207–51.
[2] Y. X. Zhang and K. S. Kim, A simple displacement-based 3-node triangular element for linear and geometrically nonlinear analysis of laminated composite plates. Computer Methods Applied Mechanics and Engineering. **(2005)**, Vol. 194, pp. 4607–4632.
[3] Y. X. Zhang and C. H. Yang, A family of simple and robust finite elements for linear and geometrically nonlinear analysis of laminated composite plates. Composite Structures. **(2006)**, Vol. 75, pp. 545–552.
[4] S. J. Lee, J. N. Reddy and F. R. Abadi, Nonlinear finite element analysis of laminated composite shells with actuating layers. Finite Elements in Analysis and Design. **(2006)**, Vol. 43, pp. 1 – 21.
[5] B. N. Singh, A. Lal and R. Kumar, Nonlinear bending response of laminated composite plates on nonlinear elastic foundation with uncertain system properties. Engineering Structures. **(2008)**, Vol. 30, pp. 1101–1112.
[6] M. D. V. Hari Kishore, B. N. Singh and M. K. Pandit, Nonlinear static analysis of smart laminated composite plate. Aerospace Science and Technology. **(2011)**, Vol. 15, pp. 224–235.
[7] A. K. Baltacioglu, O. Civalek, B. Akgoz and F. Demir, Large deflection analysis of laminated composite plates resting on nonlinear elastic foundations by the method of discrete singular convolution. International Journal of Pressure Vessels and Piping. **(2011)**, Vol. 88, pp. 290-300.
[8] B. S. Reddy, A. R. Reddy, J. S. Kumar and K. V. K. Reddy, Bending analysis of laminated composite plates using finite element method. International Journal of Engineering. Science and Technology. **(2012)**, Vol. 4, No. 2, pp. 177-190.
[9] J. Alamatian and M. E. Golmakani, Large deflection analysis of the moderately thick general theta ply laminated plates on nonlinear elastic foundation with various boundary conditions. Mechanics Research Communications. **(2013)**, Vol. 51, pp. 78– 85.
[10] M. E. Golmakani and J. Alamatian, Large deflection analysis of shear de formable radially functionally graded sector plates on two-parameter elastic foundations. European Journal of Mechanics A/Solids. **(2013)**, Vol. 42, pp. 251 – 265.
[11] O. Civalek, Nonlinear dynamic response of laminated plates resting on nonlinear elastic foundations by the discrete singular convolution-differential quadrature coupled approaches. Composites: Part B. **(2013)**, Vol. 50, pp. 171–179.
[12] J. N. Reddy, Mechanics of laminated Composite Plates and Shells. Second Edition CRC Press. **(2004)**.
[13] R. D. Cook, D. S. Malkus and M. E. Plesha, Concepts and applications of finite element analysis. John Willy and Sons Pte. Ltd. Singapore. **(2000)**.

THE EFFECT OF ATTACK ANGLE OF BOREHOLE FAILURE RELATED TO BEDDING PLANE

Md. Shmasuzzoha
Titas gas transmission and distribution co. ltd., Dhaka, Bangladesh, SPE-3462274, MIEB-22270, ME
(zoha.shamsu@gmail.com).

ABSTRACT: Attack angle (a_{at}) is the angle between the wellbore and the bedding plane, it's normally taken as acute angle. The array of bedding plane, borehole position and the dip/strike angle of formation are important parameters if anyone want to apply the in-situ stresses equations for determining failure criterion, rock strength and want to develop models of wellbore failure. Azimuth, position of wellbore, fracture angle, failure Plane and attack angle are considered confusing to determine at a time. The assessment of in-situ stress and analysis of borehole failure due to instability and the relation of attack angle with inclination borehole represent one of the most critical factors when evaluating borehole stability that causes borehole failure. A lot of scientists and engineers specially Aadnoy and Chenevert [2,3] showed that at a certain angle rock failed at very low load condition. This paper focused, analyzed and used the data from the Aadnoy et.al [3] models to address the existing problem on this matter.

According to this research, attack angle had been changed with different azimuth although inclination was same. So it's important for testing the bedding exposed with different azimuth with constant inclination. It found that attack angle was the lowest value on the down dip position and the highest value on the up dip Position. Aadnoy et.al. [3] paper did not address about the effect of attack angle and azimuth. This Paper and my research confirmed that attack angle is affected the azimuth angle definitely which ultimately will affect the result of bedding exposed position. Attack angle depends on the relative position of bedding plane and a plane that contain horizontal stress. So it has to be confirmed what are the dip angle and azimuth before taking the drilling action in to a formation. This paper analyzed the 3D effect of attack angle with changing azimuth for a constant inclination on bedding plane. Interestingly paper got that bedding exposed is not only depends on inclination but also depends on dip of the formation, attack angle and azimuth [1].

Keywords: Drilling, Borehole Stability, In-Situ Stress, Attack angle, Bedding Plane

1. INTRODUCTION

The increasing demand for well bore stability analysis during the planning stage of a field arises from economic considerations and the escalating use of deviated, extended reach and horizontal wells. The purpose of wellbore stability modeling is to create a safe operating window of annular pressures (mud pressures and mud weight) such that the designed fluid is high enough to ensure wellbore stability and low enough to ensure no loss of fluid. Problems generally build up in time, starting with the fragmentation of the borehole wall, followed by transfer of the fragments to the annulus and finally-if hole cleaning is insufficient-culminating in such difficulties as a tight hole, packing off, filling of the hole, stuck pipe, etc. To develop a model of well bore collapse/fracture; in-situ stress, pore pressure, in-situ stress orientation, wellbore trajectory, attack angle and relevant rock strength data are the important factors. Rock strength is high when force vectors are applied at a high angle to bedding. At lower angles, on the order of 15° and 30°, stratal compressive strength is low. For this case, rock failure will occur along bedding planes. This type of rock behavior is often termed "plane of weakness" [1-3].

Sedimentary rocks have a laminated structure, with directional elastic properties as well as directional shear and tensile strengths. Anderson 1951, Jaeger 1960, Aadnoy 1987 [1, 3, 10] gave a thorough analysis of the various loading scenario that explain bedding failure. A common way to model shear failure using Jaeger's approach is to use the Mohr Coulomb failure model, but vary the cohesive strength and the angle of internal friction, depending on the loading relative to bedding plane inclination and attack angle. On the basis of Jaeger, the plane of weakness was introduced in the oil industry by Aadnoy [2]. The modeling of highly inclined boreholes, he investigated the effects of wellbore inclination, anisotropic elastic rock properties, anisotropic stresses, and anisotropic rock strength. Before doing to the massive drilling the estimation of in-situ stress is needed by applying pilot drilling can be made borehole orientation, attack angle and azimuth. The In-situ stresses can be

resolved into a vertical (overburden, σ_v) and two horizontal stresses such as maximum stress (σ_H) and minimum stress (σ_h) which are generally unequal.

Layered rocks such as shale often exhibit different properties along or across bedding planes. According to Aadnoy et.al. [2], rock strength is high when force vectors are applied at a high angle to bedding. This works assumed for developing model that linear-isotropic plane strain conditions, all in-situ stresses are principal and directed horizontally and vertically. The key in this analysis is that when a well is drilled, the rock surrounding the hole must take the load that was previously taken by the removed rock. As a result increases stress concentration around the wall. If the rock is not strong enough, the borehole will fail. In that case, the attack angle is related to the bedding plane, well direction, dip, strike angle and azimuth. Attack angle 0^0 means wellbore is parallel to bedding plane and 90^0 means the wellbore is vertical to the bedding plane. Attack angle is the most important plane because, if favorable conditions exist (10^0 < Attack < 30^0) plane of weakness may occur at very low load condition [1, 2, 9].

1.1 failure plane and bedding plane

Failure plane means in what plane the wellbore/specimen will fail. One can analyze failure plane by Mohr-coulomb and tri-axial test (under different load condition) and can be determined angle of fracture (α) from a specimen shown in figure1. This may be considered a complex matter when one think on underground condition, because of complex in-situ stresses and pore pressure are acting and changing that matter due to depletion of the reservoir. Here, α is the angle between applied force and failure plane during tri-axial core-testing and β is the angle between applied force and bedding plane during tri-axial core testing. One thing for reader don't confused about γ and β, γ is related for wellbore inclination from vertical, on the other hand β is related to Core-plug. If you want to compare attack angle and β, they are equivalent, but they are considered in different positions. Where, ϕ is friction angle and a_f is angle between failure and bedding plane. So the array of bedding plane, borehole position and the dip/strike angle of formation are important parameters if anyone want to apply the in-situ stresses equations for determining failure criterion, rock strength and want to develop models of wellbore failure [1,2,9].

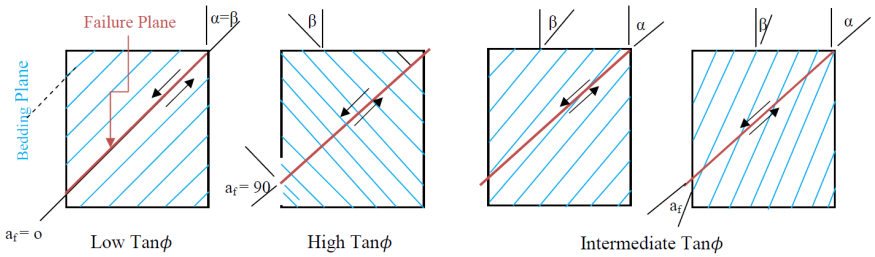

Fig.1: Failure plane Vs Bedding plane with variation of angle [1, 2, 9]

2. EFFECT OF BEDDING PLANE WITH DIFFERENT ATTACK ANGLE AND LAMINATION

Two conditions determine whether the rock fails along a weakness plane or not; the relative magnitude of the two normal stresses and the angle between the borehole and the bedding plane (attack angle). During modeling of highly inclined boreholes, researchers [1-10] investigated the effects of wellbore inclination, anisotropic elastic rock properties, anisotropic stresses and anisotropic rock strength. It was shown that under certain conditions, the rock would fail along planes of weakness. Because of the geo-mechanical properties of shale (high Pp alignment of phyllosilicates due to overburden digenesis), slip surfaces may exhibit significantly higher potential to fails as compared to stronger rock units, such as limestone and sandstone[1-2]. Vertical wellbores drilled at 45^0 to the weak bedding plane in artificial shale. As per shear stress thumbs rule, the maximum shear stress direction will follow the bedding plane and the material is so weak in this direction that the evolved shear stress would be a potential challenge for material failure, figure-2(a). Fig. 2(b) shows physical model of deviated wellbores drilled parallel to the bedding plane. The

maximum shear stress direction will be 45^0 to the weak plane and the material is relatively competent in this direction. Therefore, evolved shear stress would not be a challenge for the material. However, material failure may happen through induced cracking along the weak bedding plane. Drilling a well along the bedding plane is also considered to pose a high risk of mechanical borehole stability. The remaining models shown in Fig. 2c deviated well at an angle $\geq 70^0$ to the bedding plane and figure 2d horizontal well are relatively less challenging with respect to material failure.

Moreover, induced crack and shear stress direction are indicated in the model. Hypothetically, induced crack effects in this model will not be as critical as compared to previous 2(a, b) model. Fig. 2 (d, e) presents two different sets of physical models, consisting of vertical (Fig. 2d) & horizontally (Fig. 2e) oriented bedding plane with different attacking angles. Vertical well with 0^0 attacking angle (Fig. 2d) and vertical weak bedding plane, maximum shear stress acting at 45^0 to the borehole, induced cracking is the highest concern for instability. Fig. 2e deviated well drilled at 45^0 to the horizontally oriented weak bedding plane. We have seen that in deviated trajectories the maximum shear stress is acting along the bedding plane. Shear failure is the highest concern in such conditions. But the material failure risk analysis will be the same as discussed in the aforesaid models. The most important features will be the attacking angle between the borehole and the weak bedding plane. In general, for any combination of weak bedding plane & attacking angle orientation, the evolved shear stress direction along the weak bedding plane pose a risk for initiating material failure [1, 9].

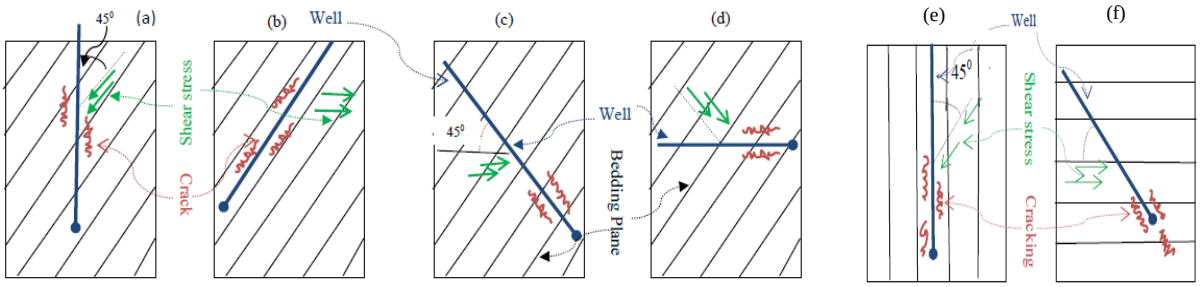

Fig.2: Wells drilled in different angles to the bedding plane [1,9]

3 MODEL REVIEW

Elastic properties like bulk modulus, Young's modulus and poison's ratio, show directional properties [2-5]. Rock strength is high when force vectors are applied at a high angle to bedding. At lower angles, on the order of 15^0 and 30^0, strata compressive strength is low, then, rock failure will occur along bedding planes. This type of rock behavior is often termed 'Planes of weaknesses'. Bedding planes of shale mainly affect high angle and horizontal wells drill close to the minimum horizontal stress direction [2].

Four failure criterions are reviewed to access borehole stability and failure related to bedding plane, namely Mohr-coulomb, Drucker-Prager, Mogi-Coulomb and modified Lade criteria [1]. These failure criteria are combined with linear and Isotropic rock mechanics behavior. Results indicate that the modified Lade, Mogi-Coulomb criteria tend to be more realistic than the Mohr-coulomb and druck-Prager criteria for these evaluations. This paper will consider only mechanical failure instead of chemical failure. Mechanical wellbore instability is caused by applying mud of insufficient weight, which will create greater hoop stresses around the borehole wall and excessive hoop stresses cause in rock failure. Critical parameters are plane of weakness in the rock strength, the relative normal stress values on the borehole, and the relative angle between the borehole and bedding Plane [2-9]. Haimson, Herrik and Aadnoy [1] are all conclude that collapse occurs at the position of the borehole that corresponds to the direction of the least in-situ stress, normal to the axis of the hole. He also concluded that if the least in-situ stress is normal to the plane of the borehole axis and the axis is normal to the bedding plane is different, The directional shear strength come into play and potential collapse will occur $15^0<\beta<35^0$ [2].

4. DEVIATED BOREHOLE IN BEDDED ROCK

Fig.3 shows a deviated borehole in bedded rock [2]. Two infinitesimally small pieces of rocks are shown on the borehole wall. The borehole typically fail at $\theta=0^0$ (Case A) or 90^0 (Case B). If the applied stress in the x direction is the smallest, the borehole will fail as in case A and the y direction is the smallest direction the borehole will fail in Case B. For a typical collapse, the radial stress is the smallest, according to Mohr-coulomb criterion; we can avoid axial stress of laboratory data (as an intermediate pressure). The radial stress is the minor principal stress and the tangential stress (hoop stress) is the major principal stress. The redial stress is always in a principal stress direction, tangential stress is not exactly in principal stress direction because some shear stress components change the direction slightly. The equivalent (as well) core plug shown in Fig**.** 3a, for case A the tangential stress acts parallel to the bedding plane, Therefore $\beta=0^0$, for this case regardless of inclination between borehole and bedding plane, one shear data set are applied for all borehole angles. In case B, tangential stress is applies at an angle with respect to the bedding plane and values now $\beta=\gamma$, But directional shear stress come into account with respect to bedding plane.

The layered rock at the borehole wall is shown as a core plug. For case A, the weakness plane is not exposed and a stable borehole exists. For case B, the plane of weakness is exposed for certain wellbore/bedding plane inclinations, leading to an unstable borehole [1,2]. Note in Fig.3 that the bedding inclination of the core plug (β) is equivalent to the borehole versus bedding inclination for the actual well (a_{at}). If the in-situ stress tensor is aligned with the bedding plane, the inclination γ also applies to the bedding plane. For a dipping bedding plane, the relative orientation between borehole and bedding plane is: $\gamma-k_{dip}$, where k_{dip} is the formation dip. If there is a small stress contrast between σ_x and σ_y, within the sensitive borehole/bedding orientation, other failures such as bedding weakness may occur. It depends on the degree of planes weakness. This paper took stress of states and field data from Aadnoy [2] paper. Limitation of my model assumed linear elastic rock, integer of inclination angle and 0.5* integer of azimuth. This model can run even minimum value of that if the computer has capacity to run , otherwise you can have to take time to obtain result.

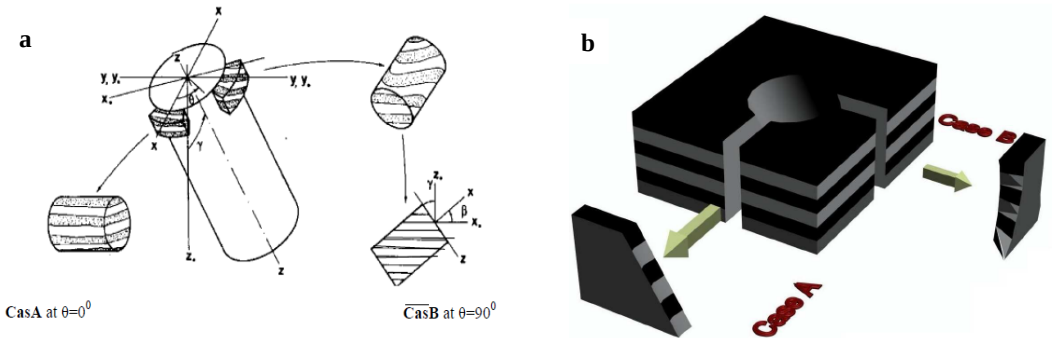

Fig.3: (a) test plug bedding plane at related to well bore position [2] (b) Test plug bedding plane 3D view [1]

5 FIELD CASE DATA AND OUR MODEL DEVELOPMENT

This paper reproduced the following spread sheet Fig 4b and introduced new matter which was optimum well path [7]. This research got same result of paper [2] and ran our model with formation dip angle, result shown that formation dip affected bedding exposed areas. This work obtained the angle of optimum well path was about 48.20 degree from maximum principal stress (σ_H) by applying Alajmi, Islam [7,9] equations. This result was close to the Aadnoy et.al. [2] paper result, that was 45^0 from the maximum horizontal stress. We got attack angle 67^0 (shown in 3D Fig. 4a that was definitely differed from Aadnoy et.al.[2] result. Their well direction data were azimuth $N60^0E$, well inclination 30^0, strike $S50^0E$ and dip 53^0SW. So it has be needed further research about the conflict of Aadnoy [2] and our findings. Our model view and result has been shown in the Fig. 6. Any user can introduce field data to obtain their different values such as type of fault, bedding exposed and safe positions, optimum well path, no of well data by applying our enhanced model.

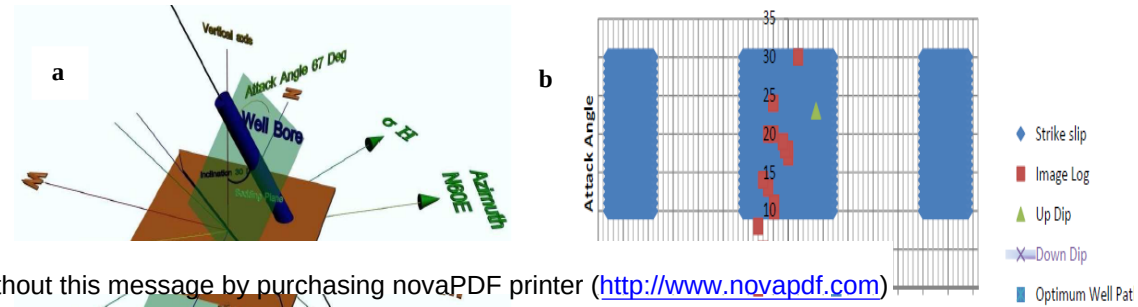

6. ATTACK ANGLE (3D EFFECT) AND DIFFERENT AZIMUTH WITH CONSTANT INCLINATION

Azimuth is the angle of well direction from True North (or Sometimes taken from σ_H) and taken positive Clockwise from north normally. The following figures (Fig. 6 and Fig.4a) showed the effect of attack angle with changing the azimuth. We certainly found that although inclination does not change, attack angle changes with the azimuth. So it is important for testing the bedding exposed with different azimuth with constant inclination. This research also found that attack angle is the lowest value on the down dip position and the highest value on the up dip Position. From the picture (Fig -5,7) dip is a formation properties with related to strike direction, so attack angle is a function of dip and strike also, although both of them are geological properties. Dip and strike give true picture of the underground with 3D view of a well.

7 RESULTS AND DISCUSSION

According to this study, if the angle between borehole and bedding is zero or 90 degrees, the wells would be more stable. The study provided invaluable pre-drill wellbore stability analysis of a complex geological structure. This study shows that planes of weakness in bedded rocks may lead to severe borehole collapse problems. However, in the three dimensional space there are combinations of wellbore inclinations, attack angle and azimuth where the weak planes are not exposed to failure.

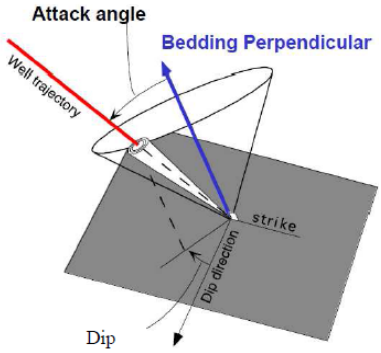

Fig.5: Measuring attack angle and Dip [1]

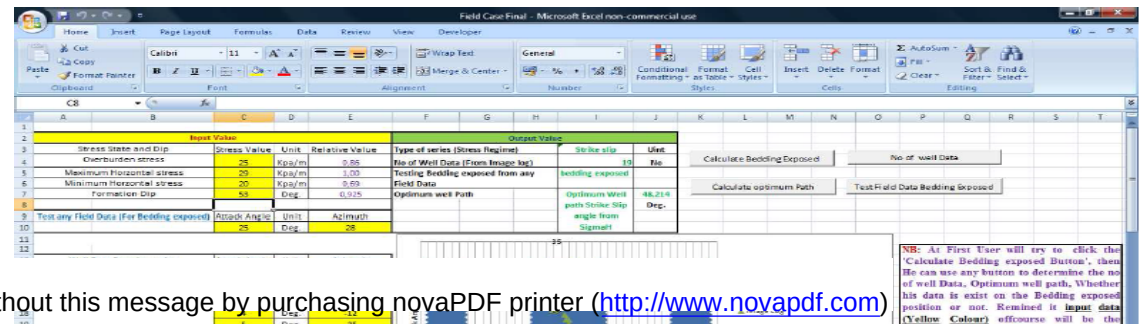

High tectonic in-situ stress in one direction, the borehole may be made very stable toward collapse by inclining it in the direction of the least in-situ stress [2, 3, 4], hence plane of weakness does not come into play at all. On the other hand inclining the borehole in the direction of maximum horizontal in-situ stress gives the conditions for the weakness plane to apply, with resultant collapse problems between 10 and 40^0 inclination. Generally deeper the well, the more likely the borehole is to become sensitive towards collapse. According to M-C shear failure theory and Jaeger's 1960 weakness- plane theory found that more inclination is sensitive for collapse. For laminated rocks the weakness plane makes the rock strongly sensitive towards collapse in the range of 10 and 40^0 inclinations for relax depositional basin. In general the fracturing gradient decreased with increased borehole inclination [3,4].

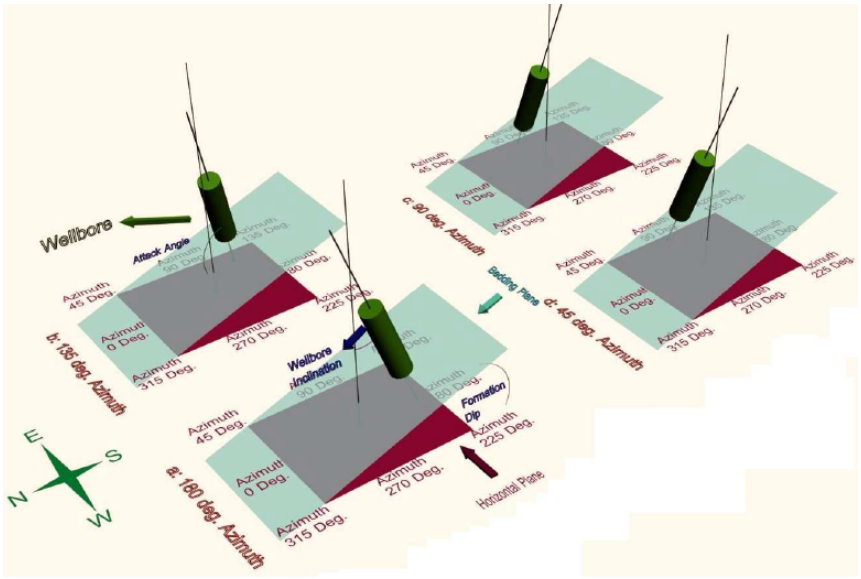

Figure 7: Attack angle Vs azimuth with constant inclination on a bedding plane, 3D effect [1]

Azimuth is the angle of well direction from true north (or sometimes taken from σ_H) and taken positive with clockwise from north normally. The figure 7 showed the effect of attack angle with changing the azimuth. We certainly found that invariable of inclination attack angle changed with the azimuth. So it's mostly important for testing the bedding exposed with different azimuth with constant inclination. This research found that lowest value of attack angle was on the down dip position and the highest value on the up-dip position. Dip is a formation properties with relate to strike direction, so attack angle is a function of dip and strike also, both are geological properties. Aadnoy et.al.[2] paper did not address about the effect of attack angle and azimuth. This paper confirmed that attack angle is affected the azimuth angle definitely which ultimately will affect the result of bedding exposed position. From figure 4a and fig 7 the (3D view) attack angle changed with different azimuth although inclination was same. Attack angle depends on the relative position of

bedding plane and a plane that contain horizontal stress. So it has to be confirmed what are the dip angle and azimuth before taking the drilling action in to a formation. One should take clear idea about the above planes before running our model [1]. After introducing the field data into the model, new thing was that model can be able to determine the optimum well path and know whether the well data is secured or exist on the bedding exposed position [4b]. You can see details works and drew the different azimuth of wellbore position shown in the 3D view of Fig. 6 and paper [1] such as 0^0, 45^0, 90^0, 135^0, 180^0, 225^0, 270^0, and 315^0.

8 CONCLUSION AND RECOMMENDATION

The failure behavior of anisotropic laminated rocks may be described by the Single plane of weakness theory or by variable coefficient approach depending on rock behavior (Cohesive strength and internal friction). In case of relaxed depositional basins, the borehole is sensitive to collapse/fracture for a range of 10 to 35^0 of inclination to bedding. This may be applicable only to laminated rocks and the phenomenon of plane of weakness. The critical parameters are planes of weakness in rock strength, the relative normal stress values on the borehole, and the relative angle between the borehole and bedding plane (attack angle). The wells, which are drilled into 0 or 90 degrees of attack angle, are more stable. It is also found that relative position of wellbore and bedding plane is more important compared to the rock anisotropy. According to the research regarding 3D is that the attack angle changes with changing azimuth having the inclination unchanged. Before conclusion, one should correlate the model (even this model) results with the laboratory results. This research addressed attack angle with borehole inclination and azimuth relation clearly. The difference of this research finding regarding up-dip and down-dip positions from those of Aadnoy et. al. [2] field data can be further analyzed and justified by means of further study.

ACKNOWLEDGEMENTS

I would like to thank Dr. Mahbubur Rahaman, associate Professor, department of PMRE, BUET and Dr. Eirik Karstad, Associate professor, Department of petroleum engineering, University of Stavanger, Norway who have given lot of advice about my M.Sc. thesis, VBA programming and this research paper .I convey plenty of thanks to Manik Chandro Roy, Director, MF-Asia, Bangladesh and Mr. Tarik, CSE final year Student, BUET, Bangladesh. They spent innumerous time helping us to write codes in VBA. Thanks also must be given to Mr. Sobahan, assistant engineer, TGTDCL, Bangladesh and Nasif Md. Tanjim (Sammo), Civil engineering, BUET, Bangladesh. They also spent plenty of time helping us producing 3D effect of attack angle by Studio-3D max.

REFERENCES

[1] Shamsuzzoha, Md., "Analysis of bore hole failure related to bedding plane", Master's thesis, at university of Stavanger, Norway June- 2011.
[2] Aadnoy B.S., Hareland G., Kustamsi A. , Hajes J. 'Borehole failure related to bedding plane', UiS, University of Calgary, AB, Canada and BG Group, Calgary, AB, Canada. ARMA-09-106, July-2009a.
[3] Aadnoy B. S.; Iain Cooper; Stefan Z. Miska; Robert F.Mitchell; and Michael L. Payne. 'Advanced Drilling and well Technology'—SPE, Page 301-440, 2009b.
[4] Aadnoy, B. S., Chenevert, M.E., "Stability of highly inclined boreholes". In Proceedings at the IADC/SPE drilling conference, New Orleans, March 15–18,1987a, SPE 16052.
[5] Aadnoy B.S.,'Stability of highly inclined boreholes' SPE, Rogaland Regional C., , SPE, University of Texas. SPE drilling Engineering, December-1987, SPE-18736.
[6] Aadnoy B.S., Chenevert M.E., 'Modeling of the Stability of highly inclined boreholes in anisotropic rock formations', SPE-19213, Rogaland U., September-1988.
[7] Al-Ajmi, A.M. and Zimmerman, R.W., " A new well path optimization model for increased mechanical borehole stability", Int J Pet Sci Eng 69, 53-62, 2009.
[8] Chenevert M.E., Gatlin C., 'Mechanical Anisotropies of Laminated Sedimentary Rocks' by, Jr. Member AIME, Member AIME., The University of Texas, Austin , Tex. SPE-890, March-1965.
[9] Islam M.A., 'Modeling and Prediction of Borehole Collapse Pressure during Underbalanced Drilling in Shale' , PhD Thesis at NTNU, November-2010.

[10] Zoback, M.D. 'Reservoir Geo-mechanics', Cambridge University press, ISBN 978-0-521-77069-9, 2010.

STUDY OF THE EFFECT OF FINITE ELEMENT MESH QUALITY ON STRESS CONCENTRATION FACTOR OF PLATES WITH HOLES

Sharaban Thohura*[1] & Dr. Md. Shahidul Islam[2]
[1]Department of Mathematics, Jagannath University Dhaka, Bangladesh
[2]Department of Naval Architecture and Marine Engineering, Bangladesh University of Engineering & Technology, Dhaka, Bangladesh
*corresponding email: sthohura@gmail.com,

ABSTRACT: The effect of mesh quality on stress concentration around the circular holes in an infinite plate subjected to uniform tensile force at the edges of the plate has been studied by using Finite element Method. The aim of the authors is to determine how structural discontinuities alter stress distributions and how the mesh quality influences these stresses. Different models have been used in this study with variable number and quality of elements from model to model. Four-node quadrilateral membrane element (2 degrees of freedom per node) has been used in meshing the computational domain. The mesh quality has been defined as a combination of two criteria such as element quality and enough number of elements in the mesh. The quality of the surface mesh should be good to get acceptable finite element results. Element quality is defined by two factors namely: Distortion factor and Aspect ratio. Based on these two factors an object oriented program in C++ has been developed. The results have been shown in tabular form and graphically. The computed results show good agreement with the published theoretical results. The finite element formulation is carried out in the analysis using NASTRAN-PATRAN software. Finally a correct meshing approach is prescribed to model structures with single or multiple holes which is essential for a finite element analyst.

Keywords: Stress Concentration Factor, Mesh quality, mesh seed, Finite element Analysis.

NOMENCLATURE

A	Plate length
d	Hole diameter
E	Modulus of Elasticity
H	Plate width
K_{tg}	Stress concentration factor
t	Thickness of the plates
σ	Stress
$\sigma_{\max}$	Maximum stress
σ_x	Normal stress in x-direction
σ_y	Normal stress in y-direction
σ_z	Normal stress in z-direction
σ_Y	Yield stress of the material
σ_{VM}	Von Mises stress
τ_{xy}	Shear stress along xy direction
τ_{yz}	Shear stress along yz direction
τ_{zx}	Shear stress along zx direction
ε	Normal strain
υ	Poisson's ratio

1. INTRODUCTION

Configuring the structures with discontinuities is one of the most important topics in the construction of ships, aero-planes, cars etc. Whenever the cross–section of a structural member changes suddenly, a structural discontinuity arises. The application of finite element method (FEM) to the analysis of

discontinuous structural systems has received a significant interest in recent years. Examples of problems in which discontinuities play prominent role in the physical behavior of a system are numerous. From mathematical point of view, analytical solutions are possible only for a limited class of such problems. The complexities of the structures, material properties and of boundary conditions, have progressively led to the predominance of numerical models based on finite elements and finite differences. For cases in which discrete representation of discontinuities is required, the finite element approach provides the best modeling to date.

In the past, stress analyses were performed analytically or experimentally, which could be both difficult and time consuming, especially when dealing with discontinuities. Many times an accurate solution was not possible due to the complexity of the discontinuity configuration. However, with the advent of Finite element method (FEM), theses analyses can now be performed with a degree of accuracy. Considering the importance of structural discontinuity, an extensive research work has been carried out by naval architects, offshore and ocean engineers, hydro dynamists and mathematicians. Until now, the stress concentration factor for various isotropic structures is investigated. Heywood[1], Peterson[2] and Pilkey[3] have investigated various isotropic shapes with wide range of holes. Howland[4] determined the solution of the problem of a long isotropic rectangular plate with a centered hole subject to a tension load. Peterson has developed good theory and charts on the basis of mathematical analysis and presented excellent methodology in graphical form for evaluation of stress concentration factors in isotropic plates with different types of abrupt change. Heywood[1] introduced various equations for long length and finite width plate with different opening shapes.

In Finite Element Method (FEM) a complex region defining a continuum is discretized into simple geometric shapes called finite elements or meshes. The generation of a finite element mesh during modeling is one of the uttermost challenging tasks[5]. Recently; most finite element codes in the modeling market are capable of producing automatic meshes[5]. The art of designing a suitable finite element mesh still needs constant human intervention, especially to problem associated with discontinuities such as cracks and holes[5, 6]. Generation of poor mesh would lead to the formation of incorrect output with elegant graphic display. So the effect of mesh quality plays a significant role in Finite element analysis. Without this knowledge erroneous result can be produced which can lead to design of a faulty structure. To get accurate result in less modeling time is also very important in the industries now a day because it saves computing ability and time which optimizes production cost. Hence it needs attention for proper design and analysis of meshes of such structural discontinuities.

In the present study, the stress concentration around circular holes in an infinite plate subjected to uniform tensile force at the edges of the plate has been studied by using Finite element Method and the effect of mesh quality on stress concentration factor will has been studied as well. The aim of this study is to make a guideline for proper meshing of the domain. In the first part a finite element model of a rectangular plate with a circular hole has been made and analyzed it to find out stress concentration factor and compared it with the value found from the formula given by Pilkey[3]. After finding out the correct approach of meshing the model has been extended for multiple holes.

2. FORMULATION OF THE PROBLEM

To study the distribution of stresses and determination of SCF, a thin steel plate with a central single hole and plate with multiple holes have been modeled as static, solid, structural, linear and isotropic material model. To define the material property we have taken the Modulus of Elasticity E is 30×10^6 psi and Poisson's ratio υ is 0.3. The element behavior is a plane stress with thickness. The Figure 1 below is a display of a two-dimensional model of a thin rectangular steel plate with a central circular hole. The length A, width H and the thickness t of the plate are 20 inch, 20 inch and 0.4 inch respectively and the diameter of the circular hole is 2 inch. The plate has been placed under constant tensile stress σ (400psi), acting in a perpendicular direction to the width at the edges of the plate.

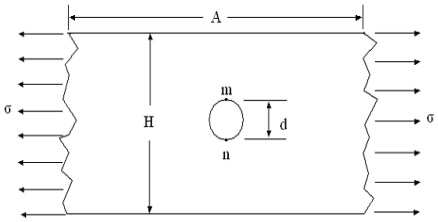

Fig.1: Plane stress of a finite width element with a circular hole.

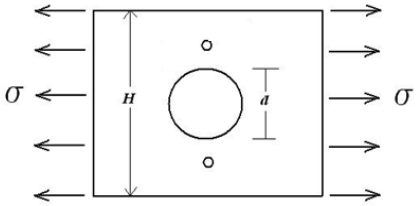

Fig. 2. A plate with a center hole and additional holes in a plane perpendicular to the loading direction

Figure 2 shows a plate with a center hole and two additional smaller holes in a plane perpendicular to the loading direction. For modeling and analysis we placed an additional hole of 0.5 inch diameter (in the quarter mode) and placed its centre 5.5 inch away from the centre of the central hole (remaining length above center hole/2 = 9/2 = 4.5). All other dimensions and parameters are kept same.

3. THEORETICAL STRESS CONCENTRATION FACTOR

As is well known the theoretical stress concentration factor (SCF) for normal stress is defined[2, 7] as

$$K_{tg} = \frac{\sigma_{\max}}{\sigma} \qquad (1)$$

where $\sigma_{\max}$ is the maximum stress in the body and σ is the stress on gross section taken as reference stress. The value of this factor depends very much on the abruptness of discontinuity, and it follows that it is desirable to design the structures in the neighborhood of a discontinuity so as to keep this factor as low as possible.

Stress concentration Formula for plate with a hole is defined as Pilkey & Pilkey[3]

$$K_{tg} = 0.284 + \frac{2}{1-d/H} - 0.600\left(1-\frac{d}{H}\right) + 1.32\left(1-\frac{d}{H}\right)^2 \qquad (2)$$

where K_{tg} is the stress concentration factor based on gross stress.

4. MESH GENERATION AND MESH QUALITY

The creation of meshing in finite element models is the most important step in the entire analysis since the decision made at this point will affect the accuracy and the economy of the solid model. Thus the choice of mesh for various analyses is crucial. An element or mesh that is good in one problem area such as magnetic field may be poor in another such as stress analysis. Even in a specific problem area an element may behave well or badly, depending on particular geometry, loading and boundary conditions. It is generally accepted that simplex triangular elements are inferior when compared to bilinear quadrilaterals. According to Brauer[8], for reasons of better accuracy and efficiency, quadrilateral elements are preferred for two- dimensional meshes and hexahedral elements for three-dimensional meshes. This preference is clear in structural analysis and seems to also hold for other engineering disciplines[8]. In view of that four-node quadrilateral membrane element (2 degrees of freedom per node) has been used in meshing the computational domain. The mesh quality has been defined as a combination of two criteria such as element quality and enough number of elements in the mesh. The quality of the surface mesh should be good to get acceptable finite element results. Element quality for quadrilateral element is defined by two factors namely: Distortion factor and Aspect ratio.

Zhu et al.[9] considered a quadrilateral element satisfactory if all its internal angles θ fall within $90^o \pm 45^o$ and was considered as unsatisfactory if θ exceeds the limit $90^o \pm 60^o$. Lo and Lee[10] found that the first condition appeared to be too strict, so a more flexible range of $90^o \pm 52.5^o$ was used for quadrilateral interior angles. In the present study Lo and Lee's range is chosen for acceptable quality of a quadrilateral element. The optimum shape for a quadrilateral is a square with interior angles 90º. The distortion factor for quadrilateral element, F_q is defined as,

$$F_q = \sqrt{\sum_{i=1}^{4} (\delta\theta_i)^2} \quad where\ \delta\theta_i = \left|\frac{\pi}{2} - \theta_i\right|, i = 1,2,3,4 \qquad (3)$$

It can be seen that F_q would attain a minimum value of zero for a perfect square and the acceptable range of $90^o \pm 52.5^o$ defined by Lo and Lee[10] would correspond to $F_q \leq 105^\circ$. In this study any element exceeding this range is considered unacceptable.

In contrast, Aspect ratio of a quadrilateral element is defined as the ratio of the largest to the smallest length of the sides of the element. The best possible value of the aspect ratio is 1. In meshing the computational domain our aim is to obtain the value of the aspect as much as close to 1. Based on these two factors an object oriented program in C++ has been developed. It calculates each element internal angles and computes the distortion factor. Finding out the maximum and minimum edge length of each element it also calculates the aspect ratio. Finally the average distortion factor of the mesh and element of worst distortion factor is found out. The output of the program for different models in our analysis for determining element quality is summarized
in the Table 1.

5. FINITE ELEMENT ANALYSIS

To conduct the Finite element analysis different models have been used with variable number and quality of elements from model to model. For modeling purposes, one quarter of plate is being subjected to the analysis due to the symmetrical appearance of the structure about horizontal and vertical axis. Application of uniform stress at the edges was also being applied with the help of symmetrical boundary conditions.

6. RESULTS AND DISCUSSION

Our first finite element model-1(Fig. 3) for the problem has 27 nodes and 16 quadrilateral elements. From the output of the program in c++, it is seen that the distortion factors of the elements are all within the acceptable range but the aspect ratio of all the elements are too high. Where a value of 5 may be too high, here only 8 elements have aspect ratio below 5.The stress distribution for the model 1 is shown in Fig. 9. From the figure it is seen that the maximum stress developed is 589 psi. So the stress concentration factor is 589/400 = 1.4725, where the value of theoretical stress concentration factor is 3.0354. From this result it is clear that quality of the mesh is not good enough and we have to refine our mesh.

To improve our result the seeding (seeding simply means locating the coordinate of nodes) biased nodes criteria has been used. Biased nodes are placed along a line in increasing or decreasing space with respect to one another. This method has been used to refine the mesh at a high stress concentration area of a model for better analysis. A model with biased nodes results in decreased computing time since fewer elements are used. One method to increase the accuracy is to make the elements as geometrically uniform as possible. This was done by seeding the right number of nodes at the right place.

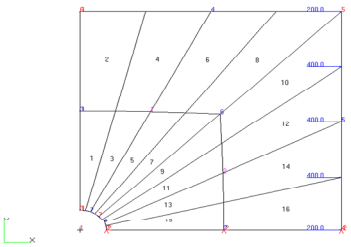

Fig. 3: Mesh of Model 1

Table 1: Summary of the output of the program for determining aspect ratio and distortion factor

Model no.	Bad quad faces, distortion factor more than 105	Average distortion factor	Average Aspect ratio	Quad with worst distortion factor	Quad with worst aspect ratio
1	nil	46.930409	17.208737	10, 79.888361	7, 33.521971
2	nil	46.067674	2.060350	10, 82.165659	71, 5.428534
3	nil	43.483030	1.654446	40, 87.386379	1, 4.786649
4	nill	40.684585	1.498629	35, 87.386379	1, 3.444965
5	368, 113.669069 369,23.092536 373, 115.273151 403, 112.877625	31.843396	1.555439	369, 123.092536	107, 3.922250

Quad means 4-noded quadrilateral membrane element

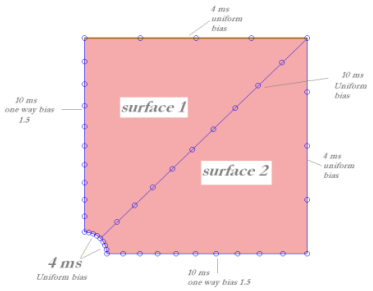

Fig. 4 Mesh seed for model 2

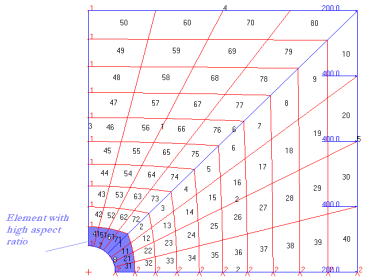

Fig. 5 : Mesh of Model 2

To create second finite element model for our problem two surfaces were created as in Fig. 4. Each edge is then divided as shown in Fig. 4. The word ms means mesh seed which represents number of subdivisions. One way bias 1.5 means largest subdivision is 1.5 times larger from the smallest one. Based on theses seeding the mesh of model 2 (Fig. 5)) is generated. The model has 99 nodes and 80 quadrilateral elements. From the output of the program in c++ for model 2 it is seen that all the elements have acceptable distortion factor but the elements surrounding the hole (the quad no.1, 11,

21, 31, 41, 51, 61, 71) have larger aspect ratio 3.8 to 5.4. The result file (distribution of stresses) is shown in Fig 10. From the figure it is seen that the maximum stress developed is 1040 psi. So the stress concentration factor is 1040/400 = 2.6. Since the mesh quality of the elements near the hole is not satisfactory in Model 2 and also we know that the stress concentration occurs at that region, we are intended to refine our mesh. For this reason, in our next model we rearrange mesh seeds though the number of nodes and elements are same as Model 2.

The next model has mesh seed as Fig 6. The mesh of model 3 is shown in Fig. 7. The model has 99 nodes and 80 quadrilateral elements. From the output of the program in c++ , we see that only four members (fewer than Model 2) have aspect ratio larger than 3. The result file is shown in Fig. 11. From the figure it is seen that the maximum stress developed is 1180 psi. So the stress concentration factor is 1180/400 = 2.95.

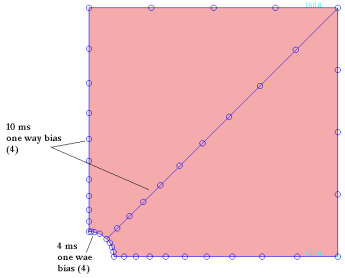

Fig. 6 Mesh seed for model 3

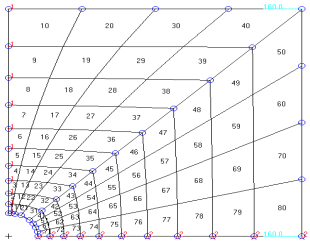

Fig. 7: Mesh of Model 3

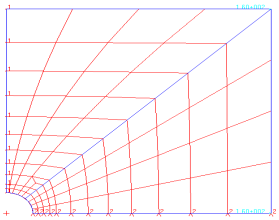

Fig. 8 : Mesh of Model 4

The mesh remaining same (same seeding as in Fig. 6) as model 3 but the elements near the hole are subdivided (along the larger length of the elements) to modify the aspect ratios. As a result, the number of nodes in the next model (Model 4) becomes 117 and the number of element is 96.The mesh of the Model 4 is shown in Fig. 8. From the output of the program, we see that only one element has aspect ratio larger than 3. The result is shown in Fig. 12. From the figure it is seen that the maximum stress developed is 1040 psi. So the stress concentration factor is 1230/400 = 3.075.

The result our analysis for different model has been shown in the tabular form in Table 2

Table 2: Summary of models and their out put

Model No.	Mesh generation & mesh quality						SCF calculation & comparison				
	No. of Nodes	No. of Elements	Average DF	Average AR	Maximum AR	No. of elements (AR more than 3)	Applied In-plane stress, σ (psi)	Maximum stress developed, σ_{max} (psi)	Numerical K_{tg}	Theoretical K_{tg}	% difference
1	27	16	46.930	17.21	33.52	16	400	589	1.4725	3.0354	51.49
2	99	80	46.070	2.06	5.43	9	400	1040	2.6	3.0354	14.345
3	99	80	43.480	1.65	4.80	4	400	1180	2.95	3.0354	2.8
4	11	96	40.685	1.50	3.44	1	400	1230	3.075	3.0354	1.3
5	7492	416	31.843	1.55	3.92	8	400	1250	3.125	unknown	

DF = Distortion factor; AR = Aspect ratio

The graphical representations of the result files (stresses in X-component) for different models for single hole are shown in the following figures:

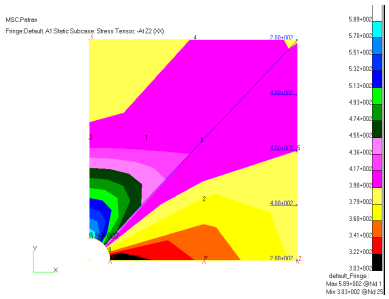

Fig. 9 : Result of Model 1

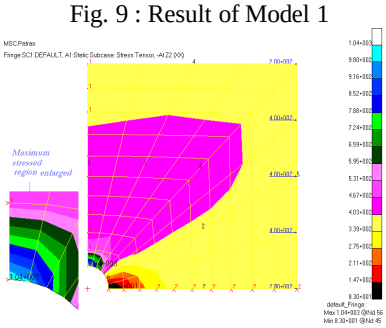

Fig. 10 : Result of Model 2

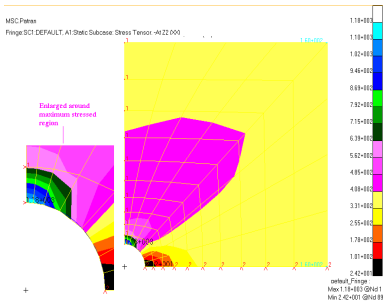

Fig. 11 : Result of Model 3

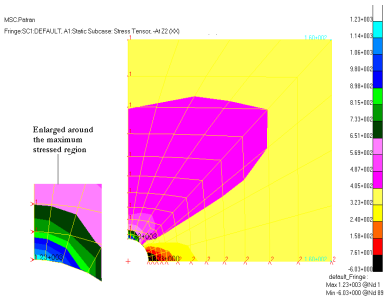

Fig. 12 : Result of Model 4

After finding out the correct approach to mesh a model, our next problem which is not listed in Pilkey[3] is a plate with a center hole and two additional smaller holes in a plane perpendicular to the loading direction. We placed the additional holes to see the effect of stress concentration in the region where originally the maximum stress developed. The mesh seed and mesh of the model with multiple holes are shown in the Fig. 13 and Fig. 14 respectively. The result is shown in Fig. 15. From the figure it is seen that the maximum stress developed is 1250 psi. So the stress concentration factor is 1250/400 = 3.125 (more than 3.075, the stress concentration found from previous problem). So we see that the addition of holes will not make the situation better but will worsen the case. Now we get two additional regions with stress concentration (extreme edges of the smaller hole).

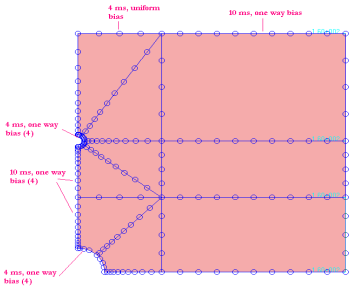

Fig.13 Mesh seed for model 5(multiple holes)

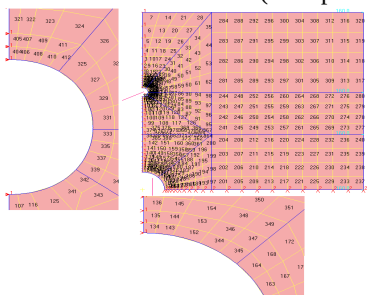

Fig. 14. Mesh of model 5(multiple holes)

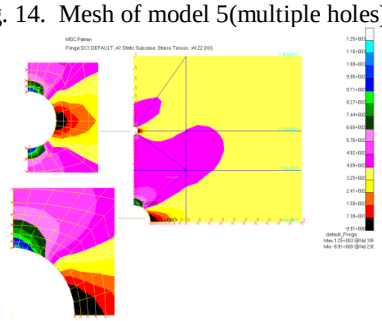

Fig. 15: Result of the model 5(multiple holes)

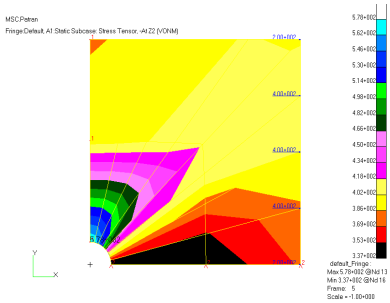

Fig. 16 Von mises stress for model 1

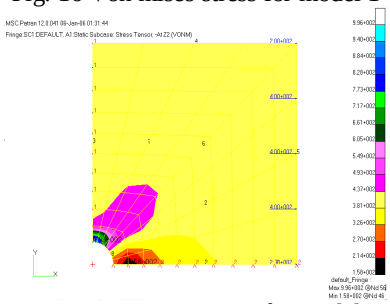

Fig. 17 Von mises stress for model 2

7. VON MISES STRESS

In this section the results are shown (for all models) in terms of Von Mises stress. Von Mises stress is a geometrical combination of all the stresses (normal stress in the three directions, and all three shear stresses) acting at a particular location. If the Von Mises stress exceeds the ultimate strength, the material ruptures at that location. The graphical representations of the result files in case of von mises stress for different models for single hole and multiple holes are shown in the following figures and So we now summarize the results in the following Table 3.

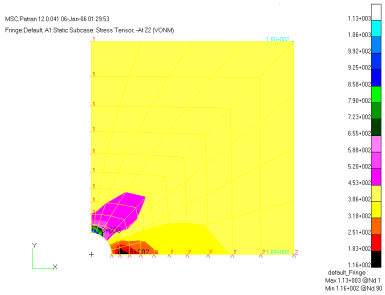

Fig. 18 Von mises stress for model 3

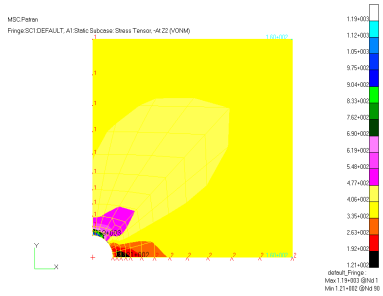

Fig. 19 Von mises stress for model 4

Table 3: Stress concentration factor in terms of Von Mises stress

Model No.	σ_{max} (Maximum Von Mises stress)	σ (Von Mises stress at the edge nodes where pressure applied)	K_{tg} (Numerical)	K_{tg} (theoretical)	% difference
1	578.00	400	1.445	3.0354	52.40
2	996.00	400	2.490	3.0354	17.97
3	1130.0	400	2.825	3.0354	6.900
4	1190.0	400	2.975	3.0354	1.990
5	1220.0	400	3.050	unknown	0.480*

* With respect to the K_{tg} of column 5

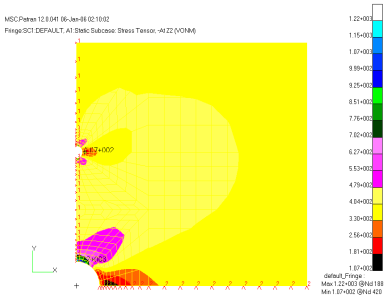

Fig. 20 Von mises stress for model 5(multiple holes)

8. CONCLUSION

This work clearly demonstrates the robustness of the finite element method in handling real life problems. Finite element analyses of holes are imperative because holes are used in engineering components and structures for bolts, rivets etc., and we need to know the stresses and deformation which occur near them. When generating a finite element mesh, one can expect more accurate results with more refined mesh (smaller size but larger number of elements within a confined area). However as the model gets larger (In FEA, larger model does not mean larger geometry, but rather the complexity due to the number of elements used), the computer will spend more time to generate the results of the analysis. It is often very important to minimize the computing time without a significant loss in the accuracy of the solution. In order to achieve satisfying results with minimum computing time, there are several techniques. One method that we have used in our analysis seeding biased nodes. In this study the main target was to perform a FEM analysis on a structural problem concerning stress concentration around a hole in the middle of an infinitely long plate to validate the formula for the problem and by this to find out correct meshing of the domain. The following conclusions can be drawn from the present study:

1. A reliable program in c++ is developed which can effectively check the quality of 2-dimensional quadrilateral finite element mesh. To achieve correct result a good quality mesh is necessary and for evaluating if the mesh is good enough, this program is very much essential.
2. After performing a number of investigations (only four are given) a reliable meshing technique is proposed, using which a mesh consisting of a minimum number of elements can be generated for achieving accurate results.
3. It is found from the analyses that element aspect ratio has a great impact on the finite element results. Our aim is to achieve the best value of the aspect ratio which is 1 but in our analysis the maximum value of the aspect ratio is 3.44 in high stress region. Also care should be given to keep elements having higher aspect ratio away from region of high stress concentration and numbers of these elements should be diminutive.
4. Though the distortion factor of value zero means perfect square (the best possible), but for geometric constraints achieving this value is not always possible. From the analyses we made, it is found that the average distortion factor of the mesh should not be more than 40.

5. After investigating the results, the formula (equation 1) given by Pilkey[3] is found reasonably accurate.

REFERENCES

[1] Heywood, R.B. *Designing by photoelasticity*. Chapman and Hall, 1952.
[2] Peterson, R.E. *Stress concentration factors*.John Wiley & Sons, 1974.
[3] Pilkey, W.D. *Peterson's stress concentration factors*. New York: John Wiley & Sons Inc., 3rd edition, January 14, 2008.
[4] Howland, R.C.J. On the stresses in the neighborhood of circular hole in a strip under tension. *Phil. Trans. Roj. Soc*., Vol. 229, 1929,pp. 49-86.
[5] Anderson, T.L. (2005), Fracture Mechanics Fundamentals and Applications, 3rd Edition: CRC press, Taylor & Francis Group, 6000 Broken Sound Parkway NW, Suite 300, Boca Raton, FL 33487-2742
[6] Roland, W.L., Perumal, N., and Kankanhalli, N.S. (2004), Fundamentals of the Finite Element Method for Heat and Fluid Flow: John Wiley & Sons Ltd, Southern Gate, Chichester, West Sussex PO19 8Q, England.
[7] Wang, Q.Z. Simple formulae for the stress concentration factor for two – and three-Dimensional Holes in Finite Domain. *J. of strain analysis*, 37, 2002, pp.259-264.
[8] Brauer, J.R., ed., What Every Engineer Should Know About Finite Element Analysis, Marcel Decker Inc., 1993.
[9] Zhu, J. Z., Zienkiewicz O. C., Hinton, E. and Wu, J. A., "A new approach to the development of automatic quadrilateral mesh generation", International Journal for Numerical Methods in Engineering, Vol. 32, pp.849-66, 1991.
[10] Lo, S. H. and Lee, C. K., "On using meshes of mixed element types in adaptive finite element analysis", Finite Elements in Analysis and Design, Vol. 11, pp.307-36, 1992

DESIGN AND FABRICATION OF A SPEECH RECOGNITION ROBOT

S. I. Sharker*, F. A. Amin*, M. A. R. Sarkar**

*Department of Mechanical Engineering, Bangladesh University of Engineering and Technology (BUET), Dhaka, Bangladesh

**Professor, Department of Mechanical Engineering, Bangladesh University of Engineering and Technology (BUET), Dhaka, Bangladesh

Abstract

A speech recognition system converts spoken words to electrical signals which can be received by a processor: in which voice is a means of interaction between human and machine.

The objective was to design and build a robot that could perform some navigation tasks by speech command. It was achieved by using Arduino microcontroller board which uses C++ programming, and by using a speech recognition module. The module is trained with all the voice commands and it also acts as a storage device for the sound files of the commands. When a speech input is given through a microphone, its frequency is compared and matched with all the previously trained commands. If it matches exactly with any of the stored sound, the microcontroller will receive a specific signal to perform the corresponding task.

Keywords

voice recognition, speech recognition, speech synthesis, C++, robot, human-machine interaction, speech training.

Introduction

The Robotics Institute of America (RIA) defines a robot as "a reprogrammable, multi-functional manipulator designed to move materials, parts, tools, or specialized devices through variable programmed motions for the performance of a variety of tasks." [1] The speech recognition robot is capable of understanding and synthesizing human speech for communication. It takes speech input as commands and performs the corresponding tasks.

The term “voice recognition” refers to the recognition system of only a particular voice in response to a command, which attempts to identify the person speaking, based on their unique vocal sound. But “speech recognition” refers to the pattern recognition of the sound regardless of the speaker. [2] Currently, the robot is programmed to function if the correct command is given by anyone, but it can also be programmed so that it can only be operated by the person who trained it, which can be very useful for password protection.

The robot now responds to five commands: forward, backward, left, right and stop. More commands can be added as required, simply by training the commands into the module.

Voice Command Training

The module needs to be connected to a computer for training of the voice commands, i.e., to add a new command to the storage. It must be connected through a serial port. A very user-friendly Graphical User Interface (GUI) makes voice command training relatively easy. Different groups can be made for storage of different sets of commands and these groups can later be called during coding on a compatible microcontroller. A microphone is attached to the input pins of the speech recognition module, and it picks up sound from its surrounding environment. The command to be trained is spoken in the microphone twice consecutively to ensure that the exact command is stored. The module filters the input and converts it to digital signal and stores the command. If any error happens, command training will be cancelled. Errors may happen when the user's voice is not heard correctly, there is too much background noise or when the second word heard is too different from the first one. The microphone used as the input device in this robot is an omnidirectional electret condenser microphone with the following specifications [3]:

- Sensitivity -38dB (0dB=1V/Pa @1KHz)
- Load Impedance 2.2K
- Operating Voltage 3V
- Almost flat frequency response in the range 100Hz – 20kHz

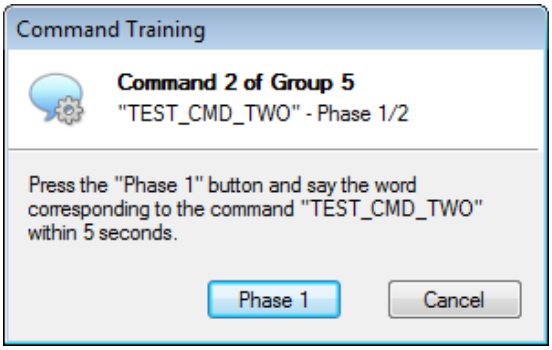

Figure: Guided training dialog on the user interface [4]

Speech Recognition System

One major advantage of this particular design of speech recognition robot is that it can function entirely independently, i.e., it does not need to be connected to a computer for speech recognition or speech synthesis, once the commands have been trained on it. The microcontroller and the module along with the microphone are onboard the robot.

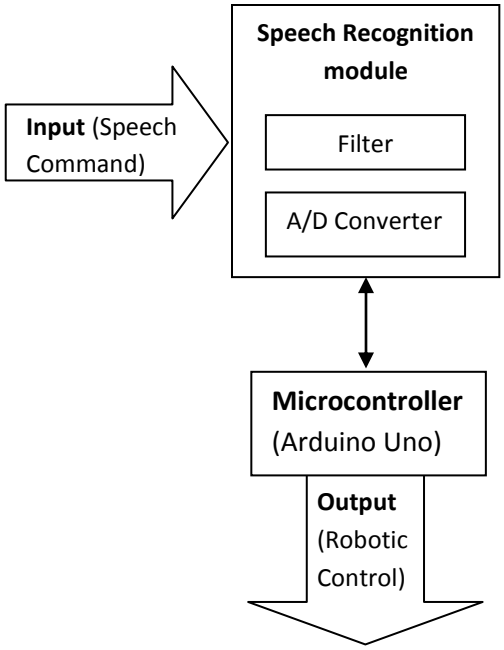

Figure: Block diagram of the speech recognition system

The general concept of the speech recognition system is that, it takes speech command as input through the microphone, the module filters it and converts it to digital signal and sends it to the microcontroller connected through the receiver (RX) and transmitter (TX) pins.

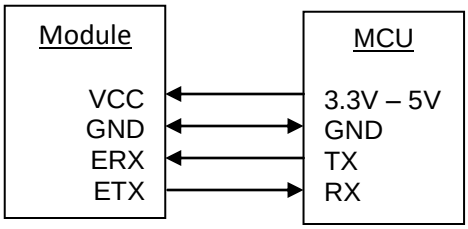

Figure: Connecting speech recognition module with MCU [5]

The initial configuration at power on is 9600 baud, 8 bit data, no parity, 1 bit stop. The baud rate can be changed later to operate in the range 9600 - 115200 baud.

The microcontroller then compares and matches the signal with those stored in the module during training. If the signal matches with the stored signal, the microcontroller performs the function as required by it provided in the codes written on it, for example, sending pulses to the motors for rotation, so that the robot can move forward. If, however, the signals do not match, it discards the signal and gets ready to receive another.

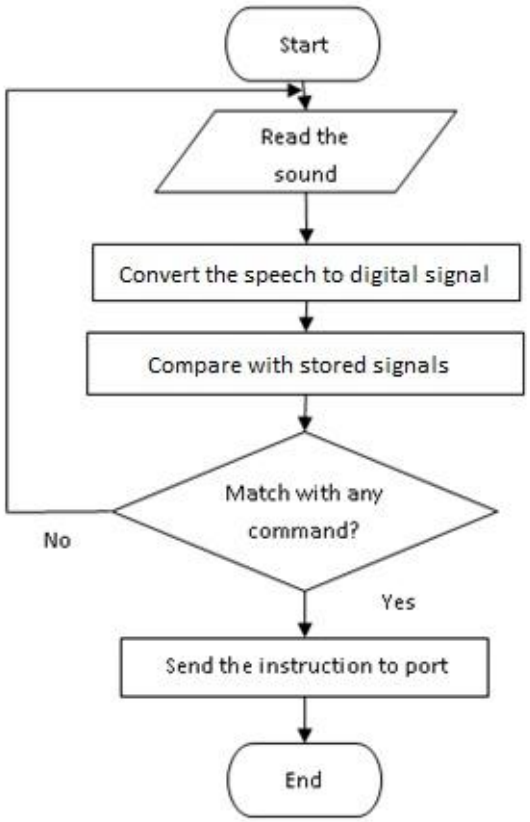

Figure: Flowchart of the speech recognition system

Hardware and Software

Since the robot is capable to move independently, without the need of a computer connection, a number of hardware are required in order to make this possible. The most important hardware are listed:

i. Speech Recognition Module
ii. Microcontroller
iii. Motor driver IC
iv. DC Geared motors

The Speech Recognition Module used is a multi-purpose module designed to easily add versatile, robust and cost effective speech recognition capabilities to virtually any application. The module can be used with any host with an UART interface powered at 3.3V – 5V. It has a simple and robust documented serial protocol to access and program through the host board. Communication with the computer is through an easy-to-use and simple Graphical User Interface (GUI) to program (or train) voice commands.

The microcontroller receives the digital signal converted from speech by the module. The microcontroller selected for this purpose is Arduino UNO which can be connected directly to the module through the receiver (RX) and transmitter (TX) pins. The Arduino can also be used as a USB/Serial adapter to connect the module to the computer. Arduino is an open-source electronics prototyping platform based on flexible, easy-to-use hardware and software. [6] An Arduino board consists of an Atmel 8-bit AVR microcontroller with complementary components to facilitate programming and incorporation into other circuits. The software consists of a standard programming language compiler and a boot loader that executes on the microcontroller.

The motor driver IC used to control the DC geared motors is L293D. It is a quadruple high-current half-H driver. The L293D is designed to provide bidirectional drive currents of up to 600-mA at voltages from 4.5 V to 36 V. It is designed to drive inductive loads such as relays, solenoids, dc and bipolar stepper motors, as well as other high-

current/high-voltage loads in positive-supply applications. [7] L293D is a 16-pin IC which can control a set of two DC motors simultaneously in any direction.

The software used for speech recognition using the speech recognition module is called the Commander. It has simple GUI for connecting the module and training of the voice commands. The software used for programming the robot using Arduino is written C++. The Arduino IDE comes with a software library, which makes many common input/output operations much easier. The Arduino Integrated Development Environment (IDE) is a cross-platform application written in Java. [8]

Conclusion

A system for reliable speech recognition has been designed and developed, and it has been detailed in this paper. This system can be made highly efficient and effective if stringent environmental conditions are maintained. Success rate of speech recognition is very high when spoken from a close range and it decreases as the distance increases. Also, background noise adversely affects the rate of speech recognition but this can be increased by using better filtering methods and better quality microphones. There is also a way to connect a speaker to the module so that it can give audio output as desired by the programmer. For that, it is needed to upload a sound table to the module. Response time from giving a command to performing the corresponding function is quite fast. Also, it can function entirely independently, i.e., it does not need to be connected to a computer for speech recognition or speech synthesis. All these characteristics make this particular design of speech recognition robot a better choice for most applications.

References

[1] Kuttan, Appuu. *Robotics.*

[2] "The Mailbag LG #114". www.linuxgazette.net.

[3]User Manual http://download.tigal.com/veear/EasyVR_User_Manual_3.4.2.pdf

[4]EasyVR Datasheet. www.ewerksonline.com/documents/EasyVR_Datasheet_2.3.pdf

[5]www.veear.eu/wp-content/uploads/veear.eu/2012/07/How-to-interface-EasyVR-to-a-PC.pdf

[6] arduino.cc

[7] L293D Datasheet www.ti.com/lit/ds/slrs008c/slrs008c.pdf

[8] en.wikipedia.org/wiki/Arduino

[9] Gosavi, Shraddha D., Khot, Uday Pandit and Shah, Seema. Speech Recognition for Robotic Control. *International Journal of Engineering Research and Application*, Vol. 3, Issue 5 (2013): 408-413

[10] Ahasan, Md. Abdullah Al, Awal, Md. Abdul and Mostafa, Sheikh Shanawaz. Implementation of Speech Recognition Based Robotic System. *International Journal of Computer and Information Technology,* Volume 1, Issue 2 (2011): 16-20

[11] Koren, Yoram. *Robotics for Engineers.*

FABRICATION AND PERFORMANCE OF AN AUTOMATIC INDUSTRIAL COOLER ROBOT

S. K. Alen[1] and M. A. R. Sarkar[2]
Department of Mechanical Engineering
Bangladesh University of Engineering and Technology
Dhaka, Bangladesh
educative.alen@gmail.com[1], rashid@me.buet.ac.bd[2]

ABSTRACT: This paper reports the fabrication and performance of an automatic industrial cooler robot. This robot is a self driven vehicle capable of detecting the high temperature zones in a grid system. It also cools that high temperature zone by means of spraying suitable cooling agent. It was fabricated with low cost locally available materials. This robot is simultaneously a combination of line follower, servo sprayer and wireless pc controlled robot. For spraying water DC-servo motor was used instead of stepper motor which ensures the sufficient torque and using RF modules for wireless PC control gives it sufficient system automation. As the program executes robot gets information from its transmitter modules and decides the highest temperature zone of the grid, then it goes to that node solving the grid and hence cooling that node with the sprayer associated with it indicates the completion of its task.

Index Terms: Industrial robot, cooler robot, servo motor, wireless pc interfacing

1. INTRODUCTION

Automation in the industrial systems is a very important tool for the rapid economic development of a country. In Bangladesh, proper system automation is necessary in different industrial systems. Robotics has become a very common application in most of the developed countries. High Performance, high accuracy, lower labor cost and the ability to work in hazardous places have put robotics in an advantageous position over many other such technologies. Third world countries like Bangladesh however, are still not very familiar with the use of robots. There are two reasons behind this. Firstly, the high initial costs in importing robots and associated softwares and secondly the misconceptions of the capabilities of robots as day to day essential applications. This industrial cooler robot can be considered as a mobile robot or a mobile platform that can locate high temperature zones and cool that heated object by means of spraying fluid/gas or any desired coolant and keeping the temperature at an optimum level. This is done automatically i.e. without the help of any human interference by implementing programs in electronic circuits, so in any condition the robot knows what to do, where to go. An operator can issue a force command to start cooling or to switch priorities and it can be controlled via PC through wireless communication. It follows a line ideally a white line that is marked on the ground. The line may consist of bends, turns and dead ends etc and the improved version of this robot would deal with all types of path characteristics with a high precision. The basic objective of this robot is to provide cost effective solutions for industrial applications, commercial applications and security applications, but not restricted to them. Slightly modified version of this robot may be creatively used even for home applications too. In case of a growing country like Bangladesh one of the major fields of an autonomous robot is in industries, power plants and in places where high heat is produced. This industrial cooler robot is built for that specific demand.

2. ROBOT FEATURES

This robot is a combination of some basic robotic features. Line follower is a machine that can follow a path. The path can be visible like a black line on a white surface (or vice-versa) or it can be invisible like a magnetic field. Sensing a line and maneuvering the robot to stay on course, while constantly correcting wrong moves using feedback mechanism forms a simple yet effective closed loop system [1]. This cooler robot was developed based on a vision based system to navigate the robot through a white line marked in the black surface. It also extracted some features in the sensor based systems as well. Although it is fully autonomous it can still be controlled wirelessly by PC command. This vehicle is also capable of storing important environmental data and can communicate

with the operator. This vehicle is actually a prototype of a self driven vehicle capable of locating and cooling various hot zones located in a industry or in any High heated environment.

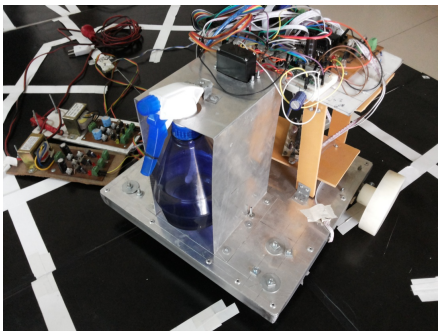

Fig. 1. Robot with its transmitter module and power supply circuits

The features of this robot can be listed as the followings

- Line follower
- Grid solver
- Automatic temperature based cooling system
- Wireless pc control

Figure-1 shows a snapshot of all the circuit boards and mechanism used for making this industrial cooler robot.

Robot can follow line in an arena containing varying gradient lines, sharp turns, lines having different thickness and even gaps in tacks. And also cools different parts of a machine by sensing temperature, the machine/part with highest temperature is given first priority. To enable the user to halt/force command the robot a control scheme is required. This robot uses wireless communication and can be controlled by simple commands through PC.

3. MECHANICAL FEATURES

This robot is the combination of following mechanical parts:

- 4-wheeler (2-DC motor Controlled Drive wheels, 2-castor wheels) of 30cm*30cm*20cm dimension.
- Two storied circuit board and a controller board frame.
- Servo motor controlled water-sprayer booth.

Mechanical Structure

Aluminum sheet was selected for the material of the frame. Dimension of the robot is very small because it is developed for modeling the system. Main purpose of this work is to propose this concept of automation in industries. The frame is 30cm* 30cm* 20 cm. Water sprayer chamber was mounted on the frame at the front side of the robot. Figure-2 shows the structure of the bot.

The robot is four wheeler, two wheel casters are used and driving wheels are connected with the DC geared motors. Circuit boards are mounted in a two storied frame which is located at the back end of the robot.

Servo Motor Operation

The most important part while making this robot is to choose the suitable motor for operating the joints. Though DC motor and stepper motor are widely used on various operations [2] but in this case servo motor is chosen for its high precession in rotary motion.

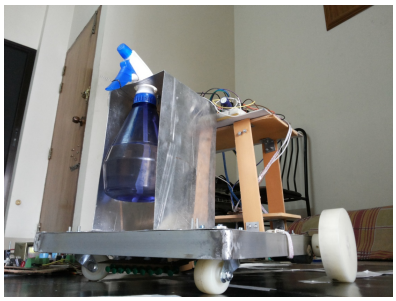

Fig. 2. Mechanical Structure of the Robot

Fig. 3. Servo Motor (SG-5010)

A Servo Motor is defined as an automatic device that uses an error-correction routine to correct its motion. A motor, control board, and a potentiometer connected to the output shafts is the major components of a servo motor. Figure-3 shows a servo motor of Towerpro SG-5010.

Servos are extremely useful in robotics and automation. Servo motors are used specifically where the motor must be able to operate at a range of speeds without overheating, operate at zero speed while being able to retain its load in a set position.

In this case Towerpro SG-5010 model servo motor is chosen and the specification of this motor as follows:

Model: TowerPro SG-5010
Modulation: Analog
Torque: 4.8v (8 kg-cm), 6v (11 kg-cm)
Operating Voltage: 4.8V~6.0V
Rotational Range: 180°

The average operating speeds should be considered in selecting a servomotor that can handle the job without danger of thermal overload. Figure-4 shows the continuous motor torque for a servomotor rated at 3.8 kg-m and 4,000 rpm for example [3].

Servo motors are high performance alternative to the stepper motor and the type of motor is not critical to a servo motor. Generally brushed permanent magnet DC motors are used considering their simplicity and low cost.

4. ELECTRONIC COMPONENTS

Electronic components of this industrial cooler robot are not so complicated. For controlling the sprayer servo motor, no motor controller is needed it can be directly controlled by the microcontroller. PWM of the MCU is used to control DC motor speed. And for the PC interface signal level conversion IC is used and for the wireless transmission of data from the PC to the MCU (microcontroller) RF (Radio Frequency) modules are used.

PIC18F452 Microcontroller

A microcontroller (MCU) is a computer on a chip with both input output and with inbuilt timers and counters. It is a small computer on a single integrated circuit consisting of a relatively simple CPU combined with support function such as crystal oscillator, timers etc.

The PIC18F452 microcontroller is a CMOS FLASH based 8-bit microcontroller packs that features a ‘C’ compiler friendly development environment, 256 bytes of EEPROM, self programming, 2 capture/compare/PWM functions, 8 channels of 10-bit Analog-to-Digital (A/D), 2 USART ports [4]. Figure-5 shows one PIC microcontroller and one pair of RF module.

Some general information of PIC18F452 MCU are given below:

- 4MHz-10MHz osc./clock input with PLL active
- Priority levels for interrupts
- Three external interrupt pins
- CCP pins and PWM output
- PWM resolution is 1- to 10-bit
- 1,000,000 erase/write cycle Data EEPROM

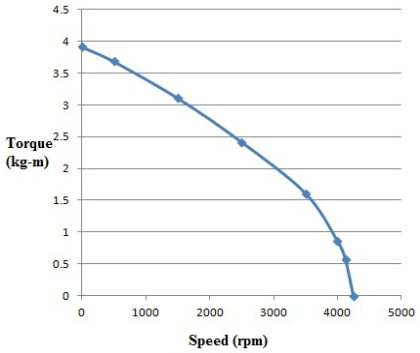

Fig. 4. Typical Servo Motor Torque-Speed Curve [3]

IC MAX232

The MAX232 IC converts signal from an RS232 serial port to signals suitable for using in TTL compatible digital logic circuits. MAX232 converts RX, TX, CTS and RTS signals. Mainly the receivers of MAX232 reduce RS-232 inputs to standard 5V TTL levels. The circuit diagram for MAX232 module is given in Fig. 6:

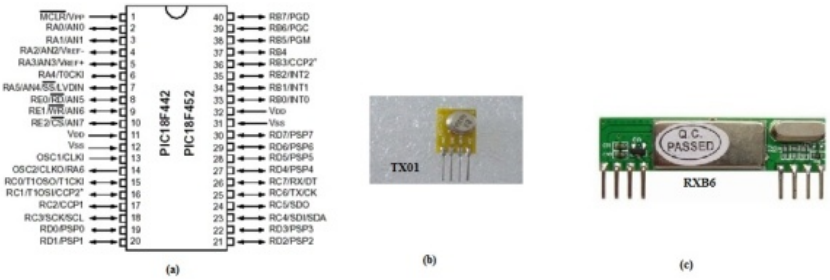

Fig. 5. (a) PIC18F452 (b) TX01 (c) RXB6

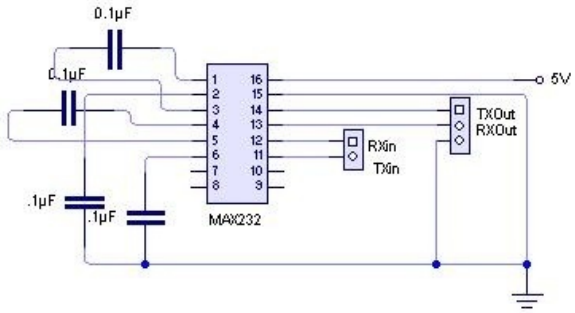

Fig. 6. MAX232 Module Connection

RF Module

Radio frequency (also RF Module) module is an integrated electronic circuit which is used for the purpose of transmission of radio signals on one of a number of carrier frequencies. In case of medium and low volume products for consumer application RF modules may be used. RF modules are for both transmitting and receiving radio signals and individual modules are manufactured for these two cases. For transmitting data from the PC and for receiving it at the MCU end the following modules are used: (a) RXB6 (b) TX01

Frequency for both of these modules is 433.92MHz. Generally 433.92MHz, 315MHz, 868MHz and 915MHz frequencies are used because of national and international regulations governing the use of radio for communication.

5. ELECTRONIC CIRCUITS

Mainly six individual circuits are needed for the electronic portion of this Industrial Cooler Robot system. Two power supply circuits providing constant 5V DC and 12V DC power supply, a servo controller circuit controlling the servo on the sprayer, a DC motor controller circuit with L293D and wireless PC control module for commanding the robot through computer are used for this robot.

Power Supply Circuit

For a constant DC 5V and 12V power supply from the 220V-50Hz AC input the following circuit of Fig. 7 is to be connected. From the AC input a bridge rectifier is used for rectifying the current. And DC output from the bridge rectifier is passed through the voltage regulator ICs LM7805 and LM7812; hence we get a constant 5V and 12V DC output from the output pin of 7805 IC and 7812 IC [5]. 1n4007 diodes are used in this circuit and for reducing noise two individual capacitors of 470uf and 1uf are used at the input and output end of LM7805 and LM7812.

DC motor control with L293D

For controlling DC motors of the wheel L293D IC is used. It receives the command from the microcontroller and defines the motor state whether the motor is to turn clockwise or anticlockwise. L293D is a H-Bridge motor controller. It uses four switches. Practical circuits comprise of other components such as diodes to mitigate the effect of back-emf.

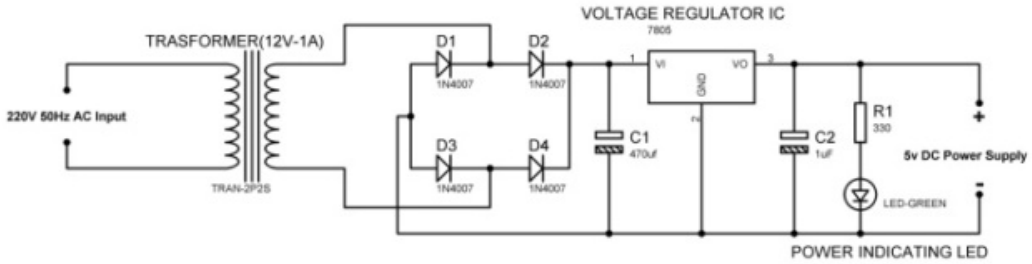

Fig. 7. Power Supply Circuit for Wireless PC Controlled SCARA

Sensor Board Circuit

An array of 10 LDR sensors is used for detecting the lines and nodes. The schematic is given in Fig. 8:

Circuit diagram for the Main circuit board

Main circuit board for the robot was built combining the MCU board, L293D controller, and LCD display circuit. Following Fig. 9 shows the main circuit schematic:

Servo Controller Circuit

For controlling the servo motors of the sprayer of the robot no motor controller is needed, it can be directly controlled with the PIC18F452 microcontroller using Pulse Width Modulation (PWM) [6].

Wireless PC Control Module

Wireless PC control module is the vital part of this project. With the help of wireless transmission of data robot can be operated within the range permitted by the radio transmitter TX01 [7]. Max232 IC is used as the signal level converter (RS232 to TTL) in this circuit and TX01 is connected with the MAX232 and it also contains an antenna which is spiral for facilitating the transmission of radio frequency. The snapshot of wireless PC control module is given in Fig. 10.

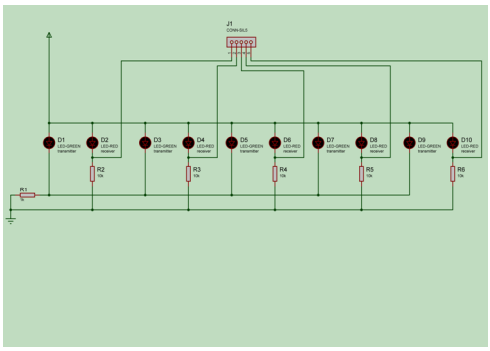

Fig. 8. Schematic Circuit Diagram for Sensor Board

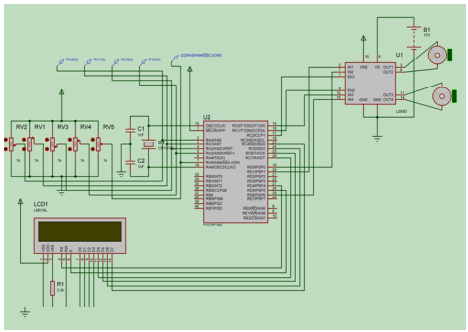

Fig. 9. Circuit board schematic for automatic industrial cooler robot

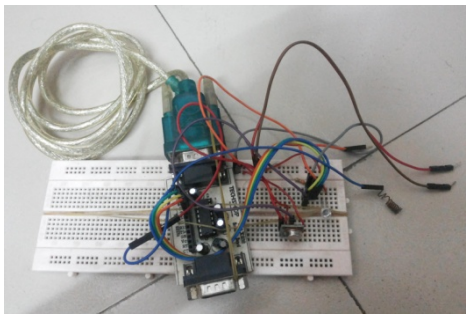

Fig. 10. Wireless PC control module

6. APPLICATION FIELDS

This robot mainly targets large industries, power plants, Server Rooms, any environment where high heat is generated. It will cool any part of a machine by sensing the temperature, thus giving the machine longer life, and also reducing any risk/danger, deformation, stress concentration etc. It can operate in any light condition because of its LDR arrangement. It can also be used for detecting uneven temperature distribution on any system/environment and cool that environment and keeping the temperature constant throughout the system. Moreover it not only cools that part it also records that data for further analysis and can give statistical report. Thus it can show the user which part of the system is more prone to failure and can mark those places as the most dangerous /unstable places in the system. Also it doesn't inspect randomly in a factory/system/ environment but uses precise sensors to monitor temperature and uses definite path, so even if there is narrow place or in a maze like layout this robot can perform its task effectively and efficiently and by following this specific path/line the robot requires the minimum surface area/path for its operation.

7. CONTROL SYSTEM AND SOFTWARE FEATURES

Control systems are an integral part of a work-cell or large complex of equipment and have the primary purpose of controlling, monitoring, analyzing, or measuring a process or other equipment [5]. Control system of this robot is quite simple. It needs only microcontroller to operate servo motor and PWM of MCU for the control of DC motor through L293D. Servo motor is run with the help of pulse width modulation of a 20 ms pulse. And this modulation can be done by the built in PWM pins of the MCU and also with the timer of the MCU required pulse can be generated. The list of some main software features is:

- Complete Button controlled PID calibration system software
- PID algorithm for following lines
- Analog to Digital converter (ADC) for taking the analog sensor values
- Radio Frequency (RF) controlled wireless communication (at a baud rate of 9600bps)
- Timer used for modulating 20ms Servo motor pulse
- Pulse-Width-Modulation for precise speed control through L293D
- USART protocol to communicate with other Microprocessors or Computers

Timer

The timer is usually used to measure the signal period. Timer needs a clock pulse for timing which can be divided into two divisions:

- Timer with internal clock
- Timer with external clock

Timer0 module used in this case and it has the following features [8]:

- Software selectable as an 8bit or 16bit timer
- Readable and writable
- Clock source selectable
- Interrupt on overflow of FFh to 00h in 8-bit

Pulse Width Modulation

PWM (Pulse Width Modulation) is the term used to describe using a digital signal to generate an analogue output signal [8]. It can generate a continuously variable analogue output without using any other integrated circuits by smoothing the PWM signal with a capacitor. Pulse coded modulation is done to communicate the angle at which the servo will turn. In spite of having some deviation from the time mentioned below, the servo expects to see a pulse every 20 milliseconds. The length of the pulse will determine how far the motor turns. A 1.5 millisecond pulse will make the motor turn to the 90 degree position (often called the neutral position). If the pulse is shorter than 1.5 ms, then the motor will turn the shaft to closer to 0 degrees. If the pulse is longer than 1.5ms, the shaft turns closer to 180 degrees. Figure-11 shows the standard time vs. angle chart for operating servo motors.

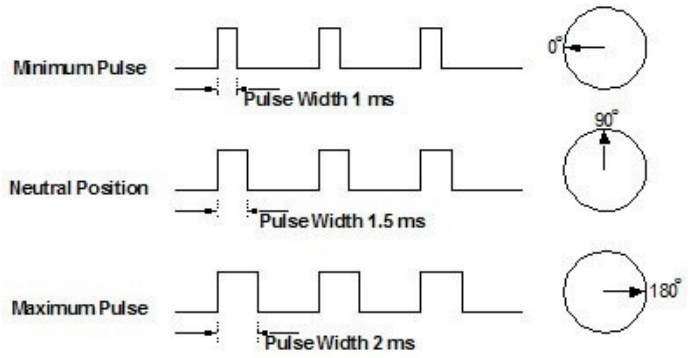

Fig. 11. The Standard Time vs. Angle Chart for Operating Servo Motors

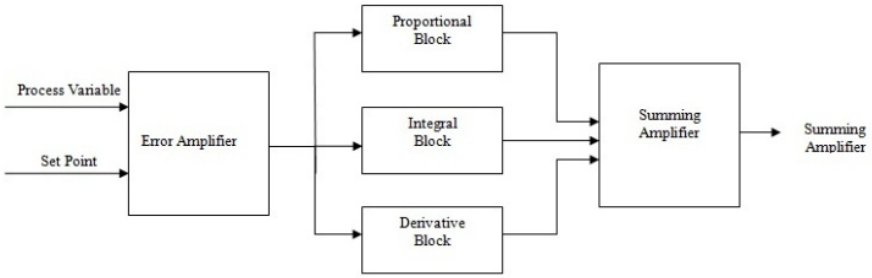

Fig. 12. Block Diagram of a typical PID controller

Proportional Integral Derivative(PID) Control

The control system primarily used in continuous process is the proportional-integral-derivative control. PID is an effective control system for continuous processes that performs two main tasks to provide feedback to a PLC (Programmable Logic Controller) [5].

- PID control keeps the output at a set level
- PID promptly and accurately changes the process level from one set point to another set point level

A typical block diagram of PID controller is given in Fig. 12:

Block Diagram of Electrical System

The complete flow diagram at the cooler end of the electrical system of this cooler robot is given in Fig-13:

This kind of robot can be of various size and shape and its components might change depending on the working area/layout/system like using different cooler for specific needs, sensing temperature using different methods. So depending on the environment or the need of the user its operation principle, component may vary but its basic operations are very simple and they are:

- Taking temperature reading at various parts/nodes and monitoring all the temperature readings at different locations of the system by using LM 35 and PIC microcontroller. There will be 8-10 LM 35 temperature modules in the system. Temperature modules will communicate with the master robot using RF.

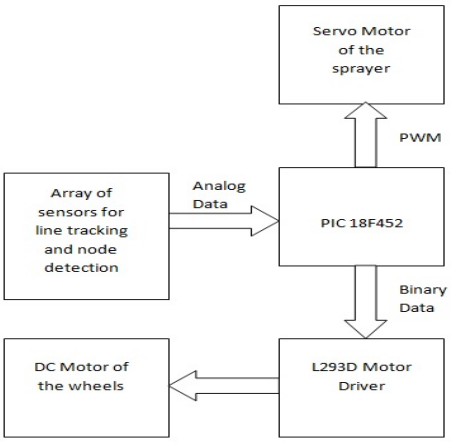

Fig. 13. Block diagram of the electrical system

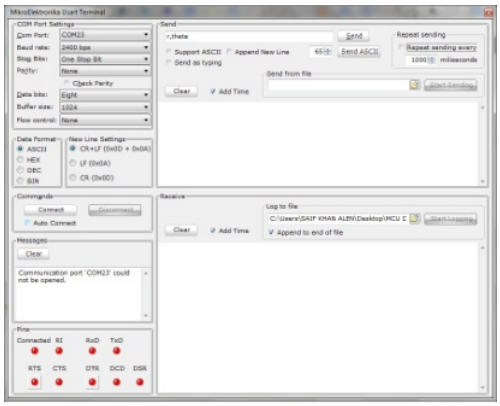

Fig. 14. USART terminal for giving command From PC

- Once an unstable region/high temperature place is found or a force command is issued mark it as first priority and locate that point in the grid.
- While going to that point, monitoring other regions and if any other heated part is detected then marking it as 2nd objective and so on.
- Cooling that point/node, marking it as cooled and storing the environment and operational data.
- After cooling moving to next priority.
- When all objectives are clear return to start position.

Serial Communication Interface

The universal asynchronous protocol - often simply called RS232. The universal synchronous/asynchronous interface is a serial channel which allows a serial bit stream of 7 or 8 bits to be shifted into and out of the MSP430, at a programmed rate, or at a rate defined by an external clock [7]. Screenshot of the software is given in Fig. 14.

To communicate from the computer 'MikroElectronika USART Terminal' is used and the communication is at a baud rate of 2400 bps. Because this TX01 module with frequency 433.92 MHz gives the best communication between the devices at a baud rate of 2400 baud per second.

8. RESULTS AND DISCUSSION

Performance of the robot was smooth due to some definite decisions and selections made during the project. Such as selecting the servo motor instead of stepper facilitated the torque required to spray water from sprayer and enhanced the precession to a large extent. Material selection such as aluminum for the robot and plastic sprayer turned out to be effective. There exists a drawback associated with the dependency on the radio frequency for transmitting the command from the PC to MCU, some noise and garbage data may be received by the RXB6 receiver.

9. SUMMARY

With the satisfactory performance of the Automatic industrial cooler Robot we can easily summarize that Industrial robots are very useful considering its industrial applications. As a wireless control system is developed for this device, this feature enhances its field of application to a large extent. Due to this computer control capability a number of Industrial cooler Robots can be simultaneously operated on the basis of individual command and individual purpose. This robot can be used in different industries in Bangladesh for achieving sufficient automation in the cooling process. Proper material selection, motor selection and easiness of its operation with a capability of wireless control of the device from the computer are the primary achievements of this work.

10. FURTHER MODIFICATIONS

Further modification of this automatic system can be done by using the latest available technology. One master robot can be used for controlling a number of slave robots which will ease the task of cooling operation. Moreover the power supply system can be replaced by boost module which is

available nowadays. Wireless remote control system for this robot can be a suitable modification. Cell phone control and object detection capability can be included in its feature. Most importantly this robot can be modified for using in the mapping of heat signature in three dimensions.

REFERENCES

[1] F. Arif, M. F. Ismail, M. S. Alam, and M. A. R. Sarkar, "Modeling and Implementation of Autonomous Robotic Vehicles with Locally Available Materials," 6th International Mechanical Engineering Conference & 14th Annual Paper Meet (6IMEC&14APM), 28-29 September 2012, Dhaka, Bangladesh.

[2] M. F. Ismail, F. Arif, M. E. Amin, J. Mojumdar, and M.A. R. Sarkar, "Fabrication of a Stair Climbing Vehicle for Industrial and Rescue applications Using Appropriate Technology," 7th International Conference on Electrical and Computer Engineering (ICECE) 2012.

[3] http://machinedesign.com/technologies/protecting-servomotors-self-destruction. (14-07-2013)

[4] http://en.wikipedia.org/wiki/. (14-07-2013)

[5] J. G. Keramas, Robot Technology Fundamentals, Delmar, a part of Cengage Learning, 1999.

[6] M. T. Das, and L. C. Dulger, "Mathematical modeling, "simulation and experimental verification of a scara robot," Journal of Simulation Modelling Practice and Theory, Vol. 13, Issue 3, pp. 257-271, April 2005.

[7] J. J. Craig, Introduction to Robotics, Addison Wesley Longman, Reading, MA, 1986.

[8] R. K. Saha, M. M. Islam, P. V. Biswas, S. D. Nath, S. Das, and K. M. M. Rahman, "Design and fabrication of Autonomous Mobile Robots," Undergraduate Thesis, Bangladesh University Of Engineering and Technology, 2009.

Fabrication of an industrial pick and place color sorting robotic arm

M. Rizwanur Rahman*, Nahid Sultan, Satyajit Mojumder, M.A.R.Sarker
Department of Mechanical Engineering
Bangladesh University of Engineering and Technology, Dhaka-1000.
*E-mail: *rishadrizwan@yahoo.com*

ABSTRACT*:* This paper presents the architecture and fabrication of an industrial pick and place color sorting robotic arm. In present days, computer aided manufacturing (CAM) system involves the industrial use of robots in different parts of the manufacturing process like material handling, product sorting, packing and other in line processes where accuracy and celerity are of main concern. This paper analyzes the mechanisms, capabilities and advantages of a simple and low cost robotic arm with 5 DOF. A prototype was developed at an intermediate stage of this research. which is able to pick up object and sort them on the basis of the color Servo mechanism was used for the motion of the actuators For the sensing of color in order to distinguish between colored objects TCS3414CS color sensor was used. An innovative design in the arm gripper has been introduced which is of very low cost and easy to fabricate locally with a higher efficiency. The authors also did real time simulations of Force and stress distribution of the model in SolidWorks.

Keywords: *Pick and place ,robotic arm, color sorting, industrial robot.*

1. INTRODUCTION

In last few decades industrial robot application has been increased in a wide range. This rapid increase is not only as a result of the impossibility of human to do that sophisticated work but also for high accuracy, precession and faster speed of human fabricated automated machines or robots. In industrial renaissance, time and man power are critical constraints. Again some hazardous heavy work in poisonous environment cannot be done at the risk of human life. So dependency on automated machines is a demand of civilization. Different types of industrial robot are being used now a days in almost all industries ranging from automobiles to micro level IC , in painting to welding, sorting to packaging, loading and unloading[1-3]. An industrial robot is defined by ISO [4] as an automatically controlled, reprogrammable, multipurpose programmable manipulator. Choosing among these three kinds of robots depends largely on speed and payload size. Among them pick and place automated arm is one of the mostly used in different industry such as food processing, automobile, electronics and in other manufacturing industries. Almost in every industry it is a very common problem that it needs to sort huge amount of product on the basis of their color. Besides, every in line processing system needs high speed sorting between odds and good products. For human it is a very time consuming and precession is never guaranteed .A robotic arm with some degrees of freedom, on the contrary, can be employed to solve this kind of problem effectively. This is a time saving and low cost technology. Several kinds of robots can be used for upstream pick-and-place: They can be broadly classified as Delta style robots, SCARA, and multi-scale articulated robots. Delta-style robots that operate from overhead with three or four long, thin arms that meet at the effector head. SCARA (selective compliant articulated robot arm) models, which are fixed-base robots with three vertical-axis (horizontal-motion) rotary arms. Multi-axis articulated robots, which can have up to six axes, with joints that can rotate in any direction [5-7]. Choosing among these three kinds of robots depends largely on speed and payload size. Another important consideration is the economical aspect. In this paper, a proper designing, choosing the right material and a proper controlling system along with the sensor is presented to make this robotic arm economic without compromising with desired accuracy and celerity. A prototype has been built to check the suitability for the design and fabrication of the robotic arm and it has been found that the arm is completely reliable with its high accuracy.

2. MECHANICAL DESIGN CONCEPTS AND STRESS ANALYSIS

2.1. MECHANICAL DESIGN

Designing was the most vital part of this research work. An arm has been developed having 5 degrees of freedom which gave the arm a wide range of working and flexibility. Different mechanical components were designed to build the prototype and the theoretical calculations were

validated with the experimental data. In figure 1(a) a CAD design prototype is shown and figure 1(b) shows a real life prototype.

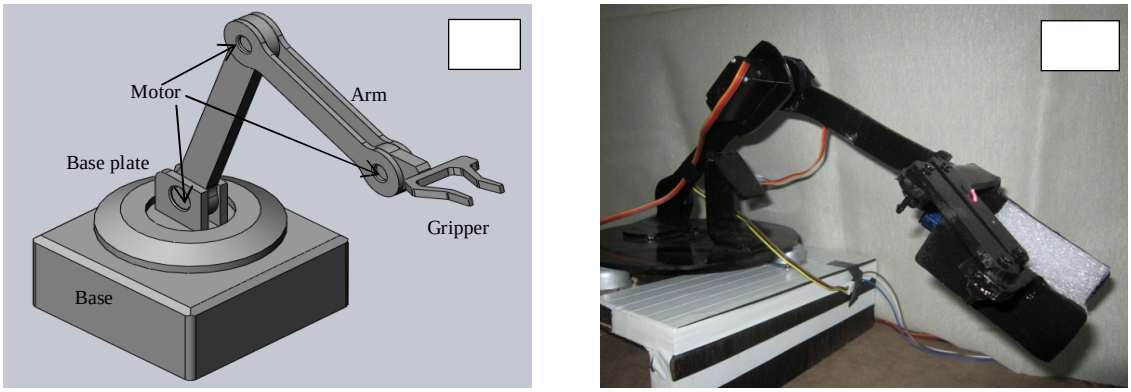

Fig:1 Design of the robotic arm.(a)prototype,(b)CAD design

Among the mechanical parts Gripper, link arm and base plate are the major ones.

2.1.1.GRIPPER: The mechanical construction incorporates an innovative design of the gripper which is considered to be one of the vital parts of the arm. As par the study of Osswald et al. [8], there are two basic approaches to determine the size and alignment of fingers. These are: Anthropomorphic and Non-anthropomorphic. An anthropomorphic alignment allows the robotic arm to inter-act with human hand more easily and humanly at the cost of complex design and cost. On the contrary, where interaction between robotic and human hand is not a necessity, rather the arm is desired to perform specific repeated job with great speed and precision, non-anthropomorphic approach is much appreciated for its simplicity in design and being more economic for production and maintenance. Since this paper presents industrial arm for sorting, picking and placing purposes, non-anthropomorphic approach was taken. The gripper was made of acrylic sheet for the prototype where it can carry a load about 1Kg.For the large scale it can be optimized and enhanced using the object type idea and physical dimension of the object. So the design of the gripper is made so flexible so that it can adjust a wide range of object without any kind of slip. A material having high friction coefficient is attached in real prototype so that the object cannot slip.

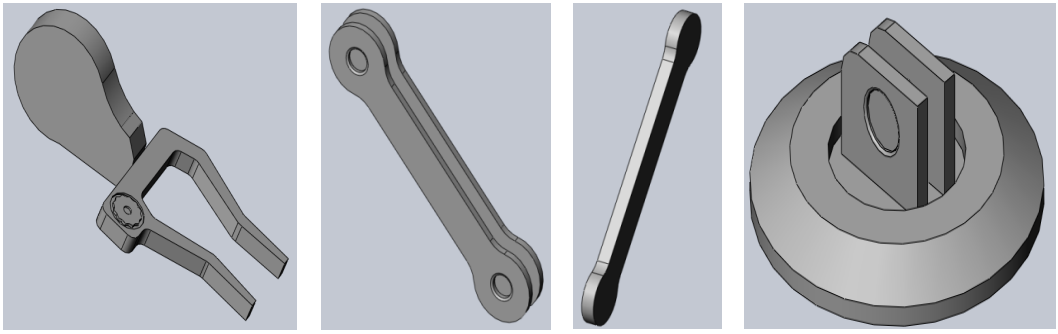

Fig 2:Design of different parts of the robotic arm

2.1.2 BASE AND ROTATING BASE PLATE: The base of the arm bears the entire load. It is to be fixed on the working platform. The strength of the material and the joints of this part are analyzed to ensure its stability. This holds a servo-motor firmly in it and on the shaft of the base motor mounted a base plate which can rotate with 360 degree with the entire arm and the object picked. Since the base plate rotates with the arm mounted upon, it is to be properly supported to avoid failure. To solve this problem 3 ball-casters were placed on the base and below the base plate to provide additional and

uniform support along with the motor shaft. To confirm the stability, loosely fitted clamps were also used to provide a slight push in the downward direction.

2.1.3 LINK ARM: The links basically make connection between the base and gripper and help to pick the objects at distance. The links were designed in such a way to provide several degrees of freedom and also were light in weight but strong in strength by choosing right material and proper shape. The buckling of the links was also analyzed and proper safety factors were determined.

2.2 MATERIALS

A wide range of material has been studied to make the mechanical structure. We studied on Aluminium, wood, stainless steel, plexi-glass, plastic for this reason. Wood was a good choice as it is easy to make drill but it is not sustainable due to the load factor. Aluminium and plastic were found to be feasible due to their mechanical properties. For Aluminium being strong and light and having a good stability against abrasion and corrosion, links of the arm and the gripper were made of it.

2.3. MECHANICAL STRESS ANALYSIS

Stress analysis has been given the most priority during the mechanical design of the robotic arm. The stress analysis has been done in the SolidWorks software package to validate the model and the critically stressed part are designed carefully. Stress is reduced introducing the chamfering, filleting and giving suitable notch to the structure. A rough stress analysis on the arm is shown in figure 3

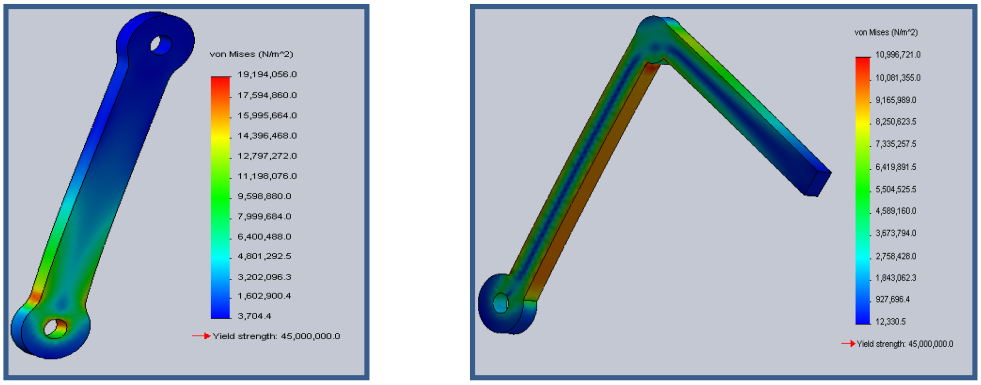

Figure:Stress analysis on the link

2.5. KINEMATICS OF THE ROBOTIC ARM

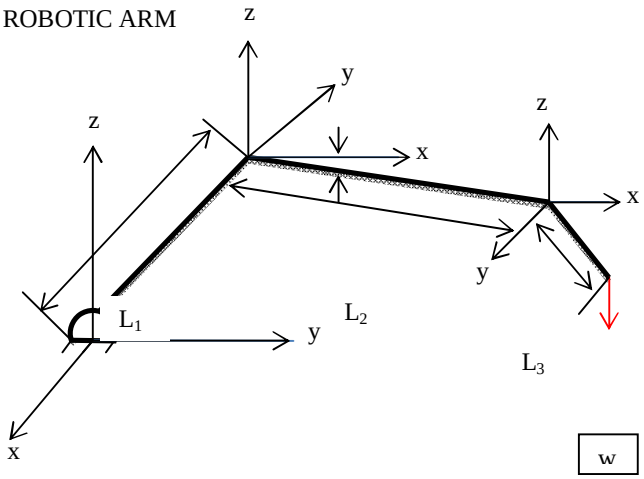

Fig: kinematics of thr robotic arm

A kinematic study was carried out to study the motion of the different links of the arm. Maximum and minimum torque at different angular position of the arm were determined which are presented in data analysis and result section of this paper. The following figure is a space diagram of the arm at a specific angular position where the first link, of length 45 cm, is at 45 degree with horizontal and the second link, 30 cm in length, at 30 degree. The third link, 15 cm, at which the gripper is affixed, is at a angular position of 50 degree. As the gripper hold the object, its weight acts downward. This weight is transmitted to all parts of the arm along with the self-weight of the links and motors attached. Analysis at different angular positions and their graphical presentation provided an accurate estimation of the torque needed for the motors used.

3. CONTROL SYSTEM

3.1 SENSOR

The control unit of the arm consists of a microcontroller ATmega 32A for I/O operations, PWM and decision making processes. For the process there is two major concerns. Firstly sensing the object accurately and secondly moving different links of the arm in order to pick and place the objects with precision and high speed. For sensing, a TCS3200 color sensor was used. TCS3200 chip is able to detect the color of light incident on it. It has an array of photodiode (a matrix of 8x8, so a total 64 sensors). These photodiodes are covered with three types of filters. Sixteen sensors have red filters over them thus can measure only the component of red in the incident light. Likewise other sixteen have green filters and sixteen have blue filters while the rest 16 sensors have clear filter. Any visible color can be broken into three primary colors. So these three types of filtered sensors helps measure the weightage of each of primary colors in incident light. TCS3200 converts the intensity of incident radiation into frequency. The output waveform is a 50% duty cycle square wave. The RGB colors thus can perfectly be detected and distinguished.

3.2. SERVO MECHANISM

For the motion of the arm, selection of motor is a major challenge. We used servo motors for precise angular position and velocity. A servo system mainly consists of three basic components - a controlled device, a output sensor, a feedback system.This is an automatic closed loop control system. Here instead of controlling a device by applying variable input signal, the device is controlled by a feedback signal generated by comparing output signal and reference input signal.
When reference input signal or command signal is applied to the system, it is compared with output reference signal of the system produced by output sensor, and a third signal produced by feedback system. This third signal acts as input signal of controlled device. This input signal to the device presents as long as there is a logical difference between reference input signal and output signal of the system. After the device achieves its desired output, there will be no longer logical difference between reference input signal and reference output signal of the system. Then, third signal produced by comparing theses above said signals will not remain enough to operate the device further and to produce further output of the system until the next reference input signal or command signal is applied to the system. Hence the primary task of a servomechanism is to maintain the output of a system at the desired value in the presence of disturbances.
To select servos, torque calculations were carried out.

3.3. VIBRATION AND NOISE CONTROL

Vibration and noise control is a key challenge in building the pick and place type robot. As the base motor rotates in high torque if there is any kind of imbalance in force the base plate can vibrate and which can be hazardous. So it is recommended that caster wheel should be used to make the rotation very smooth and vibration less. Noise is another pertinent parameter which should be controlled. There are a lot of friction among the links and plates. So noise should be kept at low level for good operating condition of the arm. Ball caster is preferable for this kind of application.

4.METHODOLOGY AND ALGORITHOM

The logic level is kept as simple as possible. It is shown in a flow chart below:

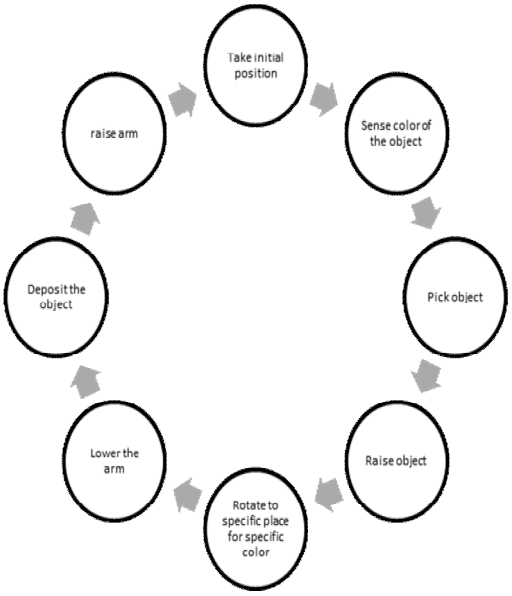

Figure: Flow chart of working principle

When the power is on at first the arm will go to its initial stage. From initial position the arm link gets down to pick the object from the conveyer. In this mean time the sensor fixed with the base sense the object's color. After picking the object from the desired place the arm raises again. Then according to the color of the object it rotates as it was preprogrammed as par the color of the object. The rotation is done by the base motor. After reaching the destination the arm is lowered. Then the motor of the gripper rotates to ungrip the object. After deposing the object into the box the arm raises again as the link motor rotates and holds its upper position.Then the base motor rotates again and takes the arm to its initial position. The rotation is done according to the sensed color. The sensing, decision making and acting according to the decision is done in the following order:

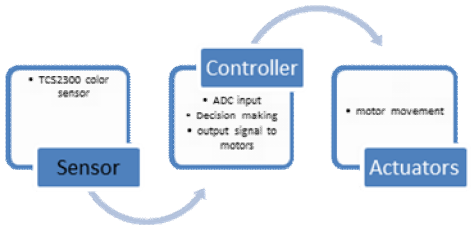

Figure: sensing and controlling

The algorithm of the robotic arm is shown in the figure

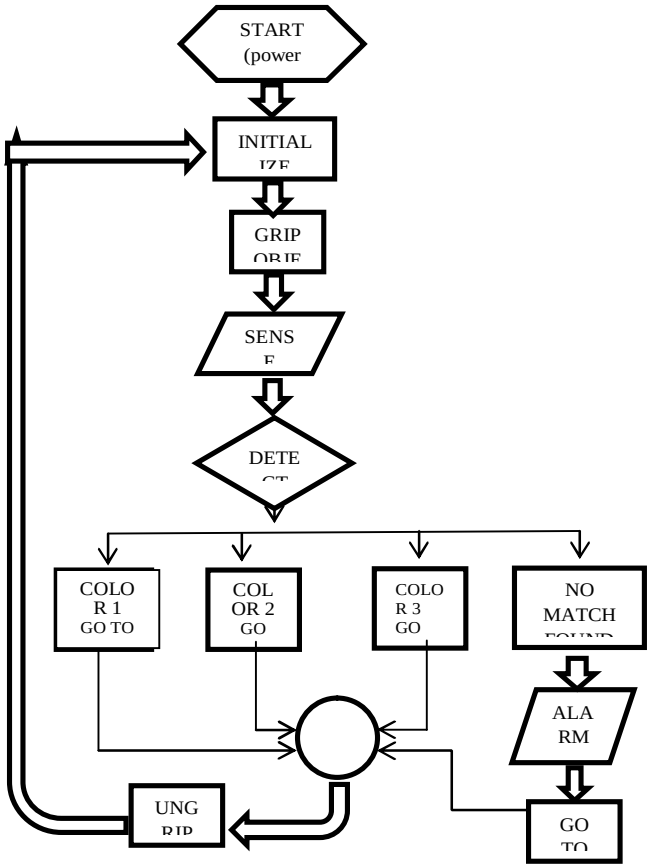

Fig: algorithm of the pick and place color sorting robotic arm

5. DATA ANALYSIS AND RESULT

Detailed data analysis has been performed for various load and angular position of the gripper, arm and base links and thus torques on respective motors were determined. Below is a graphical presentation.

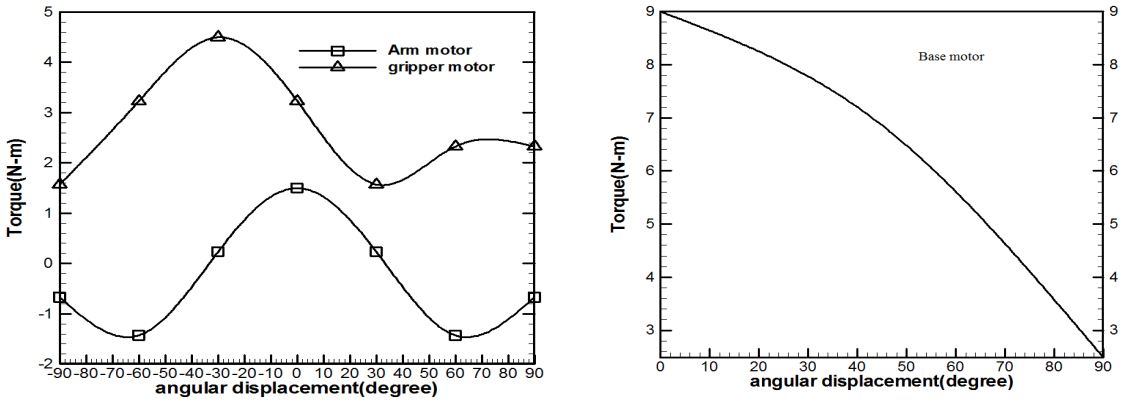

Fig: angular displacement and torque relationship

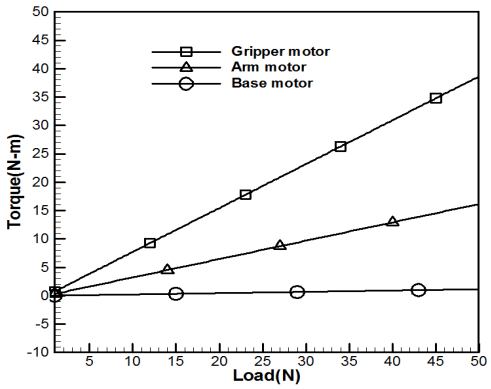

Fig: Load and torque relationship for different motor

A rigorous mathematical computation has been carried out and the result are shown in the figure .In the figure 7 first the position where the maximum torque work on different motor has been analyzed. The gripper arm shows the maximum torque at the angular position of -30 degree and the arm motor shows maximum torque for 0 degree. This torque works at the motor to hold the object properly. For the base motor maximum torque works at the 0 degree. So for the design consideration this parameter was kept in mind so that critical stress on the link and grip can be avoided.

In the later figure relationship between load and torque on different motor position has been shown. From the figure it is evident that there are critical torque and stress on the gripper as the payload increases. So the gripper should be designed properly. And in material selection gripper should be made of strong material than the arm. With the increment of load torque increased linearly.

6. APPLICATION FIELD

Robots are outfitted with wide reaches and slim arms, steady repeatability and precise tooling - all of which allows them to be extremely accurate. This high precision capability makes them a good match for pick and place applications. Pick and place robot systems have the ability to improve product quality and cycle time. Robotic movements are regulated, so the results are always the same. Quality is improved because of this regularity. Furthermore, this consistency allows the processes to take place. One of the main advantages of robotics is flexibility. Pick and place robots are easily programmable. They are able to accommodate multiple changes in product shape and type. In addition, robots provide a high level of movement flexibility. Pick and place applications can be physically demanding. They are labor-intensive, repetitive, and monotonous. Depending on the weight and size of a part, moving it from one place to another can be very demanding work. Pick and place robots are unaffected by the stresses of the application. They are able to work without taking breaks or making mistakes.Incorporating pick and place robots can effectively cut your costs. Robotic precision and reliability allow for less wasted material and more efficient use of time. Plus, the initial investment in robots is quickly recouped - making pick and place robots an extremely cost-effective solution. Today's robotic industries continue to expand. Some of the most common industries that use robots are:

- Agriculture - uses: crop harvest, animal grooming and care
- Automobile - uses: assembly, testing
- Construction - uses: welding, floor finishing
- Entertainment - uses: toys, humanoids, companions
- Health care - uses: hospitals, patient-care, surgery , research
- Laboratories - uses: science, engineering, research
- Law enforcement - uses: surveillance, patrol, etc.
- Manufacturing - uses: assembly, packing, packaging, painting, welding
- Military - uses: demining, surveillance, attack, etc.
- Mining - uses: excavation, and exploration
- Transportation - uses: air, ground, rail, space
- Utilities - uses: gas, water, and electric readings

- Warehouses - uses: material movement
- Space - uses: research, testing
- Hazardous Environments - uses: material handling
- Home - uses: cleaning, monitoring, entertainment

So in the field of robotics, specially which are produced and fabricated for industrial usage, pick and place arm stands with an special importance. And when color detecting intelligence is integrated, its significance and working field is boosted again.

7. CONCLUSION

Pick and place robot is very important from the application point of view and color sorting capability add a new dimension to its application field. Selection of motor and Degree of freedom of the entire robotic arm should be based on the application. Stress analysis shows that the arm should not be kept horizontally and a moderate design is required to achieve the wanted DOF. Sensing and controlling part can be improved and precision can be obtained varying the sensor and control unit. For low cost system, LED-LDR pair can be used for sensing, though not recommended by the authors, only if color difference is enough, only 2 or 3 colored objects to be sorted, and of course the lighting condition is always the same. From the economic point of view this kind of robotic arm is feasible. The implementation of this type of robot can be increased in Bangladesh as it costs low and its fabrication can be done locally with a reliable controlling system. So this type of robotic arm has a promising future in a developing country like Bangladesh keeping its application criteria in mind.

8.REFERENCES

[1] Yong Zhang; Chen, B.K.; Xinyu Liu; Yu Sun, "Autonomous Robotic Pick-and-Place of Microobjects," Robotics, IEEE Transactions on , vol.26, no.1, pp.200,207, Feb. 2010

[2] Nabat, V.; de la O Rodriguez, M.; Company, O.; Krut, Sebastien; Pierrot, F., "Par4: very high speed parallel robot for pick-and-place," Intelligent Robots and Systems, 2005. (IROS 2005). 2005 IEEE/RSJ International Conference on , vol., no., pp.553,558, 2-6 Aug. 2005

[3] de Rengerve, A.; Hirel, J.; Andry, P.; Quoy, M.; Gaussier, P., "On-line learning and planning in a pick-and-place task demonstrated through body manipulation," Development and Learning (ICDL), 2011 IEEE International Conference on , vol.2, no., pp.1,6, 24-27 Aug. 2011

[4] ISO Standard 8373:1994, Manipulating Industrial Robots – Vocabulary

[5] Schuler, McNamee: Industrial Electronics and Robotics.Tata McGraw-hill International Editions.

[6] Moshe Shoham: Textbook of Robotics: I Basic Concepts.Anchor Brendon Ltd.

[7] Dr. Bindu A Thomas, Stafford Michahial, Shreeraksha.P, Vijayashri B Nagvi, Suresh M (2013) Industry Based Automatic Robotic Arm, International Journal of Engineering and Innovative Technology (IJEIT)Volume 2, Issue 11, May 2013.

[8] Osswald, D., Wörn, H., "Mechanical System and Control System of a Dexterous Robot Hand", In Proceedings of the IEEE-RAS International Conference on Humanoid Robots, 2001.